



Università degli Studi dell'Aquila

Dipartimento di Scienze cliniche applicate e biotecnologiche

Dottorato di Ricerca in “Medicina Sperimentale”

Curriculum “Biotecnologie”, XXXII Ciclo

The Role of Lipocalin-2 in Bone and Muscle Physiopathology

SSD: BIO/17 – ISTOLOGIA

Dottorando:

Ponzetti Marco

Coordinatore del corso:

Prof.ssa Maria Grazia Perilli

Tutor:

Prof.ssa Nadia Rucci

A.A. 2018-2019

TABLE OF CONTENTS

CHAPTER 1: “INTRODUCTION”

1. INTRODUCTION	5
1.1 THE BONE TISSUE	5
1.1.1 BONE CELLS	6
1.2 SKELETAL MUSCLE	11
1.2.2 MUSCLE FIBER TYPES	133
1.3 MUSCLE AND BONE HEALTH IN DUCHENNE MUSCULAR DYSTROPHY (DMD)	15
1.4 LIPOCALIN-2	17
2. AIM AND OUTLINE OF THE WORK	18
3. REFERENCES	19

CHAPTER 2: “A COMPLEX ROLE FOR LIPOCALIN 2 IN BONE METABOLISM: GLOBAL ABLATION IN MICE INDUCES OSTEOPENIA CAUSED BY AN ALTERED ENERGY METABOLISM”

1. ABSTRACT	34
2. INTRODUCTION	35
3. MATERIALS AND METHODS	35
3.1 MATERIALS	35
3.2 ANIMALS	36
3.3 MICRO-CT ANALYSIS	36
3.4 BONE HISTOMORPHOMETRY	37
3.5 GLUCOSE TOLERANCE TEST	37
3.6 INSULIN TOLERANCE TEST	37
3.7 GLUCOSE-STIMULATED INSULIN SECRETION BY PRIMARY PANCREATIC ISLETS	38
3.8 EXPERIMENTS IN METABOLIC CAGES	38
3.9 GLUCOSE CONCENTRATION IN URINE	39
3.10 INSULIN, BONE TURNOVER BIOMARKER, AND LCN2 CONCENTRATIONS IN SERA	39
3.11 OSTEOBLAST PRIMARY CULTURES	39
3.12 MINERALIZATION ASSAY	39
3.13 ALP-POSITIVE COLONY FORMING UNIT ASSAY	39
3.14 OSTEOCLAST PRIMARY CULTURES	39
3.15 ADIPOCYTES ISOLATION	40
3.16 COMPARATIVE REAL-TIME RT-PCR	40
3.17 STATISTICS	40
4. RESULTS	41
4.1 BONE METABOLISM	41
4.2 ENERGY METABOLISM	47
4.3 KIDNEY ALTERATIONS	51
4.4 MOLECULAR MECHANISM	53
5. DISCUSSION	55
6. REFERENCES	58

CHAPTER 3: “LIPOCALIN-2 IN MUSCLE IN BASAL CONDITIONS AND AFTER CHALLENGE”

1. ABSTRACT.....	63
2. INTRODUCTION.....	64
3. MATERIAL AND METHODS.....	64
3.1 MATERIALS.....	64
3.2 ANIMALS.....	65
3.3 CELL LINES.....	65
3.4 PRIMARY CELL CULTURES.....	65
3.5 GRAN SASSO D’ITALIA VERTICAL RUN (VR).....	65
3.6 HUMAN SERUM SAMPLING.....	66
3.7 MICE SERUM SAMPLING.....	66
3.8 ELISA AND REFLOTRON TESTS.....	66
3.9 COMPARATIVE REAL-TIME RT-PCR.....	67
3.10 REAL TIME RT-ARRAYS.....	67
3.11 HISTOLOGY AND HISTOPATHOLOGY.....	67
3.12 STATISTICS.....	68
4. RESULTS.....	68
5. DISCUSSION.....	77
6. REFERENCES.....	78

CHAPTER 4: “LIPOCALIN 2 IN THE BONE AND MUSCLE PHENOTYPE OF THE *MDX* MOUSE MODEL OF DMD”

1. ABSTRACT.....	82
2. INTRODUCTION.....	83
3. MATERIAL AND METHODS.....	83
3.1 MATERIALS.....	83
3.2 ANIMALS.....	83
3.3 ANTI-LCN2 ANTIBODY TREATMENT.....	84
3.4 COMPARATIVE REAL-TIME RT-PCR.....	84
3.5 HISTOLOGY AND HISTOPATHOLOGY.....	84
3.6 BONE HISTOMORPHOMETRY.....	85
3.7 MICRO-CT ANALYSIS.....	85
3.8 BIODENT ® MECHANICAL TESTING.....	85
3.9 STATISTICS.....	86
4. RESULTS.....	86
5. DISCUSSION.....	100
6. REFERENCES.....	101

CHAPTER 5: “CONCLUSIONS”

CONCLUSIONS.....	104
REFERENCES.....	106

CHAPTER 6: “ACHIEVEMENTS”.....	109
--------------------------------	-----



Chapter 1

“Introduction”

Partially published in *Frontiers in endocrinology*, 2019 (doi: 10.3389/fendo.2019.00236).

M. Ponzetti and N. Rucci.

1. INTRODUCTION

1.1 THE BONE TISSUE

Bone is a specialized connective tissue, characterized by a mineralized matrix. The ceramic-like properties of hydroxyapatite, the main mineral component of the skeleton, and the polymer-like properties of type I collagen fibers, give rise to an extraordinarily resilient, hard, resistant material, with self-healing properties conferred by its cellular components¹. There are three main cellular types in the bone: osteoblasts, which form bone, osteoclasts, whose duty is to resorb bone, and bone-resident cells, osteocytes, that are essentially osteoblasts which become buried in their own matrix. Among with cartilage, tendons, ligaments and muscles, bones make up the locomotor system, allowing movement.

Perhaps surprisingly, bone is a very dynamic tissue, which exerts many important functions other than locomotion, such as being a metabolic reservoir of minerals and protection for “soft” organs²⁻⁵.

It is interesting to notice that bone undergoes constant renewal during the whole lifetime, in a process termed bone remodeling, which consists in the cyclic removal and re-deposition of bone tissue (Figure 1). Although this might seem a waste of energy, this process is actually essential for the maintenance of the mechanical properties of the tissue and for the regulation of Ca^{2+} and PO_4^{3-} serum levels. Moreover, the skeleton is now widely recognized as an endocrine organ, able to regulate not only phosphate metabolism through fibroblasts growth

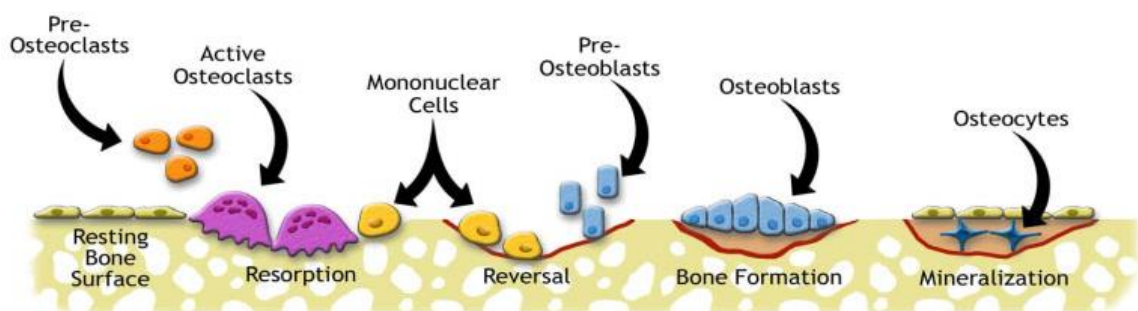


Figure 1: Bone remodelling. The bone remodeling cycle starts when bone lining cells expose the bone surface, which is now “activated” as opposed to “resting”. Next, osteoclasts differentiate and migrate to the area, forming the Howship lacuna, the part of the bone to be eroded. The lacuna is acidified to dissolve hydroxyapatite crystals, thus exposing collagen and non-collagenous proteins to proteolytic digestion by cathepsin K and other acid hydrolases. The following phase is called “reversal phase”, which starts with osteoclasts undergoing apoptosis, and giving way to macrophage-like cells called reverse cells. These cells absorb the rest of the debris from the resorption lacuna and help recruiting osteoblasts, starting the bone formation phase, characterized by the deposition of the organic part of the bone matrix, the osteoid, and the subsequent mineralization. (Source: adapted from www.orthopaedicsone.com⁶)

factor (FGF)23, but even energy metabolism, brain development, appetite and male fertility^{5,7-9}.

1.1.1 BONE CELLS

Osteoblasts

Osteoblasts are responsible for the production and deposition of bone matrix, and derive from mesenchymal stem cells (MSCs)^{2,10,11}. Indeed, MSCs can differentiate into osteoblasts after stimulation by local growth factors¹², such as Fibroblast Growth Factors (FGFs)¹³, Bone Morphogenetic Proteins (BMPs)^{14,15}, and Wingless-related integration site (Wnt)¹⁶ proteins. Later on, master osteogenic transcription factors such as Runt-related transcription factor (Runx) 2 and Osterix are required¹⁷⁻²² for their differentiation into mature osteoblasts. In the late stages of its differentiation, i.e. after its bone-depositing role has been fulfilled, the osteoblast can become a lining cell, an osteocyte, or die by apoptosis^{10,23}.

The plasma membrane of the osteoblast is rich in alkaline phosphatase (ALP), considered a marker of osteoblast-lineage cells and whose concentration in the serum is used as a marker of bone formation. In addition, osteoblast expresses receptors for parathyroid hormone (PTH), prostaglandins, oestrogens and vitamin D3.

The first phase of bone formation is the deposition of the bone organic matrix (osteoid), which is then mineralized¹¹. Osteoid exists because of a latency between matrix formation and its subsequent mineralization, which lasts approximately 10 days in humans.

Mineralization begins with the formation of hydroxyapatite crystals within the so-called matrix vesicles released by osteoblasts, which function as nucleation points for further propagation of hydroxyapatite, through the membrane, into the extracellular matrix²⁴. The formation of hydroxyapatite requires high concentrations of calcium inside the matrix vesicles, which are achieved using calcium-binding phospholipids, proteins, bone sialoprotein and calcium channel-forming annexins^{24,25}. In the second step of mineralization, hydroxyapatite crystals penetrate the membrane of matrix vesicles and grow into the extracellular matrix, initially along the period of the collagen fibrils, then filling the space among them.

In addition to depositing bone, another main function of osteoblasts is the regulation of osteoclasts by producing macrophages colony stimulating factor (M-CSF), receptor activator of nuclear factor- κ B ligand (RANKL) and osteoprotegerin (OPG), all positive (the former two) or negative (the latter) mediators of osteoclast formation and differentiation^{2,5,26-28} (Figure 2).

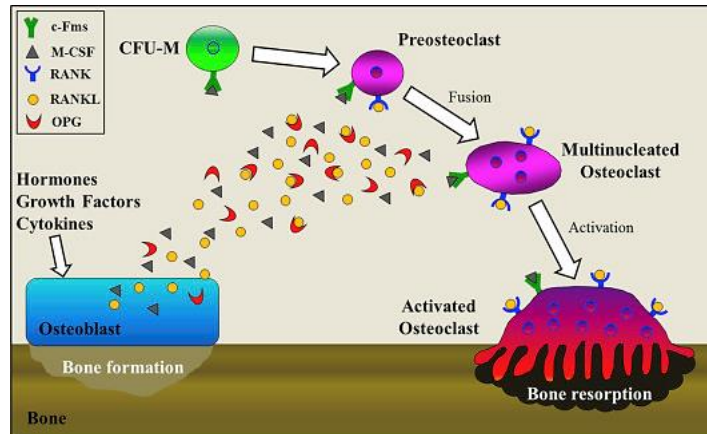


Figure 2: Osteoblasts produce osteoclast-regulating cytokines. Cartoon illustrating the mechanism by which osteoblasts regulate osteoclastogenesis through the production of cytokines such as M-CSF, RANKL (pro-osteoclastogenesis) and OPG (anti-osteoclastogenesis). (Source: adapted from Lee and Choi, 2015²⁹)

Another important function osteoblasts exert, is the regulation of hematopoiesis. In fact, mice with constitutively active PTH/PTHrP receptor in osteoblasts, have more hematopoietic stem cells (HSCs)³⁰. Moreover, a subpopulation of osteoblasts, called spindle-shaped-N-cadherin⁺CD45⁻ osteoblasts (SNOs), was directly correlated and bound to HSCs³¹. B lymphocytes differentiation from HSCs was also found to be controlled by osteoblasts³², likely due to their secretion of Interleukin (IL)7 and C-X-C Motif Chemokine Ligand (CXCL)12, both pivotal for B cells differentiation^{33,34}. This led to the establishment of a new concept, the so called “endosteal niche”, regulating haematopoiesis besides the well-known “vascular niche”^{28,35}.

Osteocytes

Osteocytes are the most abundant bone cells, representing 90-95% of the total cells in the adult skeleton^{36,10}. They were originally osteoblasts, which became “buried alive” in the bone matrix that they produced⁵. These non-proliferative, terminally differentiated cells are regularly dispersed in the mineralized matrix, connected to each other and to cells lining the bone surface through numerous dendritic processes forming gap junctions, which run inside a complex anastomosed system of canaliculi, called the osteo-canalicular network (Figure 3)³⁶⁻³⁸. The morphology of the osteocytes varies according to their age and functional activity. A young osteocyte has most of the ultrastructural characteristics of the osteoblast from which it derives, except that there has been a decrease in cell volume and organelles involved in protein synthesis and secretion.

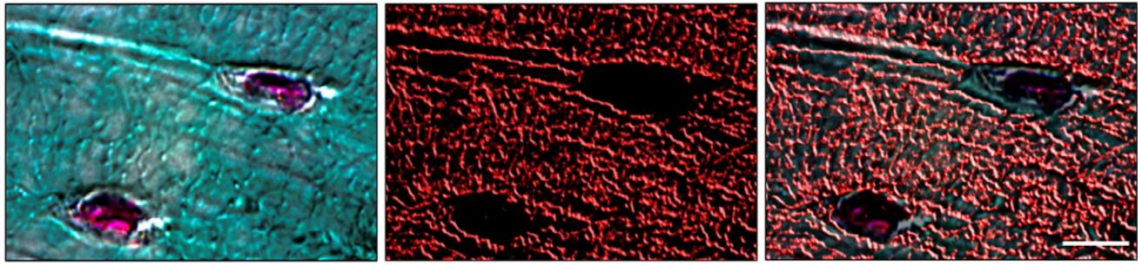


Figure 3: The osteocyte and osteo-canalicular network. Goldner trichrome staining of a cortical bone section from a paraffin embedded mouse tibia (left panel). Osteocyte canaliculi were evidenced by graphic elaboration of the picture (central panel) and merged with the original picture (right panel). Bar = 2 μ m (Source: adapted from Capulli *et al.*, 2014¹⁰)

A mature osteocyte, located deeper within the calcified bone into osteocytic lacunae, shows a further accentuation of these decreases and an accumulation of glycogen in the cytoplasm. In certain circumstance, these cells have been shown to locally resorb the bone surrounding the osteocytic lacunae, as well as to synthesise new bone matrix at the surface of these lacunae^{28,37,39-41}. The osteocytes persist in the matrix for years, playing a role as mechano-sensors, in the local activation of bone turnover^{39,40,42,43} and in the release of FGF23, a hormone that regulates the phosphate tubular reabsorption by the kidney⁴⁴.

Osteoclasts

Osteoclasts are highly specialized cells able to remove bone matrix, thus playing a crucial part in the mineral homeostasis and guaranteeing bone mechanical prowess^{27,45}.

They are giant multinucleated cells, containing 4-20 nuclei, derived from multiple cellular fusion of their mononuclear precursors belonging to the monocyte/macrophage lineage^{27,45}. To digest bone, they form resorption lacunae (a.k.a. Howship's lacunae).

At the microscopic level, nuclei are of variable morphology, reflecting the asynchronous fusion of mononuclear precursors. Osteoclasts have large Golgi apparatuses around each nucleus, abundant mitochondria, and numerous transport vesicles, lysosomes and vacuoles. These structures indicate that osteoclasts are actively involved in energy production and protein synthesis and secretion, particularly in the production of lysosomal proteins and enzymes^{27,45}.

Osteoclasts are polarized and show well-defined plasma membrane domains, namely the basolateral and the apical ones. The latter is characterized by the "sealing zone" made up of two distinct areas called the "clear zone", with few organelles, and the "sealing membrane", which faces bone directly and contains specialized adhesion structures called podosomes^{46,47}. Podosomes ensure a tight association between the osteoclast and the bone

matrix directing the assembly of the so-called “actin ring”. Proximally to the sealing zone, osteoclasts present the ruffled border, composed of specialized membrane invaginations and evaginations that allow the fusion of the lysosomal membranes and the release of the lysosomal enzymes into the resorption lacuna, and are equipped with proton pumps and the molecular machinery necessary to allow the degradation of the inorganic and organic bone matrix^{5,27,48,49}.

Finally, the basolateral membrane, presents a “functional secretory domain”, which is essential for releasing the digested matrix components into the bloodstream⁵⁰. The rest of the basolateral membrane is highly and specifically enriched in Na⁺/K⁺ ATPase (sodium-potassium pumps), HCO₃⁻/Cl⁻ exchangers, and Na⁺/H⁺ exchangers, as well as several ion channels, which allow the osteoclast to maintain electro- and pH-neutrality. This domain also expresses RANK (RANKL receptor) and c-Fms (M-CSF receptor), responsible for osteoclast differentiation^{51,52}, and the calcitonin receptor²⁷. RANKL interacts with its receptor RANK expressed by osteoclast precursors, thus recruiting TNFR-associated factors (TRAFs), which in turn trigger osteoclast differentiation by stimulating nuclear translocation of Nuclear Factor k-light-chain-enhancer of activated B cells (NFkB), activator protein 1 (AP1) complex and nuclear factor of activated T-cells, cytoplasmic, calcineurin-dependent 1 (NFATc1)⁵³. All these factors stimulate transcription of several osteoclast-specific genes, such as Tartrate Resistant Acid Phosphatase (TRAcP), calcitonin receptor, cathepsin K, Osteoclast Associated Receptor (OSCAR), alpha V β3 integrin, Metalloproteinase (MMP) 9 and Dendritic Cell-Specific Transmembrane Protein (DC-STAMP) the latter involved in osteoclast fusion (Figure 4). Of note, a vast number of inflammatory molecules, able to activate the NfκB pathway in osteoclasts, can induce osteoclast formation (Table I), which is why a number of inflammatory diseases, including rheumatoid arthritis⁵⁴⁻⁵⁶ and periodontal disease⁵⁷⁻⁵⁹, are characterized by marked bone loss due to osteoclast hyperactivation.

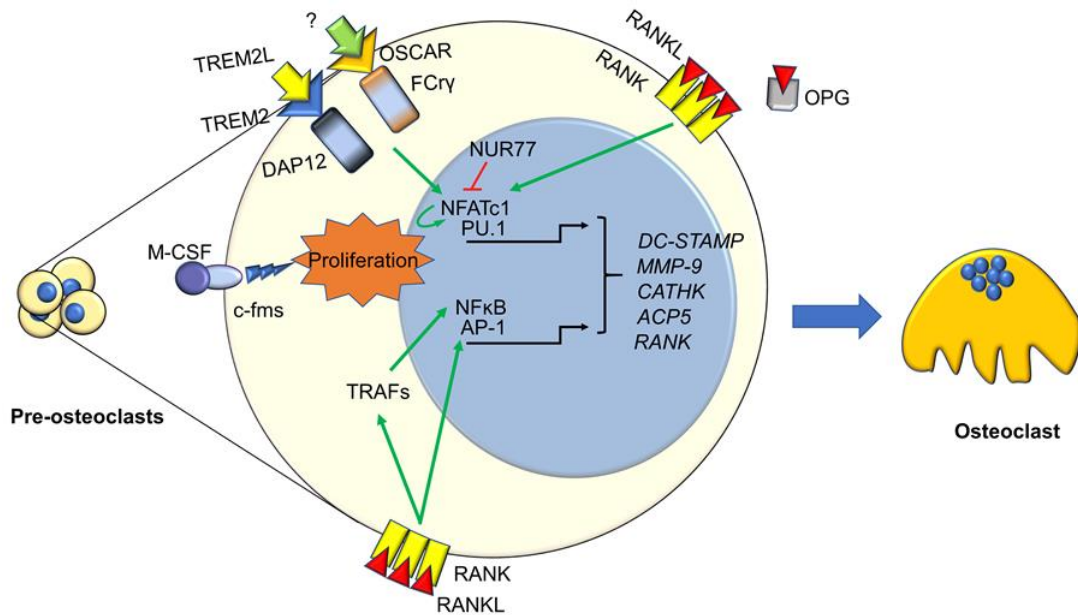


Figure 4: Molecular pathways involved in osteoclastogenesis. Osteoclasts differentiation from pre-osteoclasts involves several factors, most of which are derived from the immune system. Signaling from TREM2, OSCAR, c-FMS and RANK cause the nuclear translocation of several transcription factors activating pre-osteoclast proliferation and differentiation. These include the master osteoclastogenesis controllers NFATc1, which also self-amplifies, and NFκB, along with the early commitment factor PU.1 and AP1. This is enacted both directly by RANK, and indirectly through TRAFs and PLCγ. Osteoclastogenesis can be hindered by several factors, two key ones are the decoy receptor for RANKL, OPG, and the immune factor NUR77, which can inhibit NFATc1 stopping its self-amplification loop. The final outcome of these molecular pathways is the transcription of key osteoclast genes such as DC-STAMP, MMP9, CATHK, ACP5 and RANK, which eventually results in the generation of a mature osteoclast. (Source: Ponzetti and Rucci., 2019²⁸)

Table I: Secreted and membrane-bound immune factors promoting osteoclastogenesis

Factor	Source
RANKL	Osteoblasts, osteocytes, neutrophils, sinoviocytes, T-cells ⁶⁰⁻⁶²
TNFα	Activated leucocytes ^{63,64}
IL-1α, -1β	Activated leucocytes, osteoblasts, synoviocytes, endothelial cells ⁶⁵
IL-7	Osteoblasts, bone marrow stromal cells, leucocytes ⁶⁵
IL-8	Activated leucocytes
IL-11	Bone marrow stromal cells ⁶⁶
IL-23	Dendritic cells, Th17 T-cells ⁶⁷
IL-34	Dendritic cells, Th17 T-cells, synoviocytes, osteoblasts ^{65,67}
Prostaglandins	Bone and bone marrow cells ⁶⁸
SOFAT	T-cells ⁵⁹
IL-6	Bone marrow stromal cells, osteoblasts, macrophages, muscle, fibroblasts ^{66,69-72}
IFN-γ	T-cells, NK-cells ^{73,74}
IL-17A	Th17 cells ^{16,55,67,75}
IL-15	PG-stimulated stromal cells, NK-cells ⁷⁶

Bone marrow stromal cells/skeletal stem cells

Bone marrow stromal cells (MSCs), sometimes termed mesenchymal stem cells, albeit not taking part in bone remodelling *per se*, are worth calling “bone cells”. In fact, they are able to differentiate in chondrocytes, adipocytes, hematopoietic-supporting tissue and notably, osteoblasts⁷⁷. MSCs are highly plastic *in vitro* and *in vivo*, have very high proliferation potential, are spindle shaped, and are characterised by high activity of membrane-bound ALP⁷⁷⁻⁷⁹. In fact, they can be easily isolated from the bone marrow, cultured, and identified as ALP-positive fibroblast-like colony forming units (CFU-F)⁷⁷. MSCs are interesting from a biotechnological point of view, being able to improve bone healing when seeded on appropriate scaffolds^{80,81}. Indeed, MSCs can differentiate into osteoblasts after stimulation from local growth factors¹², such as Fibroblast Growth Factors (FGFs)¹³, Bone Morphogenetic Proteins (BMPs)^{14,15}, and Wnt¹⁶ proteins. Later on, master osteogenic transcription factors such as Runt-related transcription factor (Runx) 2 and Osterix are required¹⁷⁻²² for their differentiation into mature osteoblasts. MSCs or MSC-like cells can be obtained from a variety of tissues, including fat⁸², bone marrow, placenta⁸³ and even urine⁸⁴, making it easy to obtain autologous MSCs, which already made their way into regenerative cell therapy and a number of new applications are currently in study^{85,86}. Another stem cell type that can give rise to osteoblast, is the skeletal stem cell (SCC). The boundary between MSC and SSC is not clear-cut, and the two are often considered the same cell type, with the only difference being the anatomical location, and the commitment stage of SSC, which are thought to be at a stage where they already express Runx2 hence being restricted to the osteo-chondro lineage⁸⁷. This provides SSCs with less plasticity, but more phenotypical stability and predictability^{87,88}. However, more work is needed to clearly define how their commitment is carried out, which would make them excellent candidates for regenerative cell therapy, even more so than MSCs⁸⁸.

1.2 SKELETAL MUSCLE

Skeletal muscle comprises about 40% of the entire body weight, and can account for as much as 75% of all the proteins in the body⁸⁹. It contributes to many body functions, including energy metabolism, thermogenesis, posture maintenance, vision, digestion. However, its main function is surely to allow movement and, most importantly, breathing⁸⁹. A typical skeletal muscle is organized into parallel fibers, bundled up and bound to each other by scarce connective tissue, to eventually form an elongated shape, enlarged in the longitudinal middle. The two extremities are in continuation with tendons. This arrangement, together with the unique ability of muscles to contract and relax, allows movement⁴. The size of

muscles is generally defined by the number and size of muscle fibers (Figure 5), although fat infiltration, oedema, and connective tissue may influence it in pathological conditions^{90,91}. Muscle fibers, which can be long up to several centimeters, are actually a single cell. These cells are formed by fusion of mononuclear precursors (myoblasts),

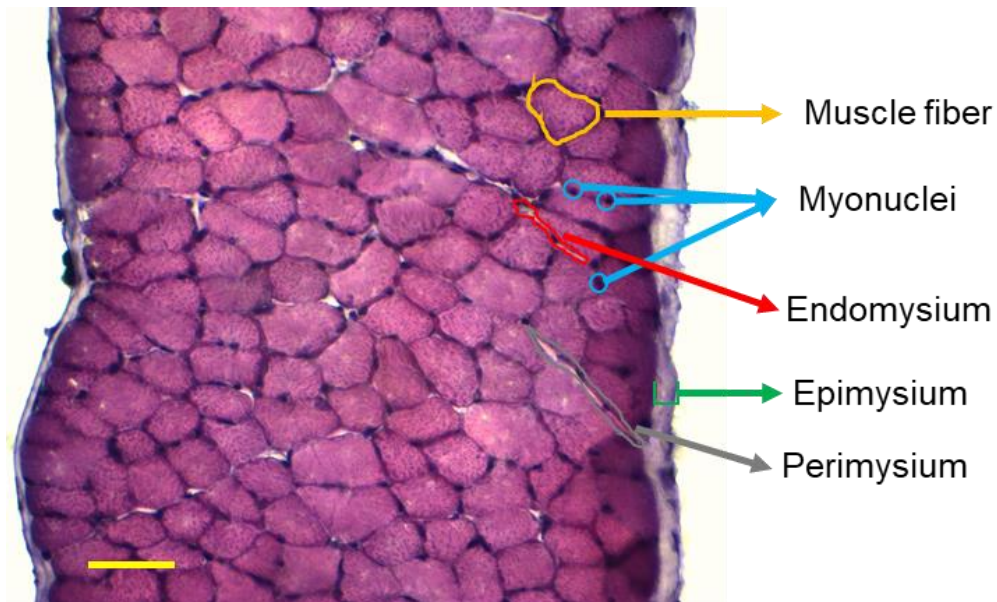


Figure 5: Appearance of mouse skeletal muscle cross-sections of diaphragm stained with hematoxylin-eosin. The figure shows an image of a wild-type mouse diaphragm cross-sections, with some important structures indicated in different colors. Bar=100 μ m

eventually forming large multinucleated *syncytia*. However, the distance among the various nuclei, requires a local regulation of protein synthesis, which is performed by the local nucleus(i), hence dividing the large muscle fiber in “nuclear domains”⁹². Muscle cells are post-mitotic, but several adult stem cells, named satellite cells because of their position in respect to muscle fibers, are present in every muscle⁹²⁻⁹⁴. These cells are known to decline in number with age, and to contribute to several aspects of muscle physiology such as exercise adaptation and damage repair⁹²⁻⁹⁴, since they proliferate and differentiate into mature muscle fibers when stimulated by myogenic factors⁹⁴. Individual muscle fibers are surrounded by a loose connective tissue called endomysium, which also contains nerves and blood vessels⁴. Fascicles are then surrounded by a similar but thicker connective tissue, the perimysium, and entire muscles are encased into the epimysium, a fibrous connective tissue that isolates them from their surroundings^{4,89}. The cytoplasm of muscle fibers, named sarcoplasm, is separated from the endomysium by the sarcolemma, i.e. the muscle cell membrane, which in turn is associated with a complex of several membrane proteins that are physically connected to the microtubules and the extracellular matrix, giving muscle cells

structural resilience. The absence or dysfunction of these protein complexes results in severe muscle damage⁹⁵.

Skeletal muscle is 80% proteins⁹⁶, the majority of them organized in myofilaments⁴, mainly composed by actin and myosin. Myosin is the main molecular motor that allows muscle contraction, by using actin as “rails”. There are as much as eleven subtypes of myosin described in mammals, some of which are also expressed in cardiac muscle⁸⁹. Together, thick filaments of myosin and thin filaments of actin bundle up to form sarcomeres, extremely regular structures that represent the smallest contractile unity in muscle, and confer it its typical striated appearance (Figure 6)^{4,89,97}.

Muscle contraction results in the sliding of a group of myosin heads along actin beads, which culminates in the shortening of the sarcomere. Contraction puts significant strain on the musculoskeletal system, which is easily able to handle it in physiological conditions but can be lethal when specific mechanical or repair elements are missing, such as in the case of Duchenne Muscular Dystrophy.

1.2.2 MUSCLE FIBER TYPES

In the human body, different muscles are significantly variable in terms of relative predominance of fiber types⁸⁹. The most widely used definition of fiber type is the following: type I (fatigue resistant, slow, oxidative), type IIA (intermediate metabolic properties, fast, oxidative), type IIX (fatiguable, fast, glycolytic)⁹⁸. Differences are due to heterogeneity in myosin energy requirements and energy production proteins relative presence. The type of muscle fibers have some degree of plasticity, and depend on metabolic and functional requirements, as well as exercise status, and may vary with pathological conditions, for example, cancer-induced cachexia, or muscular dystrophies^{98,99}. Contraction speed mainly relates to the extent of the sarcoplasmic reticulum, while fatigue tolerance and oxidative capacity primarily depend on mitochondria content. In fact, the most important determinant

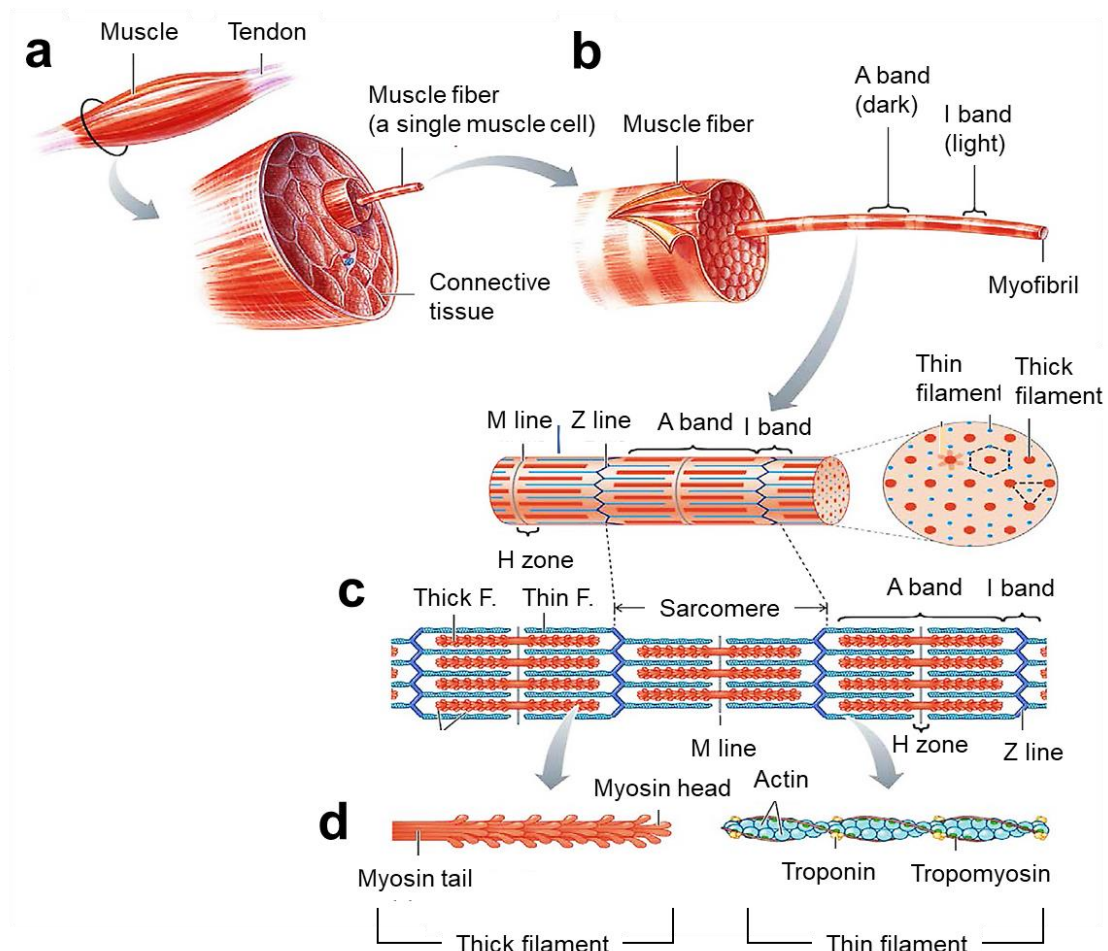


Figure 6: Structure of skeletal muscle, from macro- to nano-scale. (a) Skeletal muscle is formed by parallelly-oriented muscle fibers, eventually converging in one or two tendons, anchoring muscles to bone or cartilage structures. (b) Muscle fibers, representing single muscle cells, are formed by myofibrils, which show light (I) and dark (A) bands. Cross-sections of A bands show the presence of regularly spaced thick and thin spots, representing filaments of myosin (thick filaments) and actin (thin filaments). The I bands are areas where thick and thin filaments do not overlap and are only observable in relaxed or not fully-contracted muscles, where this band almost disappears following the sliding of myosin heads on actin beads. Two lines are also visible in longitudinal section: the Z line, which is mainly formed by actin, crosslinked by α -actinin, and the M line, formed by crosslinked myosin tails, as well as other important proteins such as CK and titin (which extends from the Z line to here). (c) The space between two contiguous Z-lines is termed sarcomere, which is the minimum contractile unit in skeletal muscle, and the M-line represents its middle. (d) detailed representation of myosin and actin structures, with two important proteins evidenced on actin, tropomyosin and troponin. The former binds actin masking its myosin-binding sites, and the latter binds the former, and is able to enact its release from actin, when bound to calcium ions, which starts muscle contraction when sufficient ATP is present. (Source: adapted from Frontera et al., 2015⁸⁹)

of ATP consumption rate and force generation is the isotype of myosin present in the muscle fiber. Type I fibers have the lowest ATP usage rate, IIx have the highest, and IIa are in the middle¹⁰⁰, also reflecting their purpose, since type I fibers are mainly found in tonic and stance muscles, while IIx are needed in muscles performing finer but low-duration movements. The identification of different fiber types may therefore be indicative of metabolic shifts, or various pathological conditions. Notably, the same muscle fiber may express different myosin isoforms in different nuclear domain, especially in response to

exercise, aging, and some pathological conditions^{101,102}. Furthermore, other muscle proteins such as troponin T⁹⁸ have been found to be expressed in type I (slow troponin) and type II (fast troponin) in specific different isoforms. Several transcription factors such as MyoD and myogenin have been shown to play a role in fiber type definition⁸⁹.

1.3 MUSCLE AND BONE HEALTH IN DUCHENNE MUSCULAR DYSTROPHY (DMD)

Duchenne Muscular Dystrophy (DMD) is a rare X-linked genetic disorder, caused by mutations in the largest gene in the genome: dystrophin (*DMD*)¹⁰³. Its incidence is the highest known for rare genetic diseases, affecting up to 1/4000 male live birth¹⁰⁴. The *DMD* gene accounts for 0.1% of the genome and has a wide range of mutations that have been recognized as causative for DMD. About 60–65% of these mutations are deletions, 30% are point mutations (frameshift or early nonsense) and 5–15% are gene duplications^{105,106}. There are 2 known mutational hotspots in this gene, one being located between exons 45–55, and one between exons 2-19¹⁰⁷. Different mutations cause different clinical manifestations, where milder changes in protein structure or only partial reduction of expression may cause Becker Muscular Dystrophy (BMD) instead of DMD, which is a much more forgiving form of the disease^{108,109}. Lack of dystrophin causes such severe effects, since this protein is crucial in the maintenance of sarcolemmal stability during muscle contraction, as it coordinates a protein complex connecting the actin cytoskeleton to the extracellular matrix (Dystrophin-Associated Glycoprotein Complex, DAGC, Figure 7)^{110,111}. Lack of this protein causes muscle damage following contraction, which increases calcium intake of the fiber, further exacerbating contraction and damage¹¹². Muscle necrosis contributes to the establishment of a chronic inflammatory milieu in muscle, summoning inflammatory cells and causing further damage^{113–115}. Another important factor impairing muscle health in DMD is disuse and mechanical unloading^{95,116,117}. In fact, boys affected by DMD are usually forced on a wheelchair by 10-15 years of age^{104,118,119}. At the muscle level, DMD is characterized by weakness, which tends to localise in the areas from neck to elbow and from thigh to knee, and rapidly progressive muscle degeneration, which may happen in different ways. Typically, muscles undergo atrophy, oedematous or compensatory hypertrophy, fibrosis, and fatty infiltration, all of which result in impaired muscle function¹²⁰. Sadly, heart and diaphragm defects typically lead to cardio-respiratory crises and death by age 30-35 despite mechanical ventilation and steroid therapy¹²⁰. The already low quality of life of DMD patients, becomes even direr in the case of fragility fractures: when this happens, even early in life, DMD boys become wheelchair bound and never get up^{104,118,119,121–123}. It is therefore clear that finding a cure for the disease is absolutely crucial, but bone health is not

to be underestimated in giving patients the best possible quality of life, especially considering that fractures are present in up to 30% of them¹²³.

As stated in the previous paragraphs, inflammatory mediators, which are increased in DMD, are usually also activators of osteoclastogenesis, and some of them also reduce osteoblast differentiation^{28,65}.

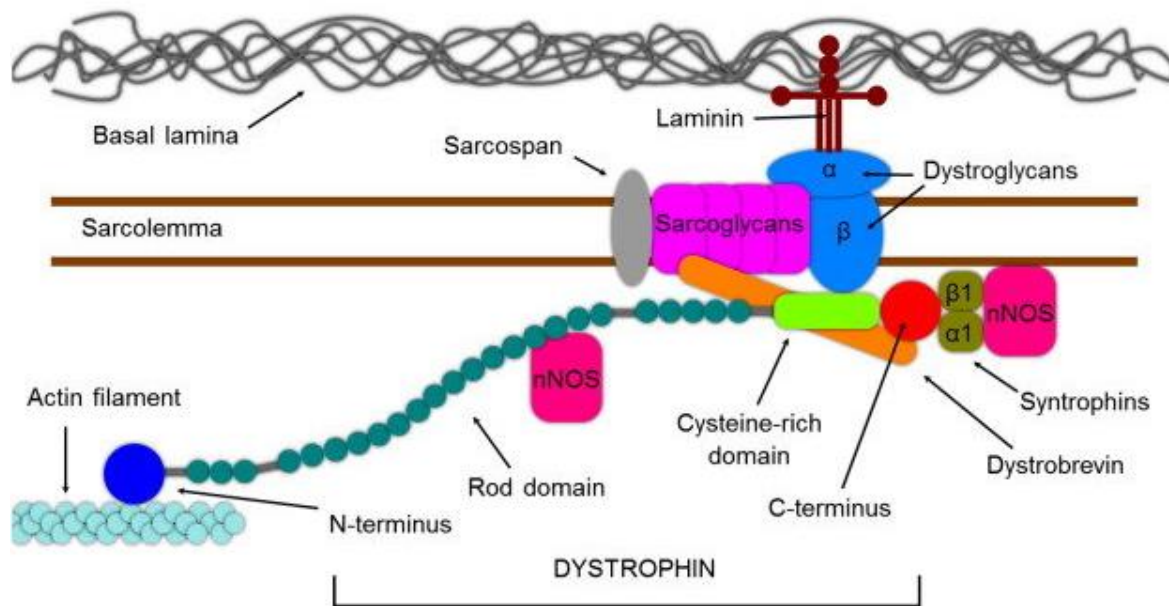


Figure 7: The dystrophin-associated glycoprotein complex (DAGC). Dystrophin is a large (>400KDa) structural protein that is present in myofibers as well as the central nervous system. In striated muscle, it has a very important role during muscle contraction: it anchors actin filaments in the myofiber, to the basal lamina of the endomysium. On the N-terminus, dystrophin binds cytoskeletal actin. The central domain of dystrophin is also termed “rod domain” due to its structure and is able to bind neuronal nitric oxide synthase (nNOS) in addition to providing mechanical stability. The C-terminus is indirectly responsible for the link to the basal lamina, since it binds dystrobrevin and β -dystroglycans through a cysteine-rich domain. The former provides binding sites for sarcoglycans ($\alpha, \beta, \gamma, \delta$), which together with sarcospan and β -dystroglycans, span through the sarcolemma. Sarcoglycans and β -dystroglycans bind α -dystroglycans, which binds laminin, thus connecting the basal lamina to intracellular actin. The C-terminus of dystrophin also binds $\alpha 1$ and $\beta 1$ syntrophins, which provide further binding sites for nNOS. (Source: adapted from Douglas et al., 2013¹²⁴)

This is due to at least 3 main factors: i) the already-mentioned inflammatory cascade that the disease causes, ii) mechanical unloading of bone, eventually leading to bone loss and iii) the standard of care for DMD which is glucocorticoids, known to further foment bone loss, causing glucocorticoid-induced osteoporosis (GIOP)^{118,119,121,123,125,126}. Glucocorticoids also delay the onset of puberty, interfering with normal sex development, which reduces testosterone, further reducing bone mass¹²³. Another crucial aspect to consider in DMD bone health is the treatment state-of-the-art. In general, the main treatment strategies available for osteoporosis are aimed at blocking osteoclastic bone resorption (anti-resorptive therapy) or increasing bone deposition (anabolic therapy). The former class of drugs are mainly Bisphosphonates and Denosumab (anti-RANKL monoclonal antibody), which kill or

prevent differentiation of osteoclasts. The latter is further divided in parathyroid hormone (PTH)-mimics, including Teriparatide and Abaloparatide, and Wnt pathway signaling activators, including Romosozumab (anti-Sclerostin monoclonal antibody) and BHQ880/LY2812176 (anti DKK1 antibodies, still in early pre-clinical stage)^{127,128}. However, most of them come with side effects in pediatric children: antiresorptive drugs “freeze” the bone, preventing normal bone modeling and remodeling and may cause atypical fractures, bone pain, and osteonecrosis of the jaw, along with dental eruption delay^{127,129–132}. On the other hand, anabolic PTH-mimics have been “black boxed” due to risk of osteosarcoma in pediatric patients¹³³. Romosozumab and anti-DKK1 agents may be a good therapeutic option in DMD patients, but safety and effectiveness of either have not been established in children, and more animal and human studies are needed to assess the effectiveness of either therapies. These considerations suggest that more research is needed to find therapeutic targets that could improve bone health in DMD patients without adding more side effects. An interesting target candidate, Lipocalin-2 (LCN2) will be presented in the following paragraph.

1.4 LIPOCALIN-2

Lipocalin-2 (LCN2) is a small (22-25kDa depending on species) glycoprotein that was first discovered and purified in 1993 by Kjeldsen and colleagues¹³⁴. LCN2 is also classified as an adipokine because it is produced and secreted by adipocytes¹³⁵, and is also able to bind iron and small hydrophobic molecules¹³⁶. LCN2 is expressed in many tissues, and partakes in several different physiopathologic phenomena, including thermogenesis, bone metabolism, kidney physiology and diabetes. It belongs to the lipocalin superfamily, which includes at least 20 members sharing a characteristic beta barrel secondary structure such as adipocyte fatty acid binding protein, apolipoprotein D, and retinol-binding protein 4¹³⁶. LCN2 is also involved in inflammation, being regulated by IL1 β ¹³⁷, TNF α ¹³⁸, IL17¹³⁹ and Nf κ B¹⁴⁰, and being able to induce IL6 and RANKL in osteoblasts¹⁴¹, as well as CCL2 and immune infiltration in retina¹⁴². It is also known to bind MMP-9, increasing its stability and thus its activity over time, which is important for neutrophil extravasation and cancer invasion and metastasis¹⁴³. This protein is surrounded by a certain degree of controversy, and probably the mechanisms regulating its expression are complex and still poorly understood. As an example, in kidney it is now widely considered a biomarker for kidney injury^{144–146}, but while many reports state that it is protective for kidney injury^{146–149}, other reports state that this factor is irrelevant^{150,151} or even correlates with negative indicators of kidney health¹⁵². Another representative example is thermogenesis: while some investigators show that Lcn2-

KO mice have impaired thermogenesis¹⁵³, others show the exact opposite¹⁵⁴. A large body of literature is present on LCN2 and its links with energy metabolism, so it's unsurprising to find that some controversy is present in that field too^{148,154-159}.

LCN2 responds to lack of mechanical stimulation in both bone and muscle, being upregulated under mechanical unloading in mouse models as well as in humans^{141,160,161}. As mentioned, its overexpression stimulates the production of IL6 and RANKL, which in turn promote osteoclastogenesis, all while reducing osteoblast differentiation, thus targeting both of the main remodeling cells negatively¹⁴¹. It is also intriguing to notice that *MDX* mice, which are a mouse model for DMD, have increased LCN2 expression in their femurs¹⁴¹. This disease presents with both mechanical unloading and inflammation, both closely related to LCN2, hence suggesting a further link among bone, muscle physiopathology and this protein.

2. AIM AND OUTLINE OF THE WORK

LCN2 has gained more and more attention in the last 10 years, and our group has pioneered the research related to its role in mechanical unloading in bone. The present PhD thesis is aimed at expanding our knowledge in this matter and understanding whether LCN2 may be a viable therapeutic target to prevent bone loss in specific musculoskeletal diseases, such as DMD.

In particular, in **Chapter 2**, we conduct a study aimed at evaluating whether animals lacking LCN2 have any bone and energy phenotype, with some insight on kidney as well. In **Chapter 3** we analyze the role this protein has in exercise biology in mice and humans, with specific regards to muscle. The role of LCN2 in muscle and bone physiopathology is further investigated in **Chapter 4**, where we explore the role of this protein in bone and muscle health of *MDX* mice, recapitulating DMD. In **Chapter 5**, we present some conclusions drawn from the present PhD thesis as well as critical literature reviewing, to discuss future directions and the possible impact of the work in modulating bone health in inflammatory muscle diseases. Further rationale for the investigations will be provided in the relevant chapters.

3. REFERENCES

1. Miller, E. J. & Martin, G. R. The Collagen of Bone. *Clin. Orthop. Relat. Res.* **59**, (1968).
2. Baron, R. Anatomy and Ultrastructure of Bone. in *Primer on the Metabolic Bone Diseases and Disorders of Mineral Metabolism*. (ed. Favus MJ) 1–12 (2003).
3. Nather, A. Ong, H.J.C. and Aziz, Z. Structure of Bone. in *Bone Grafts and Bone Substitutes* (World Scientific Publishing Co Pte Ltd, 2005).
4. S. Adamo, M. De Felici, A. Dolfi, A. Filippini, M. Grano, A. Musarò, C. Nervi, G. Papaccio, A. Salustri, E. Ziparo, N. Bernardini, C. Boitani, L. Bonsi, M. Bouchè, P. Brun, R. Canipari, R. Castriconi, P. Castrogiovanni, C. Ciccarelli, P. De Cesaris, M. De, D. V. *Istologia di Monesi*. (2018).
5. Cappariello, A., Ponzetti, M. & Rucci, N. The ‘soft’ side of the bone: Unveiling its endocrine functions. *Horm. Mol. Biol. Clin. Investig.* **28**, (2016).
6. No Title.
<https://www.orthopaedicsone.com/display/Clerkship/Describe+the+process+of+bone+remodeling>.
7. Karsenty, G. & Ferron, M. The contribution of bone to whole-organism physiology. *Nature* (2012) doi:10.1038/nature10763.
8. Di Girolamo, D. J., Clemens, T. L. & Kousteni, S. The skeleton as an endocrine organ. *Nature Reviews Rheumatology* (2012) doi:10.1038/nrrheum.2012.157.
9. Oury, F. *et al.* Osteocalcin regulates murine and human fertility through a pancreas-bone-testis axis. *J. Clin. Invest.* (2013) doi:10.1172/JCI65952.
10. Capulli, M., Paone, R. & Rucci, N. Osteoblast and osteocyte: games without frontiers. *Arch. Biochem. Biophys.* **561**, 3–12 (2014).
11. Lian, J. B., Stein, G. S. & Aubin, J. E. *Bone formation: maturation and functional activities of osteoblast lineage cells. Primer on the metabolic bone diseases and disorders of mineral metabolism* (2003).
12. Hill, P. A., Tumber, A. & Meikle, M. C. Multiple extracellular signals promote osteoblast survival and apoptosis. *Endocrinology* (1997) doi:10.1210/endo.138.9.5370.

13. Yao, Z., Xing, L., Qin, C., Schwarz, E. M. & Boyce, B. F. Osteoclast precursor interaction with bone matrix induces osteoclast formation directly by an interleukin-1-mediated autocrine mechanism. *J. Biol. Chem.* **283**, 9917–9924 (2008).
14. Scott Thies, R. *et al.* Recombinant human bone morphogenetic protein-2 induces osteoblastic differentiation in w-20-17 stromal cells. *Endocrinology* (1992) doi:10.1210/endo.130.3.1311236.
15. Ishikawa, H., Kitoh, H., Sugiura, F. & Ishiguro, N. The effect of recombinant human bone morphogenetic protein-2 on the osteogenic potential of rat mesenchymal stem cells after several passages. *Acta Orthop.* **78**, 285–292 (2007).
16. Moon, R. T., Bowerman, B., Boutros, M. & Perrimon, N. The promise and perils of Wnt signaling through β -catenin. *Science* (2002) doi:10.1126/science.1071549.
17. Ji, C., Chen, Y., Centrella, M. & McCarthy, T. L. Activation of the insulin-like growth factor-binding protein-5 promoter in osteoblasts by cooperative E box, CCAAT enhancer-binding protein, and nuclear factor-1 deoxyribonucleic acid-binding sequences. *Endocrinology* (1999) doi:10.1210/endo.140.10.7061.
18. Javed, A. *et al.* runt homology domain transcription factors (Runx, Cbfa, and AML) mediate repression of the bone sialoprotein promoter: evidence for promoter context-dependent activity of Cbfa proteins. *Mol. Cell. Biol.* **21**, 2891–2905 (2001).
19. Gutierrez, S. *et al.* CCAAT/enhancer-binding proteins (C/EBP) beta and delta activate osteocalcin gene transcription and synergize with Runx2 at the C/EBP element to regulate bone-specific expression. *J. Biol. Chem.* **277**, 1316–1323 (2002).
20. Nakashima, K. *et al.* The novel zinc finger-containing transcription factor osterix is required for osteoblast differentiation and bone formation. *Cell* **108**, 17–29 (2002).
21. Komori, T. *et al.* Targeted disruption of Cbfa1 results in a complete lack of bone formation owing to maturational arrest of osteoblasts. *Cell* **89**, 755–764 (1997).
22. Shui, C., Spelsberg, T. C., Riggs, B. L. & Khosla, S. Changes in Runx2/Cbfa1 expression and activity during osteoblastic differentiation of human bone marrow stromal cells. *J. Bone Miner. Res.* **18**, 213–221 (2003).
23. Clarke, B. Normal bone anatomy and physiology. *Clinical journal of the American Society of Nephrology : CJASN* (2008) doi:10.2215/CJN.04151206.

24. Kirsch, T., Harrison, G., Golub, E. E. & Nah, H. D. The roles of annexins and types II and X collagen in matrix vesicle-mediated mineralization of growth plate cartilage. *J. Biol. Chem.* **275**, 35577–35583 (2000).
25. Clarke Anderson, H. *The role of matrix vesicles in physiological and pathological calcification. Current Opinion in Orthopaedics* vol. 18 (2007).
26. Suda, T. *et al.* Modulation of osteoclast differentiation and function by the new members of the tumor necrosis factor receptor and ligand families. *Endocr. Rev.* **20**, 345–357 (1999).
27. Cappariello, A., Maurizi, A., Veeriah, V. & Teti, A. The Great Beauty of the osteoclast. *Arch. Biochem. Biophys.* **558**, 70–78 (2014).
28. Ponzetti, M. & Rucci, N. Updates on osteoimmunology: What’s new on the cross-talk between bone and immune system. *Front. Endocrinol. (Lausanne)*. **10**, (2019).
29. Lee, S. H. & Choi, Y. Communication between the skeletal and immune systems. *Osteoporos. Sarcopenia* **1**, 81–91 (2015).
30. Calvi, L. M. *et al.* Osteoblastic cells regulate the haematopoietic stem cell niche. *Nature* (2003) doi:10.1038/nature02040.
31. Zhang, J. *et al.* Identification of the haematopoietic stem cell niche and control of the niche size. *Nature* (2003) doi:10.1038/nature02041.
32. Zhu, J. *et al.* Osteoblasts support B-lymphocyte commitment and differentiation from hematopoietic stem cells. *Blood* (2007) doi:10.1182/blood-2006-08-041384.
33. Egawa, T. *et al.* The earliest stages of B cell development require a chemokine stromal cell-derived factor/pre-B cell growth-stimulating factor. *Immunity* (2001) doi:10.1016/S1074-7613(01)00185-6.
34. Miller, J. P. *et al.* The earliest step in B lineage differentiation from common lymphoid progenitors is critically dependent upon interleukin 7. *J. Exp. Med.* (2002) doi:10.1084/jem.20020784.
35. Zhu, J. & Emerson, S. G. A new bone to pick: Osteoblasts and the haematopoietic stem-cell niche. *BioEssays* (2004) doi:10.1002/bies.20052.
36. Lee, N. K. *et al.* Endocrine Regulation of Energy Metabolism by the Skeleton. *Cell* (2007) doi:10.1016/j.cell.2007.05.047.

37. Bonewald, L. F. Osteocytes. in *Primer on the Metabolic Bone Diseases and Disorders of Mineral Metabolism* (ed. Rosen, C. J.) 22–27 (2008).
38. Noble, B. S. The osteocyte lineage. *Archives of Biochemistry and Biophysics* (2008) doi:10.1016/j.abb.2008.04.009.
39. Teti, A. & Zallone, A. Do osteocytes contribute to bone mineral homeostasis? Osteocytic osteolysis revisited. *Bone* (2009) doi:10.1016/j.bone.2008.09.017.
40. Bélanger, L. F. Osteocytic osteolysis. *Calcified Tissue Research* (1969) doi:10.1007/BF02279101.
41. Qing, H. & Bonewald, L. F. Osteocyte remodeling of the perilacunar and pericanalicular matrix. *International journal of oral science* (2009) doi:10.4248/ijos.09019.
42. Cullinane, D. M. The role of osteocytes in bone regulation: Mineral homeostasis versus mechanoreception. *J. Musculoskelet. Neuronal Interact.* (2002).
43. Blaber, E. A. *et al.* Microgravity Induces Pelvic Bone Loss through Osteoclastic Activity, Osteocytic Osteolysis, and Osteoblastic Cell Cycle Inhibition by CDKN1a/p21. *PLoS One* (2013) doi:10.1371/journal.pone.0061372.
44. Bonewald, L. F. & Wacker, M. J. FGF23 production by osteocytes. *Pediatr. Nephrol.* **28**, 563–568 (2013).
45. Väänänen, H. K. & Laitala-Leinonen, T. Osteoclast lineage and function. *Archives of Biochemistry and Biophysics* (2008) doi:10.1016/j.abb.2008.03.037.
46. Marchisio, P. C. *et al.* Cell-substratum interaction of cultured avian osteoclasts is mediated by specific adhesion structures. *J. Cell Biol.* **99**, 1696–1705 (1984).
47. Schachtner, H., Calaminus, S. D. J., Thomas, S. G. & Machesky, L. M. Podosomes in adhesion, migration, mechanosensing and matrix remodeling. *Cytoskeleton* vol. 70 572–589 (2013).
48. Schlesinger, P. H., Blair, H. C., Teitelbaum, S. L. & Edwards, J. C. Characterization of the osteoclast ruffled border chloride channel and its role in bone resorption. *J. Biol. Chem.* **272**, 18636–18643 (1997).
49. Baron, R. Polarity and membrane transport in osteoclasts. *Connect. Tissue Res.* **20**, 109–120 (1989).

50. Hirvonen, M. J., Fagerlund, K., Lakkakorpi, P., Väänänen, H. K. & Mulari, M. T. K. Novel perspectives on the transcytotic route in osteoclasts. *Bonekey Rep.* **2**, (2013).
51. Burgess, T. L. *et al.* The ligand for osteoprotegerin (OPGL) directly activates mature osteoclasts. *J. Cell Biol.* (1999) doi:10.1083/jcb.145.3.527.
52. Lacey, D. L. *et al.* Osteoprotegerin ligand is a cytokine that regulates osteoclast differentiation and activation. *Cell* (1998) doi:10.1016/S0092-8674(00)81569-X.
53. Xu, F. & Teitelbaum, S. L. Osteoclasts: New Insights. *Bone Res.* **1**, 11–26 (2013).
54. Noh, J. W. *et al.* Safety of TNF- α antagonists in the treatment of rheumatoid arthritis and ankylosing spondylitis: 5-year single-center experience. *Int. J. Rheum. Dis.* (2010).
55. Stadhouders, R., Lubberts, E. & Hendriks, R. W. A cellular and molecular view of T helper 17 cell plasticity in autoimmunity. *Journal of Autoimmunity* (2018) doi:10.1016/j.jaut.2017.12.007.
56. Sato, K. & Takayanagi, H. Osteoclasts, rheumatoid arthritis, and osteoimmunology. *Current Opinion in Rheumatology* (2006) doi:10.1097/01.bor.0000231912.24740.a5.
57. Kawai, T. *et al.* B and T lymphocytes are the primary sources of RANKL in the bone resorptive lesion of periodontal disease. *Am. J. Pathol.* (2006) doi:10.2353/ajpath.2006.060180.
58. Hienz, S. A., Paliwal, S. & Ivanovski, S. Mechanisms of bone resorption in periodontitis. *J. Immunol. Res.* (2015) doi:10.1155/2015/615486.
59. Jarry, C. R. *et al.* Secreted osteoclastogenic factor of activated T cells (SOFAT), a novel osteoclast activator, in chronic periodontitis. *Hum. Immunol.* (2013) doi:10.1016/j.humimm.2013.04.013.
60. Hashizume, M., Hayakawa, N. & Mihara, M. IL-6 trans-signalling directly induces RANKL on fibroblast-like synovial cells and is involved in RANKL induction by TNF- α and IL-17. *Rheumatology* (2008) doi:10.1093/rheumatology/ken363.
61. Fujiwara, Y. *et al.* RANKL (Receptor Activator of NF κ B Ligand) produced by osteocytes is required for the increase in B cells and bone loss caused by estrogen deficiency in mice. *J. Biol. Chem.* (2016) doi:10.1074/jbc.M116.742452.

62. Magdalena Coetzee, M. C. K. Osteoprotegerin-Receptor Activator of Nuclear Factor-[kappa]B: Mechanism of Action between Osteoblasts and Osteoclasts. *South. Med. J.* (2004).
63. Li, P. *et al.* Systemic Tumor Necrosis Factor α Mediates an Increase in Peripheral CD11bhigh Osteoclast Precursors in Tumor Necrosis Factor α -Transgenic Mice. *Arthritis Rheum.* (2004) doi:10.1002/art.11419.
64. Yao, Z. *et al.* Tumor necrosis factor- α increases circulating osteoclast precursor numbers by promoting their proliferation and differentiation in the bone marrow through up-regulation of c-Fms expression. *J. Biol. Chem.* (2006) doi:10.1074/jbc.M512624200.
65. Amarasekara, D. S. *et al.* Regulation of osteoclast differentiation by cytokine networks. *Immune Network* (2018) doi:10.4110/in.2018.18.e8.
66. Girasole, G., Passeri, G., Jilka, R. L. & Manolagas, S. C. Interleukin-11: A new cytokine critical for osteoclast development. *J. Clin. Invest.* (1994) doi:10.1172/JCI117130.
67. Mori, G., D'Amelio, P., Faccio, R. & Brunetti, G. The interplay between the bone and the immune system. *Clinical and Developmental Immunology* (2013) doi:10.1155/2013/720504.
68. Raisz, L. G. Physiology and pathophysiology of bone remodeling. in *Clinical Chemistry* (1999).
69. Kudo, O. *et al.* Interleukin-6 and interleukin-11 support human osteoclast formation by a RANKL-independent mechanism. *Bone* (2003) doi:10.1016/S8756-3282(02)00915-8.
70. De Benedetti, F. *et al.* Impaired skeletal development in interleukin-6-transgenic mice: A model for the impact of chronic inflammation on the growing skeletal system. *Arthritis Rheum.* (2006) doi:10.1002/art.22175.
71. Kaneshiro, S. *et al.* IL-6 negatively regulates osteoblast differentiation through the SHP2/MEK2 and SHP2/Akt2 pathways in vitro. *J. Bone Miner. Metab.* (2014) doi:10.1007/s00774-013-0514-1.
72. Yoshitake, F., Itoh, S., Narita, H., Ishihara, K. & Ebisu, S. Interleukin-6 directly

- inhibits osteoclast differentiation by suppressing receptor activator of NF- κ B signaling pathways. *J. Biol. Chem.* (2008) doi:10.1074/jbc.M607999200.
73. Schroder, K., Hertzog, P. J., Ravasi, T. & Hume, D. A. Interferon- γ : an overview of signals, mechanisms and functions. *J. Leukoc. Biol.* (2004) doi:10.1189/jlb.0603252.
74. Tang, M., Tian, L., Luo, G. & Yu, X. Interferon-gamma-mediated osteoimmunology. *Frontiers in Immunology* (2018) doi:10.3389/fimmu.2018.01508.
75. Moon, Y. M. *et al.* IL-32 and IL-17 interact and have the potential to aggravate osteoclastogenesis in rheumatoid arthritis. *Arthritis Res. Ther.* (2012) doi:10.1186/ar4089.
76. Takeda, H. *et al.* Effect of IL-15 and natural killer cells on osteoclasts and osteoblasts in a mouse coculture. *Inflammation* (2014) doi:10.1007/s10753-013-9782-0.
77. Krebsbach, P. H., Kuznetsov, S. A., Bianco, P. & Gehron Robey, P. Bone marrow stromal cells: Characterization and clinical application. *Crit. Rev. Oral Biol. Med.* (1999) doi:10.1177/10454411990100020401.
78. Castro-Malaspina, H. *et al.* Characterization of human bone marrow fibroblast colony-forming cells (CFU-F) and their progeny. *Blood* (1980) doi:10.1182/blood.v56.2.289.bloodjournal562289.
79. Westen, H. & Bainton, D. F. Association of alkaline-phosphatase-positive reticulum cells in bone marrow with granulocytic precursors. *J. Exp. Med.* (1979) doi:10.1084/jem.150.4.919.
80. Giannoni, P. *et al.* Regeneration of large bone defects in sheep using bone marrow stromal cells. *J. Tissue Eng. Regen. Med.* (2008) doi:10.1002/term.90.
81. Kraus, K. H. & Kirker-Head, C. Mesenchymal stem cells and bone regeneration. *Veterinary Surgery* (2006) doi:10.1111/j.1532-950X.2006.00142.x.
82. Schneider, S., Unger, M., Van Griensven, M. & Balmayor, E. R. Adipose-derived mesenchymal stem cells from liposuction and resected fat are feasible sources for regenerative medicine. *Eur. J. Med. Res.* (2017) doi:10.1186/s40001-017-0258-9.
83. Antoniadou, E. & David, A. L. Placental stem cells. *Best Pract. Res. Clin. Obstet. Gynaecol.* (2016) doi:10.1016/j.bpobgyn.2015.08.014.

84. Pavathuparambil Abdul Manaph, N., Al-Hawaas, M., Bobrovskaya, L., Coates, P. T. & Zhou, X. F. Urine-derived cells for human cell therapy. *Stem Cell Research and Therapy* (2018) doi:10.1186/s13287-018-0932-z.
85. Vizoso, F. J. *et al.* Mesenchymal stem cells in homeostasis and systemic diseases: Hypothesis, evidences, and therapeutic opportunities. *International Journal of Molecular Sciences* (2019) doi:10.3390/ijms20153738.
86. Ling, X. *et al.* Exosomes from human urine-derived stem cells enhanced neurogenesis via miR-26a/HDAC6 axis after ischaemic stroke. *J. Cell. Mol. Med.* (2020) doi:10.1111/jcmm.14774.
87. Bianco, P. & Robey, P. G. Skeletal stem cells. *Dev.* (2015) doi:10.1242/dev.102210.
88. Liu, J. Q., Li, Q. W. & Tan, Z. New insights on properties and spatial distributions of skeletal stem cells. *Stem Cells International* (2019) doi:10.1155/2019/9026729.
89. Frontera, W. R. & Ochala, J. Skeletal Muscle: A Brief Review of Structure and Function. *Behav. Genet.* **45**, 183–195 (2015).
90. Fortin, M., Videman, T., Gibbons, L. E. & Battié, M. C. Paraspinal muscle morphology and composition: A 15-yr longitudinal magnetic resonance imaging study. *Med. Sci. Sports Exerc.* (2014) doi:10.1249/MSS.000000000000179.
91. Javan, R. *et al.* Generating color-coded anatomic muscle maps for correlation of quantitative magnetic resonance imaging analysis with clinical examination in neuromuscular disorders. *Muscle and Nerve* (2013) doi:10.1002/mus.23780.
92. S. Hikida, R. Aging Changes in Satellite Cells and Their Functions. *Curr. Aging Sci.* (2012) doi:10.2174/1874609811104030279.
93. MacAluso, F. & Myburgh, K. H. Current evidence that exercise can increase the number of adult stem cells. *J. Muscle Res. Cell Motil.* (2012) doi:10.1007/s10974-012-9302-0.
94. Bareja, A. *et al.* Human and mouse skeletal muscle stem cells: Convergent and divergent mechanisms of myogenesis. *PLoS One* (2014) doi:10.1371/journal.pone.0090398.
95. Thomas, G. D. Functional muscle ischemia in Duchenne and Becker muscular dystrophy. *Frontiers in Physiology* (2013) doi:10.3389/fphys.2013.00381.

96. Hoppeler, H., Lüthi, P., Claassen, H., Weibel, E. R. & Howald, H. The ultrastructure of the normal human skeletal muscle - A morphometric analysis on untrained men, women and well-trained orienteers. *Pflügers Arch. Eur. J. Physiol.* (1973) doi:10.1007/BF00588462.
97. Ottenheijm, C. A. C. & Granzier, H. Lifting the nebula: Novel insights into skeletal muscle contractility. *Physiology* (2010) doi:10.1152/physiol.00016.2010.
98. Schiaffino, S. & Reggiani, C. Fiber types in Mammalian skeletal muscles. *Physiol. Rev.* (2011) doi:10.1152/physrev.00031.2010.
99. Galpin, A. J. *et al.* Human skeletal muscle fiber type specific protein content. *Anal. Biochem.* (2012) doi:10.1016/j.ab.2012.03.018.
100. Larsson, L. & Moss, R. L. Maximum velocity of shortening in relation to myosin isoform composition in single fibres from human skeletal muscles. *J. Physiol.* (1993) doi:10.1113/jphysiol.1993.sp019964.
101. Andersen, J. L. Muscle fibre type adaptation in the elderly human muscle. in *Scandinavian Journal of Medicine and Science in Sports* (2003). doi:10.1034/j.1600-0838.2003.00299.x.
102. Greising, S. M., Gransee, H. M., Mantilla, C. B. & Sieck, G. C. Systems biology of skeletal muscle: Fiber type as an organizing principle. *Wiley Interdisciplinary Reviews: Systems Biology and Medicine* (2012) doi:10.1002/wsbm.1184.
103. Hoffman, E. P., Brown, R. H. & Kunkel, L. M. Dystrophin: The protein product of the duchenne muscular dystrophy locus. *Cell* (1987) doi:10.1016/0092-8674(87)90579-4.
104. Moser, H. Duchenne muscular dystrophy: Pathogenetic aspects and genetic prevention. *Human Genetics* (1984) doi:10.1007/BF00275183.
105. Magri, F. *et al.* Genotype and phenotype characterization in a large dystrophinopathic cohort with extended follow-up. *J. Neurol.* (2011) doi:10.1007/s00415-011-5979-z.
106. Lee, S. H., Lee, J. H., Lee, K. A. & Choi, Y. C. Clinical and genetic characterization of female dystrophinopathy. *J. Clin. Neurol.* (2015) doi:10.3988/jcn.2015.11.3.248.
107. López-Hernández, L. B. *et al.* Comparison of mutation profiles in the duchenne

- muscular dystrophy gene among populations: Implications for potential molecular therapies. *Int. J. Mol. Sci.* (2015) doi:10.3390/ijms16035334.
108. Hoffman, E. P. & Kunkel, L. M. Dystrophin abnormalities in Duchenne/Becker muscular dystrophy. *Neuron* (1989) doi:10.1016/0896-6273(89)90226-2.
 109. Koenig, M. *et al.* The molecular basis for duchenne versus becker muscular dystrophy: Correlation of severity with type of deletion. (1989) doi:10.1016/1.
 110. Ervasti, J. M. & Campbell, K. P. Membrane organization of the dystrophin-glycoprotein complex. *Cell* (1991) doi:10.1016/0092-8674(91)90035-W.
 111. Blake, D. J., Weir, A., Newey, S. E. & Davies, K. E. Function and genetics of dystrophin and dystrophin-related proteins in muscle. *Physiological Reviews* (2002) doi:10.1152/physrev.00028.2001.
 112. Petrof, B. J., Shrager, J. B., Stedman, H. H., Kelly, A. M. & Sweeney, H. L. Dystrophin protects the sarcolemma from stresses developed during muscle contraction. *Proc. Natl. Acad. Sci. U. S. A.* (1993) doi:10.1073/pnas.90.8.3710.
 113. De Paepe, B. & De Bleecker, J. L. Cytokines and chemokines as regulators of skeletal muscle inflammation: Presenting the case of Duchenne muscular dystrophy. *Mediators Inflamm.* (2013) doi:10.1155/2013/540370.
 114. Del Rocío Cruz-Guzmán, O., Rodríguez-Cruz, M. & Cedillo, R. E. E. Systemic inflammation in duchenne muscular dystrophy: Association with muscle function and nutritional status. *J. Nutr. Sci.* (2017) doi:10.1155/2015/891972.
 115. Evans, N. P., Misyak, S. A., Robertson, J. L., Bassaganya-Riera, J. & Grange, R. W. Immune-Mediated Mechanisms Potentially Regulate the Disease Time-Course of Duchenne Muscular Dystrophy and Provide Targets for Therapeutic Intervention. *PM and R* (2009) doi:10.1016/j.pmrj.2009.04.010.
 116. Jansen, M., van Alfen, N., Geurts, A. C. H. & de Groot, I. J. M. Assisted Bicycle Training Delays Functional Deterioration in Boys With Duchenne Muscular Dystrophy. *Neurorehabil. Neural Repair* (2013) doi:10.1177/1545968313496326.
 117. Jansen, M., de Groot, I. J. M., van Alfen, N. & Geurts, A. C. H. Physical training in boys with Duchenne Muscular Dystrophy: The protocol of the No Use is Disuse study. *BMC Pediatr.* (2010) doi:10.1186/1471-2431-10-55.

118. Birnkrant, D. J. *et al.* Diagnosis and management of Duchenne muscular dystrophy, part 2: respiratory, cardiac, bone health, and orthopaedic management. *The Lancet Neurology* (2018) doi:10.1016/S1474-4422(18)30025-5.
119. Birnkrant, D. J. *et al.* Diagnosis and management of Duchenne muscular dystrophy, part 1: diagnosis, and neuromuscular, rehabilitation, endocrine, and gastrointestinal and nutritional management. *The Lancet Neurology* (2018) doi:10.1016/S1474-4422(18)30024-3.
120. Mercuri, E. & Muntoni, F. Muscular dystrophies. *The Lancet* (2013) doi:10.1016/S0140-6736(12)61897-2.
121. Rufo, A. *et al.* Mechanisms inducing low bone density in duchenne muscular dystrophy in mice and humans. *J. Bone Miner. Res.* (2011) doi:10.1002/jbmr.410.
122. Bianchi, M. L. *et al.* Bone mineral density and bone metabolism in Duchenne muscular dystrophy. *Osteoporos. Int.* (2003) doi:10.1007/s00198-003-1443-y.
123. Buckner, J. L., Bowden, S. A. & Mahan, J. D. Optimizing bone health in duchenne muscular dystrophy. *International Journal of Endocrinology* (2015) doi:10.1155/2015/928385.
124. Douglas, A. G. L. & Wood, M. J. A. Splicing therapy for neuromuscular disease. *Mol. Cell. Neurosci.* (2013) doi:10.1016/j.mcn.2013.04.005.
125. Compston, J. *et al.* UK clinical guideline for the prevention and treatment of osteoporosis. *Arch. Osteoporos.* (2017) doi:10.1007/s11657-017-0324-5.
126. Canalis, E., Mazziotti, G., Giustina, A. & Bilezikian, J. P. Glucocorticoid-induced osteoporosis: Pathophysiology and therapy. *Osteoporosis International* (2007) doi:10.1007/s00198-007-0394-0.
127. Tu, K. N. *et al.* Osteoporosis: A review of treatment options. *P and T* (2018).
128. No Title. <https://clinicaltrials.gov/ct2/show/NCT01293487>.
129. Boyce, A. M., Tosi, L. L. & Paul, S. M. Bisphosphonate Treatment for Children With Disabling Conditions. *PM and R* (2014) doi:10.1016/j.pmrj.2013.10.009.
130. Diab, D. L. & Watts, N. B. Bisphosphonates in the Treatment of Osteoporosis. *Endocrinology and Metabolism Clinics of North America* (2012) doi:10.1016/j.ecl.2012.04.007.

131. Alwahhabi, B. K. S. & Alsuwaine, B. A. Long-Term use of bisphosphonates in osteoporosis. *Saudi Med. J.* (2017) doi:10.15537/smj.2017.6.19793.
132. Bhatt, R., Hibbert, S. A. & Munns, C. F. The use of bisphosphonates in children: Review of the literature and guidelines for dental management. *Australian Dental Journal* (2014) doi:10.1111/adj.12140.
133. Deal, C. The use of intermittent human parathyroid hormone as a treatment for osteoporosis. *Current rheumatology reports* (2004) doi:10.1007/s11926-004-0083-3.
134. Kjeldsen, L., Johnsen, A. H., Sengelov, H. & Borregaard, N. Isolation and primary structure of NGAL, a novel protein associated with human neutrophil gelatinase. *J. Biol. Chem.* (1993).
135. Zhang, Y. *et al.* Lipocalin 2 expression and secretion is highly regulated by metabolic stress, cytokines, and nutrients in adipocytes. *PLoS One* **9**, 1–9 (2014).
136. Lögberg, L. & Wester, L. Immunocalins: A lipocalin subfamily that modulates immune and inflammatory responses. *Biochim. Biophys. Acta - Protein Struct. Mol. Enzymol.* **1482**, 284–297 (2000).
137. Bonnemaïson, M. L., Marks, E. S. & Boesen, E. I. Interleukin-1 β as a driver of renal NGAL production. *Cytokine* (2017) doi:10.1016/j.cyto.2016.12.004.
138. Naudé, P. J. W. *et al.* Lipocalin 2: Novel component of proinflammatory signaling in Alzheimer's disease. *FASEB J.* (2012) doi:10.1096/fj.11-202457.
139. Ferreira, M. C. *et al.* Interleukin-17-induced protein lipocalin 2 is dispensable for immunity to oral candidiasis. *Infect. Immun.* (2014) doi:10.1128/IAI.01389-13.
140. Zhao, P. & Stephens, J. M. STAT1, NF- κ B and ERKs play a role in the induction of lipocalin-2 expression in adipocytes. *Mol. Metab.* (2013) doi:10.1016/j.molmet.2013.04.003.
141. Rucci, N. *et al.* Lipocalin 2: A new mechanoresponding gene regulating bone homeostasis. *J. Bone Miner. Res.* (2015) doi:10.1002/jbmr.2341.
142. Valapala, M. *et al.* Increased Lipocalin-2 in the retinal pigment epithelium of Cryba1 cKO mice is associated with a chronic inflammatory response. *Aging Cell* (2014) doi:10.1111/acel.12274.

143. Yan, L., Borregaard, N., Kjeldsen, L. & Moses, M. A. The high molecular weight urinary matrix metalloproteinase (MMP) activity is a complex of gelatinase B/MMP-9 and neutrophil gelatinase-associated lipocalin (NGAL): Modulation of MMP-9 activity by NGAL. *J. Biol. Chem.* (2001) doi:10.1074/jbc.M106089200.
144. Mishra, J. *et al.* Neutrophil gelatinase-associated lipocalin (NGAL) as a biomarker for acute renal injury after cardiac surgery. *Lancet* (2005) doi:10.1016/S0140-6736(05)74811-X.
145. Mishra, J. *et al.* Kidney NGAL is a novel early marker of acute injury following transplantation. *Pediatr. Nephrol.* (2006) doi:10.1007/s00467-006-0055-0.
146. Mishra, J. *et al.* Amelioration of ischemic acute renal injury by neutrophil gelatinase-associated lipocalin. *J. Am. Soc. Nephrol.* (2004) doi:10.1097/01.ASN.0000145013.44578.45.
147. Mori, K. *et al.* Endocytic delivery of lipocalin-siderophore-iron complex rescues the kidney from ischemia-reperfusion injury. *J. Clin. Invest.* (2005) doi:10.1172/JCI23056.
148. Lim, W. H. *et al.* Circulating Lipocalin 2 Levels Predict Fracture-Related Hospitalizations in Elderly Women: A Prospective Cohort Study. *J. Bone Miner. Res.* (2015) doi:10.1002/jbmr.2546.
149. Wang, E. *et al.* Overexpression of exogenous kidney-specific Ngal attenuates progressive cyst development and prolongs lifespan in a murine model of polycystic kidney disease. *Kidney Int.* (2017) doi:10.1016/j.kint.2016.09.005.
150. Berger, T. *et al.* Lipocalin 2-deficient mice exhibit increased sensitivity to *Escherichia coli* infection but not to ischemia-reperfusion injury. *Proc. Natl. Acad. Sci. U. S. A.* (2006) doi:10.1073/pnas.0510847103.
151. Mosialou, I. *et al.* MC4R-dependent suppression of appetite by bone-derived lipocalin 2. *Nature* (2017) doi:10.1038/nature21697.
152. Wu, J. *et al.* Urinary RBP and NGAL Levels are Associated with Nephropathy in Patients with Type 2 Diabetes. *Cell. Physiol. Biochem.* (2017) doi:10.1159/000477860.
153. Guo, H. *et al.* Lipocalin-2 deficiency impairs thermogenesis and potentiates diet-

- induced insulin resistance in mice. *Diabetes* **59**, 1376–1385 (2010).
154. Ishii, A. *et al.* Obesity-promoting and anti-thermogenic effects of neutrophil gelatinase-associated lipocalin in mice. *Sci. Rep.* (2017) doi:10.1038/s41598-017-15825-4.
 155. Wang, Y. *et al.* Lipocalin-2 is an inflammatory marker closely associated with obesity, insulin resistance, and hyperglycemia in humans. *Clin. Chem.* (2007) doi:10.1373/clinchem.2006.075614.
 156. De La Chesnaye, E. *et al.* Lipocalin-2 plasmatic levels are reduced in patients with long-term type 2 diabetes mellitus. *Int. J. Clin. Exp. Med.* (2015).
 157. Yan, Q. W. *et al.* The adipokine lipocalin 2 is regulated by obesity and promotes insulin resistance. *Diabetes* (2007) doi:10.2337/db07-0007.
 158. Jun, L. S., Parker Siddall, C. & Rosen, E. D. A minor role for lipocalin 2 in high-fat diet-induced glucose intolerance. *Am. J. Physiol. - Endocrinol. Metab.* (2011) doi:10.1152/ajpendo.00147.2011.
 159. Akelma, A. Z. *et al.* The association of serum lipocalin-2 levels with metabolic and clinical parameters in obese children: A pilot study. *J. Pediatr. Endocrinol. Metab.* (2012) doi:10.1515/jpem-2011-0477.
 160. Capulli, M., Rufo, A., Teti, A. & Rucci, N. Global transcriptome analysis in mouse calvarial osteoblasts highlights sets of genes regulated by modeled microgravity and identifies A ‘mechanoresponsive osteoblast gene signature’. *J. Cell. Biochem.* (2009) doi:10.1002/jcb.22120.
 161. Gambará, G. *et al.* Microgravity-induced transcriptome adaptation in mouse paraspinal longissimus dorsi muscle highlights insulin resistance-linked genes. *Front. Physiol.* (2017) doi:10.3389/fphys.2017.00279.



Chapter 2

“A Complex Role for Lipocalin 2 in Bone Metabolism: Global Ablation in Mice Induces Osteopenia Caused by an Altered Energy Metabolism.”

Published in JBMR, 2018 (doi: 10.1002/jbmr.3406).

M. Capulli, **M. Ponzetti**, A. Maurizi, A. S. Gemini-Piperni, T. Berger, T.W. Mak, A. Teti, N. Rucci.

1. ABSTRACT

Lipocalin 2 (Lcn2) is an adipokine that carries out a variety of functions in diverse organs. We investigated the bone phenotype and the energy metabolism of Lcn2 globally deleted mice (*Lcn2*^{-/-}) at different ages. *Lcn2*^{-/-} mice were largely osteopenic, exhibiting lower trabecular bone volume, lesser trabecular number and higher trabecular separation when compared to wild type (WT) mice. *Lcn2*^{-/-} mice showed a lower osteoblast number and surface over bone surface, and subsequently a significantly lower bone formation rate, while osteoclast variables were unremarkable. Surprisingly, we found no difference in Alkaline Phosphatase (ALP) activity or in nodule mineralization in *Lcn2*^{-/-} calvaria osteoblast cultures, while less ALP-positive colonies were obtained from freshly isolated *Lcn2*^{-/-} bone marrow stromal cells, suggesting a non-autonomous osteoblast response to Lcn2 ablation. Given that *Lcn2*^{-/-} mice showed higher body weight and hyperphagia, we investigated whether their osteoblast impairment could be due to altered energy metabolism. *Lcn2*^{-/-} mice showed lower fasted glycemia and hyperinsulinemia. Consistently, glucose tolerance was significantly higher in *Lcn2*^{-/-} compared to WT mice, while insulin tolerance was similar. *Lcn2*^{-/-} mice also exhibited polyuria, glycosuria, proteinuria and renal cortex vacuolization, suggesting a kidney contribution to their phenotype. Interestingly, the expression of the glucose transporter protein type 1, that conveys glucose into the osteoblasts and is essential for osteogenesis, was significantly lower in the *Lcn2*^{-/-} bone, possibly explaining the in vivo osteoblast impairment induced by the global Lcn2 ablation. Taken together, these results unveil an important role of Lcn2 in bone metabolism, highlighting a link with glucose metabolism that is more complex than expected from the current knowledge.

2. INTRODUCTION

Lipocalin 2 (Lcn2), also known as neutrophil gelatinase-associated lipocalin (NGAL), is a widely expressed protein that has been found to exert many different functions. It belongs to the lipocalin superfamily, which includes at least 20 secreted proteins, such as adipocyte fatty acid binding protein, apolipoprotein D, and retinol-binding protein 4¹. Lcn2 is involved in inflammation, chronic renal failure, energy metabolism, and tumor development and progression². It is also known to bind matrix metalloproteinase 9 (MMP-9), increasing its stability and thus its activity over time, which is important for neutrophil extravasation and cancer invasion and metastasis. Lcn2 is also classified as an adipokine because it is produced and secreted by adipocytes³. Furthermore, a complex and not yet well understood role has recently been suggested for this molecule in the regulation of energy metabolism³⁻⁸. We previously demonstrated an involvement of Lcn2 in bone metabolism, pointing to this molecule as a mechanoresponding factor that is upregulated under mechanical unloading in mouse models and in humans^{9,10}. Moreover, Lcn2 overexpression reduces osteoblast differentiation and stimulates the production of interleukin (IL)-6 and Receptor Activator of Nuclear factor Kappa B Ligand (RANKL), which in turn promote osteoclastogenesis¹⁰. Based on these findings, here we aimed at characterizing the bone phenotype of Lcn2 knock out (*Lcn2*^{-/-}) mice, hypothesizing a high bone mass condition. Instead, to our surprise, we found that systemic ablation of Lcn2 induced a remarkable osteopenic phenotype, due to an impairment of osteoblast differentiation and activity, which conflicts with our previous observation that Lcn2 overexpression impairs osteogenesis¹⁰. We reconciled these results demonstrating that the effect of Lcn2 global ablation on bone is caused by an altered energy metabolism rather than by an intrinsic impairment of osteoblast activity. Our data are partially at variance with the observations of Mosialou et al.¹¹, who ruled out any effect of Lcn2 deficiency on the bone phenotype and demonstrated alterations in energy metabolism to some extent different from those observed in our study. We believe that, altogether, the results described so far by us and others suggest that the network of interactions mediated by Lcn2 is extremely complex, requiring further work to be fully elucidated.

3. MATERIALS AND METHODS

3.1 MATERIALS

Dulbecco's modified minimum essential medium (DMEM), Roswell Park Memorial Institute 1640 (RPMI) medium, α modified Minimum Essential Medium (α MEM), fetal bovine serum (FBS), penicillin, streptomycin, and trypsin were from GIBCO (Uxbridge,

UK). Sterile plastic ware was from Falcon Becton-Dickinson (Cowley, Oxford, UK) or Costar (Cambridge, MA, USA). TRIzol reagent, primers and reagents for RT-PCR were from Invitrogen (Carlsbad, CA, USA). The brilliant SYBR Green QPCR master mix was from Stratagene (La Jolla, CA, USA). The infinity hexokinase kit for glucose determination (cat# TR15421) and the osteocalcin (OCN; cat# NC0450271) ELISA kits were from ThermoFisher Scientific (Waltham, MA, USA). The rat/mouse insulin ELISA kit (cat# EZRMI-13K) and the carboxy-terminal cross-linking telopeptide of type 1 collagen (CTX) and mouse tartrate-resistant acid phosphatase (TRAcP) immunoenzymatic kits were from Immunodiagnostic Systems-Nordic Bioscience (Herlev, Denmark). Bone alkaline phosphatase (BALP; cat# MBS281206) ELISA kit was from MyBioSource (San Diego, CA, USA). All the other reagents, including the ALP kit #85 and the TRAcP kit #386, were of the purest grade from Sigma Aldrich Co. (St. Louis, MO, USA).

3.2 ANIMALS

Lcn2^{-/-} mice (background C57BL6/J) were generated and kindly provided by Dr. Tak Wah Mak (University Health Network, Toronto, ON, Canada)¹². They are vital, with an overall normal lifespan and fertility. Bone and energy metabolism phenotypes were evaluated at 1, 3, 6, and 12 months of age in wild-type (WT) and *Lcn2*^{-/-} male and female mice. All procedures involving animals and their care were conducted in conformity with national and international laws and policies (European Economic Community Council Directive 86/609, OJ L 358, 1, December 12, 1987; Italian Legislative Decree 4.03.2014, n.26, *Gazzetta Ufficiale della Repubblica Italiana* no. 61, March 4, 2014) and the Animal Research: Reporting of In Vivo Experiments (ARRIVE) guidelines. Mice were housed in the animal facility of the University of L'Aquila, Italy, at the following conditions: temperature: 20°C to 24°C, humidity: 60%–5%, dark/light cycle: 12/12 hours. They had access to food and water ad libitum and were fed with a standard diet (Mucedola code: 4RF21) composed of 60.8% carbohydrates, 21% proteins, 3.45% fat, 6.8% fibers, 7.95% trace elements, and 12% humidity.

3.3 MICRO-CT ANALYSIS

Images of femurs previously fixed in 4% formaldehyde were acquired using the SkyScan 1174 (Bruker, Billerica, MA, USA) with a resolution of 6.7 μm (X-ray voltage 50 kV). Image reconstruction was carried out employing a modified Feldkamp algorithm¹³, using the Skyscan Nrecon software. Three-dimensional (3D) and two-dimensional (2D) morphometric parameters were calculated for the trabecular bone, 150 slides (4 mm thick) from the growth

plate. Threshold values were applied for segmenting trabecular bone corresponding to bone mineral density values of 0.6 mg/cm³ calcium hydroxyapatite. 3D parameters were based on analysis of a Marching Cubes-type model with a rendered surface¹⁴. Calculation of all 2D areas and perimeters was based on the Pratt algorithm¹⁵. Bone structural variables and nomenclature were those suggested by Bouxsein and colleagues¹⁶.

3.4 BONE HISTOMORPHOMETRY

Tibias explanted from euthanized WT and *Lcn2*^{-/-} mice were fixed in 4% paraformaldehyde, dehydrated in acetone, and processed for methyl-methacrylate embedding without decalcification. Histomorphometric measurements were carried out on 5- μ m-thick sections with an interactive image analysis system (IAS 2000; Delta Sistemi, Rome, Italy)¹⁷ and with the suggested nomenclature¹⁸. Osteoclast number/bone surface (number/mm²) and osteoclast surface/bone surface (%) were evaluated after histochemically staining the sections for TRAcP activity. Osteoblast surface/bone surface (%) was evaluated in sections stained with toluidine blue, while dynamic assessment of the mineral apposition rate (MAR) was calculated after double injection of calcein, 10 and 3 days before euthanasia. Bone formation rate (BFR) was calculated according to the following formula: $MAR \times MS \div BA$ where MS = mineralized surface and BA = bone area, as suggested by Dempster and colleagues¹⁸.

3.5 GLUCOSE TOLERANCE TEST

Three-month-old and 12-month-old WT and *Lcn2*^{-/-} mice were subjected to the glucose tolerance test (GTT) following 16 hours (overnight) fasting. Briefly, fasted glucose was measured at time 0 using the Accu-Chek Aviva System (Roche Diagnostics, Mannheim, Germany) collecting blood directly from the tail, then 2 g/kg of body weight (b.w.) of D-glucose was administered by intraperitoneal (i.p.) injection. Blood glucose and insulin levels were measured 15, 30, 60, and 120 min after D-glucose injection.

3.6 INSULIN TOLERANCE TEST

Three-month-old and 12-month-old WT and *Lcn2*^{-/-} mice were subjected to the insulin tolerance test (ITT) after 4 hours of fasting. Briefly, glucose was measured at time 0 using the Accu-Chek Aviva System, then a bolus of 0.75 U/kg b.w. of recombinant human (rh)-insulin (Humulin[®], Eli Lilly and Company, Indianapolis, IN) was administered by i.p. injection. Blood glucose levels were then measured as above after 15, 30, 60, 90, and 120 min after rh-insulin injection.

3.7 GLUCOSE-STIMULATED INSULIN SECRETION BY PRIMARY PANCREATIC ISLETS

Primary pancreatic islets were isolated from 3-month-old male mice by intraductal injection of 3 mL of collagenase P solution, according to Li and colleagues¹⁹, then pancreatic islets were recovered and cultured in RPMI medium containing 11mM glucose and 10% FBS. Seven to 10 islets were transferred in 24-well plates and glucose-starved by incubation in Krebs Ringer bicarbonate HEPES buffer (114mM NaCl; 4.7mM KCl; 1.16mM MgSO₄; 1.2mM KH₂PO₄; 2.5mM CaCl₂; 5mM NaHCO₃; 20mM HEPES; 0.2% BSA) for 45 min at 37°C. Then, the islets were incubated at 37°C in Krebs Ringer bicarbonate HEPES buffer containing 5.5mM or 16mM glucose. After 1 hour, the medium was harvested and centrifuged at 250g for 5 min. The supernatants were used to quantify the secreted insulin by ELISA kit, while the pellets were lysed to isolate the DNA. Insulin secretion was then normalized versus the DNA content.

3.8 EXPERIMENTS IN METABOLIC CAGES

Mice were acclimated for 48 hours in the experimental room, then transferred into metabolic cages (one mouse per cage) to measure food intake, water intake, and urine output. All experiments were run on a 10-hour light/14-hour dark cycle. Food intake was evaluated for 4 and 21 days²⁰. Briefly, 15 g of food were given to each mouse at the start of every light cycle. At the end of the light cycle, food was weighted again, then the difference between the starting weight and the final weight was computed to measure the food intake. This value was also used as a starting weight to determine the night cycle food intake. After one light/dark cycle, the food left in the cages was changed with 15 g of fresh food. Water intake was measured each day at the start of every light cycle. Briefly, 50 g of drinking water was weighted and given to the mice in a water bottle. At the start of the next light cycle, water weight was measured again, accounting for the water dripped out of the bottle, which was also collected by the metabolic cage, giving the amount of water drank by the mice. This value was then converted to milliliters by measuring the density of the water with an analytical scale and micropipettes. Urine was also collected, using the built-in system of the metabolic cages. Urine volumes were measured at the end of every dark and light cycle. Urine samples were then centrifuged at 500g for 15 min and supernatants were deep frozen at -80°C until use.

3.9 GLUCOSE CONCENTRATION IN URINE

The concentration of glucose in the urine collected from WT and *Lcn2*^{-/-} mice at the end of the dark cycles was evaluated using the Infinity hexokinase-based glucose detection kit, according to the manufacturer's instructions.

3.10 INSULIN, BONE TURNOVER BIOMARKER, AND LCN2 CONCENTRATIONS IN SERA

Sera from WT and *Lcn2*^{-/-} mice were used for detection of insulin, bone turnover biomarker (CTX, TRAcP, BALP, OCN), and *Lcn2* concentrations by ELISA kits, according to the manufacturers' instructions.

3.11 OSTEOBLAST PRIMARY CULTURES

Calvarias from 7-day-old WT and *Lcn2*^{-/-} mice were explanted, cleaned free of soft tissues, and digested three times with 1 mg/ mL *Clostridium histolyticum* type IV collagenase and 0.25% trypsin, for 20 min at 37°C, with gentle agitation. Cells from the second and third digestions were plated and grown in standard conditions, in DMEM plus 10% FBS. At confluence, cells were trypsinized and plated according to the experimental protocol. The purity of the culture was evaluated by the expression of the osteoblast biomarkers, *Alkaline phosphatase (ALP)*, *Runt-related transcription factor (Runx)-2*, *Parathyroid hormone (PTH)/PTH related peptide receptor, type I collagen*, and *Osteocalcin (OCN)* and by the histochemical evaluation of ALP activity.

3.12 MINERALIZATION ASSAY

Osteoblast standard medium was supplemented with 10mM β -glycerophosphate and 50 μ g/mL ascorbate (osteogenic medium). Osteoblasts were cultured for 3 weeks before evaluation of mineralization by von Kossa staining.

3.13 ALP-POSITIVE COLONY FORMING UNIT ASSAY

Femurs and tibiae of 7-day-old WT or *Lcn2*^{-/-} mice were cleaned out of soft tissues, chopped with a sterile blade, and bone marrow cells were flushed out and pooled together. Cells were pelleted at 350g for 10 min and then 500,000 cells were plated in 6-cm dishes with osteogenic medium. Medium was changed every 5 days. At the 14th day, cells were fixed in 4% paraformaldehyde and histochemically stained for ALP. Pictures were taken with a complementary metal-oxide semiconductor (CMOS) camera and the number and area of ALP-positive colonies were analyzed to estimate the amount of osteoblast progenitors in the bone marrow.

3.14 OSTEOCLAST PRIMARY CULTURES

Femurs and tibiae of 7-day-old WT or *Lcn2*^{-/-} mice were cleaned of soft tissues, chopped with a sterile blade, and bone marrow was flushed out, diluted 1:1 in Hank's balanced salt solution (HBSS), layered over Histopaque 1077 solution, and centrifuged at 400g for 30 min. Buffy coat cells were collected, washed twice with HBSS, resuspended in DMEM plus 10% FBS, and plated in culture dishes at a density of 1*10⁶ cells/cm². After 3 hours, cell cultures were washed with PBS to remove nonadherent cells and maintained for 7 days in the same medium supplemented with 50 ng/mL rh-macrophage-colony stimulating factor (rhM-CSF) and 120 ng/mL rhRANKL. Mature osteoclasts and committed precursors were detected by TRAcP histochemical staining.

3.15 ADIPOCYTES ISOLATION

Primary adipocytes were isolated from the gonadal (epididymal) white adipose tissue of 2-month-old male mice. Briefly, gonadal fat pad was collected and kept in the Adipo Buffer (120mM NaCl; 6mM KCl; 1.2mM MgSO₄; 1mM CaCl₂; 0.6mM Na₂HPO₄; 0.4mM NaH₂PO₄; 20mM HEPES) supplemented with 1% BSA and 1mM D-glucose. The tissue was digested using 2 mg of collagenase P per each gram of fat, for 1 hour at 37°C. Adipocytes were purified by serial centrifugations (180g for 3 min, three times) and plated in α MEM supplemented with 1% FBS. After 1 hour, the adipocytes were collected and processed for RNA extraction.

3.16 COMPARATIVE REAL-TIME RT-PCR

Total RNA was extracted from mouse tissues and from osteoblast and adipocyte cultures, using the TRIzol[®] method. One microgram (1 μ g) of total RNA was reverse transcribed into cDNA using Moloney Murine Leukemia Virus (M-MLV) reverse transcriptase and the equivalent of 0.1 μ g was processed using the Brilliant[®] SYBR[®] Green QPCR master mix for real-time PCR or Thermo Scientific 2X greentaq mastermix for conventional PCR. Results, expressed as fold increase, were normalized versus the housekeeping gene Gapdh.

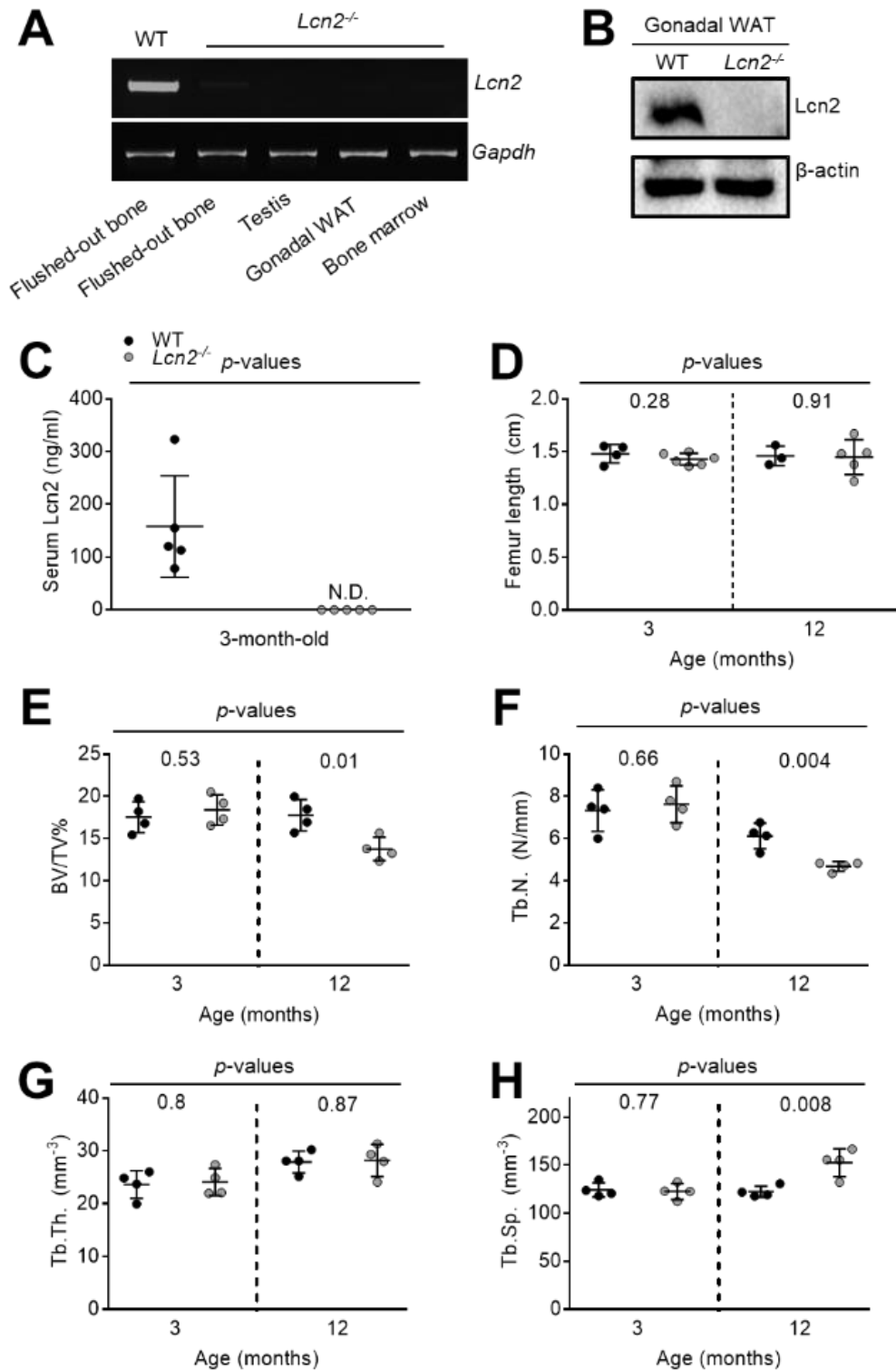
3.17 STATISTICS

Results were expressed as the mean \pm SD of at least three independent experiments or 3 to 10 mice/group, as specified in the figure legends. Results from the two sexes were analyzed separately. The sex is specified in the figure legends. Statistical analyses were performed using unpaired Student's *t* test, conducted either on raw data or on the area under the curve, according to the type of data. The statistical method is indicated in the figure legends. A *p* value <0.05 was considered statistically significant.

4. RESULTS

4.1 BONE METABOLISM

We previously showed that increased *Lcn2* expression, in response to bone mechanical unloading, impaired *in vitro* osteoblast differentiation, and enhanced osteoblast RANKL expression and subsequent osteoclast formation¹⁰. To thoroughly characterize the role of *Lcn2* in bone metabolism, we investigated the bone phenotype of *Lcn2* globally deleted mice hypothesizing an enhanced osteogenesis compared to WT mice. As expected, our *Lcn2*^{-/-} mice did not express *Lcn2* mRNA (Supporting Fig. 1A) and protein (Supporting Fig. 1B) in any tissue investigated. Consistently, circulating *Lcn2* was undetectable (Supporting Fig. 1C). The longitudinal growth of the skeleton of *Lcn2*^{-/-} mice appeared normal, as shown by gross observations and measurement of the femur length (Supporting Fig. 1D). However, to our surprise, μ CT analysis revealed that the trabecular bone volume over tissue volume was dramatically lower in *Lcn2*^{-/-} compared to WT mice at all ages analyzed (Fig. 1A,B). Consistently, evaluation of trabecular parameters revealed a significantly lower trabecular number (Fig. 1C), whereas trabecular thickness was slightly higher in *Lcn2*^{-/-} mice at 1 month of age but did not show differences with WT mice at the other ages (Fig. 1D). A higher trabecular separation was observed in *Lcn2*^{-/-} mice (Fig. 1E), whereas the cortical thickness was significantly lower only in elderly *Lcn2*^{-/-} mice (Fig. 1F). Interestingly, the trabecular bone variables in the L4 vertebrae showed no difference between WT and *Lcn2*^{-/-} mice at 3 months of age (Supporting Fig. 1E). However, we observed a significant reduction of the bone volume in the L4 vertebrae of older mice (12 months old) (Supporting Fig. 1E–H), suggesting a delayed loss of bone mass in this bone segment. To determine whether these differences in the bone structural variables were due to osteoblastic and/or osteoclastic dysfunctions, we performed histomorphometric analysis of distal femur secondary spongiosa and observed that osteoblast number and surface over bone surface were significantly lower in *Lcn2*^{-/-} mice compared to WT littermates (Fig. 2A–C). Consistently, double calcein labeling (Fig. 2D) showed reduced bone formation rate and MAR in the *Lcn2*^{-/-} mice (Fig. 2E,F). In contrast, no modulation of the osteoclast variables was observed (Fig. 2G–I), suggesting that the osteopenic phenotype of the *Lcn2*^{-/-} mice was dependent on the osteoblasts. In agreement with this hypothesis, lower serum levels of BALP (Fig. 2J) and OCN (Fig. 2K) were observed in *Lcn2*^{-/-} mice, while the serum osteoclast and bone resorption biomarkers, TRAcP (Fig. 2L) and CTX (Fig. 2M), respectively, were unremarkable. Finally, real-time RT-PCR in *Lcn2*^{-/-} marrow-depleted femurs showed a



Supporting Figure 1: Effect of *Lcn2* ablation on the bone phenotype. (A) Transcriptional expression of *Lcn2* in flushed-out bone from WT mice and in flushed-out bone, testis, gonadal white adipose tissue (WAT) and bone marrow tissues from *Lcn2*^{-/-} mice. (B) Western blot for *Lcn2* in gonadal WAT from WT and *Lcn2*^{-/-} mice. (C) ELISA assay to assess *Lcn2* levels in sera from WT and *Lcn2*^{-/-} mice. (D) Longitudinal measurements of femurs in WT and *Lcn2*^{-/-} male mice. (E-H) MicroCT analysis performed on vertebrae (L4) from WT and *Lcn2*^{-/-} male mice at 3 and 12 months of age. (E) Bone volume/total tissue volume (BV/TV %) and trabecular (F) number (Tb.N.), (G) thickness (Tb.Th.) and (H) separation (Tb.Sp.) (unpaired Student's *t*-test, number of mice per group=3-6).

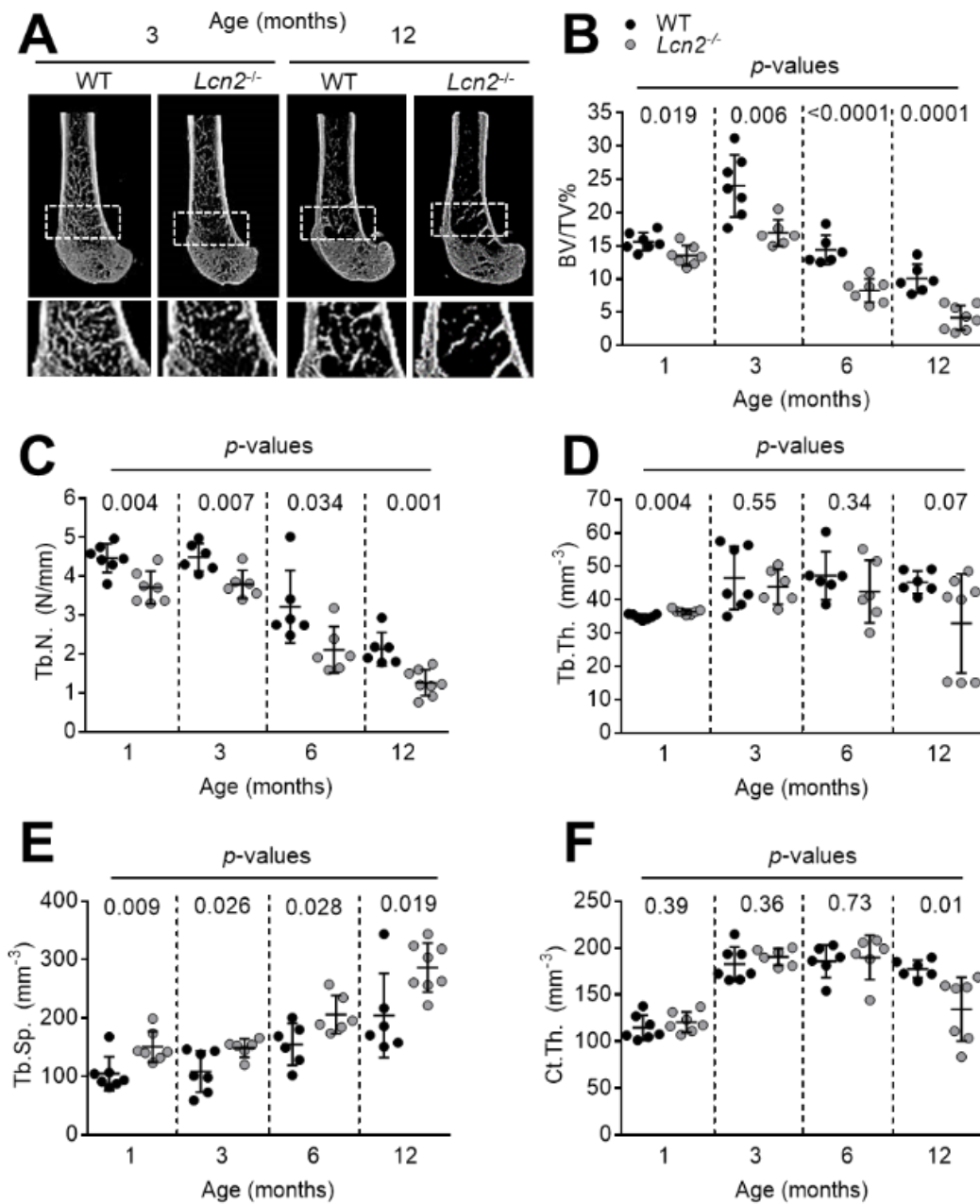


Figure 1: *Lcn2*^{-/-} mice show an osteopenic phenotype. MicroCT analysis of distal femur secondary spongiosa of WT and *Lcn2*^{-/-} male mice. (A) Representative images of femurs analyzed at the indicated ages. (B) Bone volume/total tissue volume (BV/TV %) and trabecular (C) number (Tb.N.), (D) thickness (Tb.Th.) and (E) separation (Tb.Sp.). (F) Cortical thickness (Ct.Th.) (unpaired Student's *t*-test; number of mice/group=6-7).

significant reduction of *Alp*, *Runx2*, and *Col1A2* compared to WT mice (Fig. 2N). The bone loss found in *Lcn2*^{-/-} mice was unexpected as it conflicted with our previous observation that *Lcn2* Was increased in mechanically unloaded osteopenic mice¹⁰.

To understand the mechanisms underlying this discrepancy, we first investigated which cell types expressed *Lcn2* in the bone. Interestingly, we found low transcriptional levels of *Lcn2* in marrow-depleted bones compared to the bone marrow alone and to the whole bone (Supporting Fig. 2A). Moreover, in cultured primary calvaria osteoblasts, we observed faint levels of *Lcn2* mRNA compared to marrow cells (Supporting Fig. 2B) and primary adipocytes (Supporting Fig. 2C). Similar results were observed detecting the *Lcn2* protein in bone and gonadal fat sections by immunohistochemistry, with a positive signal found in marrow cells and adipocytes but not in osteoblasts (Supporting Fig. 2D). These results confirmed previous observations^{9,10,21} but are at variance with the data reported by Mosialou and colleagues¹¹, who found a basal osteoblast expression of *Lcn2* 10-fold higher than in the other *Lcn2*-expressing organs. Given the complexity of the in vivo results, we next assessed whether the cellular changes observed in the *Lcn2*^{-/-} mice were cell-autonomous by evaluating the bone cell phenotype in vitro. Primary osteoclasts, differentiated from the bone marrow– derived mononuclear cell fraction, showed no differences in formation or function (Fig. 3A,B). Surprisingly, in contrast with the in vivo data, osteoblasts isolated from WT and *Lcn2*^{-/-} calvarias exhibited similar levels of ALP activity (Fig. 3C), with no differences in the ability to mineralize the extracellular matrix (Fig. 3D) and in the transcriptional expression of *Alp* (Fig. 3E) and *Runx2* (Fig. 3F). Because these assays can only be performed after various days of culture, which deprive the cells of environmental factors present in vivo, we speculated that the in vivo global *Lcn2* ablation affected osteoblasts by an indirect mechanism. Consistent with this assumption, *Lcn2* silencing of cultured osteoblasts by the means of specific siRNA (Supporting Fig. 3A) did not influence *Alp* and *Runx2* (Supporting Fig. 3B,C), in agreement with the observation that our osteoblasts expressed very low basal levels of *Lcn2*^{9,10,21} (Supporting Fig. 2). In contrast, a colony forming unit assay, which gives an instant picture of the in vivo situation detecting the ALP-positive osteoblast precursor pool in the freshly harvested bone marrow, showed significantly lower ALP-positive colony number (Fig. 3G) and area (Fig. 3H) in the *Lcn2*^{-/-} cultures, suggesting that global *Lcn2* ablation in vivo reduced the number of osteoblast precursors in the bone marrow. From this set of data, we concluded that the impaired osteoblast activity in *Lcn2*^{-/-} mice was not cell-autonomous.

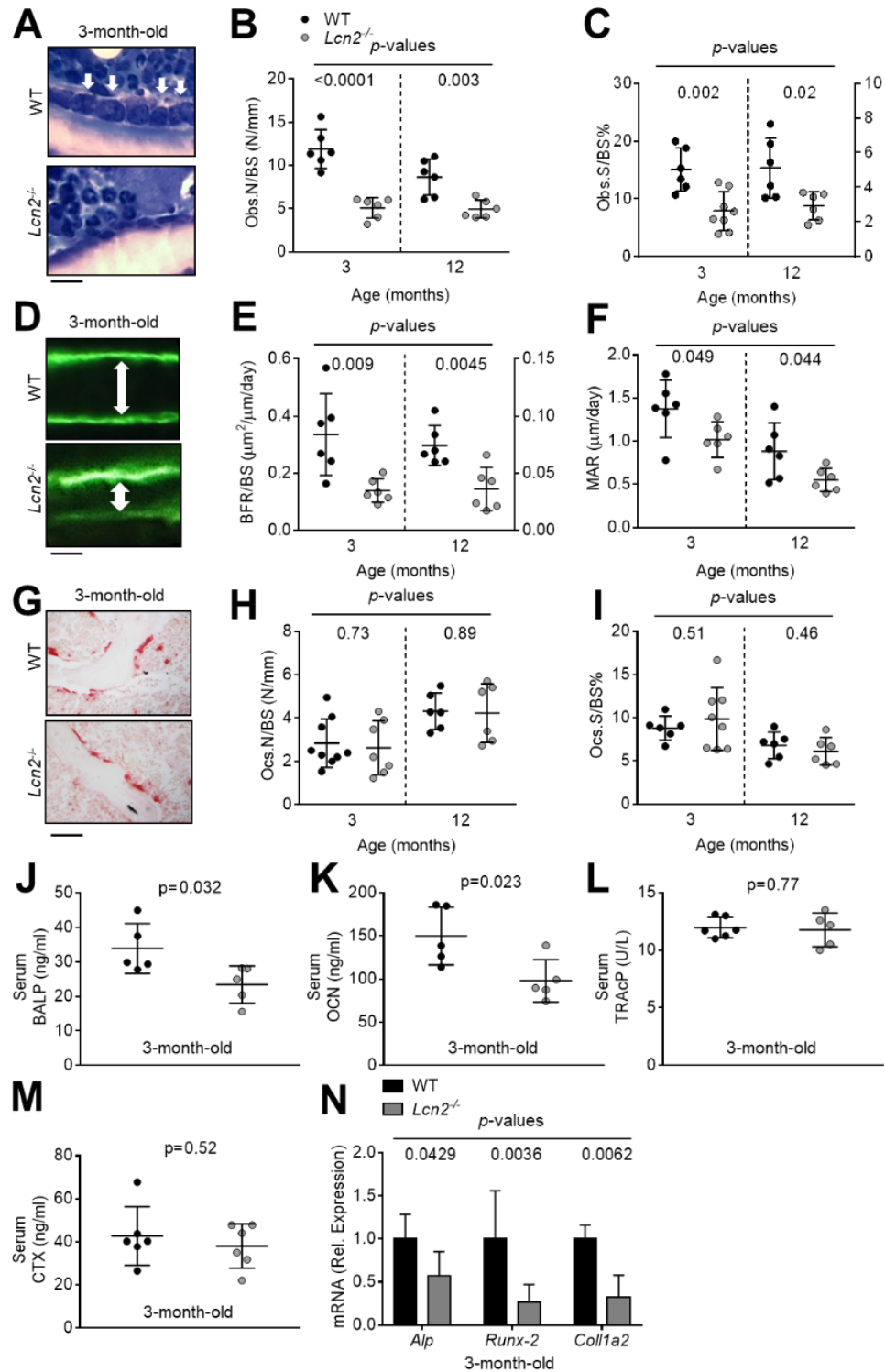
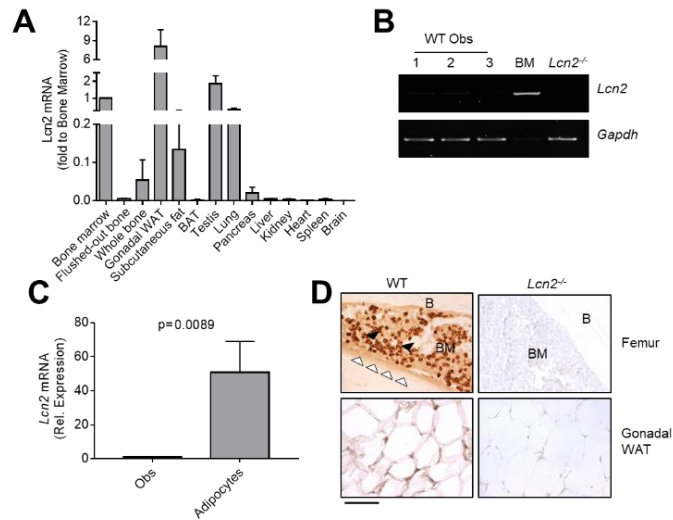


Figure 2: Histomorphometry and bone turnover biomarkers in WT and *Lcn2*^{-/-} mice. (A) Histological sections from WT and *Lcn2*^{-/-} male mouse proximal tibias stained with methylene blue/azure II to evaluate (B) osteoblast number/bone surface (ObN/BS) and (C) osteoblast surface/bone surface (ObS/BS); arrows = osteoblasts, scale bar = 5μm. (D) Double *in vivo* calcein labelling (green fluorescence; scale bar = 5μm) and evaluation of (E) bone formation rate/bone surface (BFR/BS) and (F) mineral apposition rate (MAR). (G) Histological sections of proximal tibias subjected to TRAcP histochemical assay to evaluate osteoclast (H) number (Oc.N) and (I) surface (OcS/BS) over bone surface; scale bar = 10μm. (J,K) Serum analysis of the bone formation biomarkers (J) bone alkaline phosphatase (BALP) and (K) osteocalcin (OCN). (L,M) Serum analysis of (L) TRAcP and (M) CTX. (N) Transcriptional expression of *Alp*, *Runx2* and *Collagen 1A2* in femurs (unpaired Student's *t*-test, number of mice/group=5-8).



Supporting Figure 2: Lcn2 expression. (A) Real time RT-PCR analysis of *Lcn2* mRNA levels in the tissues indicated in the abscissa. (B) Transcriptional expression of *Lcn2* in WT osteoblasts (Obs, preparations n. 1, 2, 3) in the bone marrow (BM) as positive control and in KO osteoblasts. (C) Real time RT-PCR analysis of *Lcn2* transcriptional levels in osteoblast and adipocyte primary cultures. (D) Immunohistochemistry for *Lcn2* performed on femur sections and gonadal WAT from WT and *Lcn2*^{-/-} mice (BM = bone marrow; B = bone; arrows = osteoblasts). Data are (B,D) representative or (A,C) the mean \pm SD of three independent experiments (unpaired Student's *t*-test).

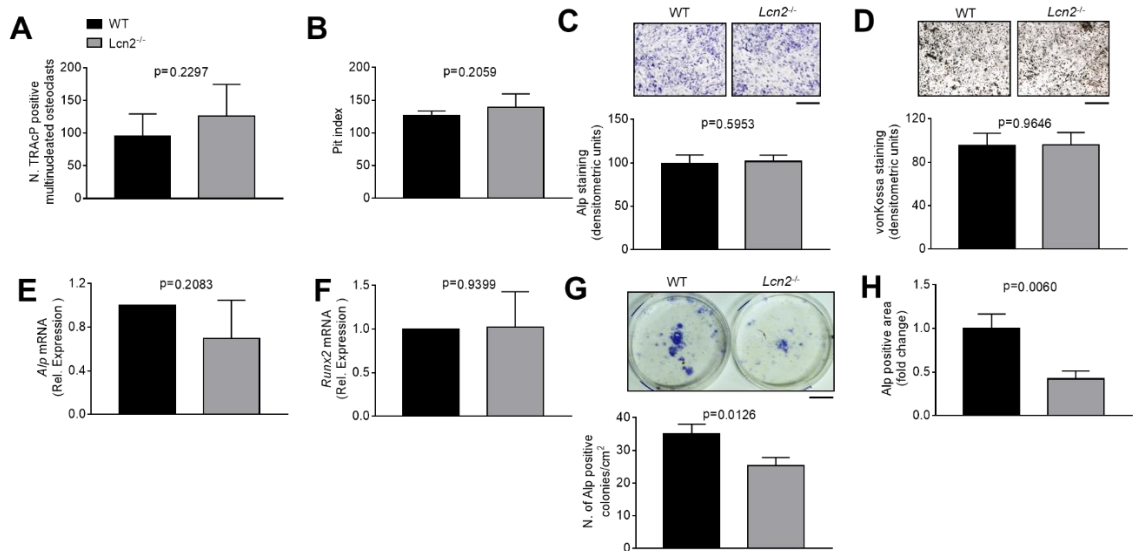
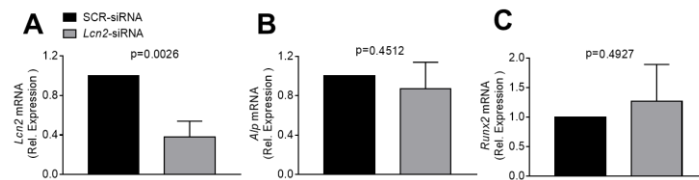


Figure 3: Effect of *Lcn2* ablation on osteoclast and osteoblast phenotype. (A,B) Purified bone marrow mononuclear cells from 7-day-old WT and *Lcn2*^{-/-} mice were allowed to differentiate in osteoclasts in the presence of 25 ng/ml rhM-CSF and 120 ng/ml rhRANKL. (A) At the end of the experiment, mature osteoclasts were detected by TRAcP histochemical staining and counted. (B) Purified bone marrow mononuclear cells were plated onto bone slices and allowed to differentiate as described in (A). At the end of the experiment, bone slices were stained with toluidine blue and the pit index calculated. (C-F) Primary osteoblasts were isolated from the calvariae of 7-day-old WT and *Lcn2*^{-/-} mice after 3 digestions with 1 mg/ml *Clostridium histolyticum* type IV collagenase and 0.25% trypsin. (C) ALP activity evaluated by histochemical assay (inset; scale bar = 50 μ m) and quantified by densitometric analysis (graph). (D) Von Kossa staining (inset; scale bar = 50 μ m) of mineralization nodules from WT and *Lcn2*^{-/-} primary osteoblasts cultured in standard medium supplemented with 10 mM β -glycerophosphate and 50 μ g/ml ascorbic acid (osteogenic medium) for 3 weeks. (E,F) Transcriptional expression of (E) *Alp* and (F) *Runx2*. (G,H) Osteogenic colony forming unit assay performed in bone marrow stromal cells flushed out from femurs of 7day-old WT and *Lcn2*^{-/-} mice. Evaluation of (G) number of ALP-positive colonies and (H) ALP-positive area; scale bar = 1mm. Results are the mean \pm SD of three independent experiments (unpaired Student's *t*-test).

These results could also reconcile our seemingly contradictory observations that both *Lcn2* overexpression¹⁰ and ablation (this study) impair osteogenesis, because the former could affect osteoblasts by a direct mechanism, while the latter could act through an indirect process involving a systemic regulation.

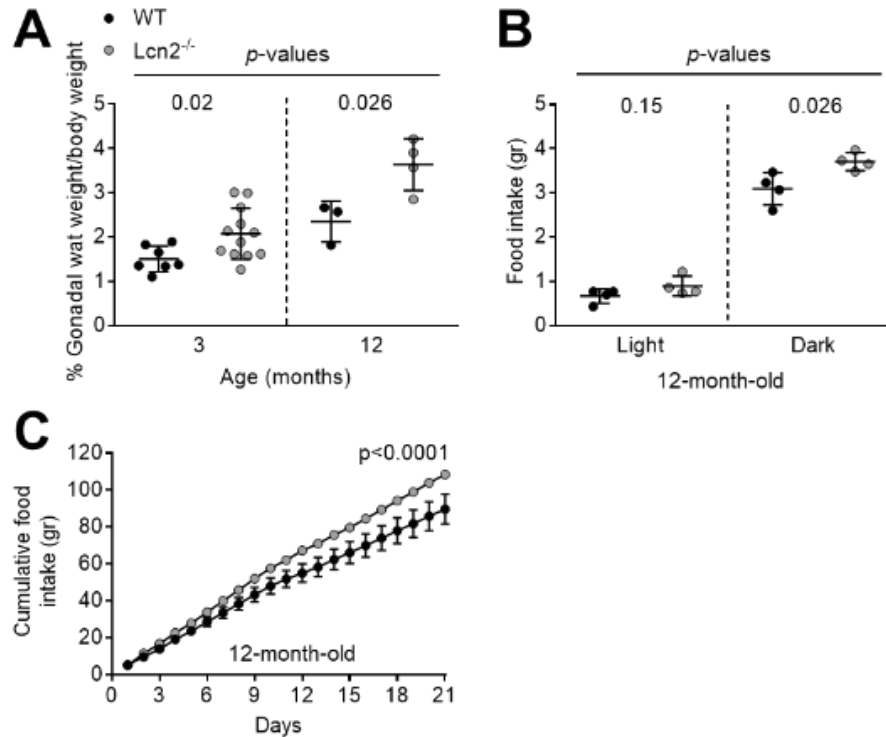


Supporting Figure 3: Silencing of *Lcn2* mRNA in WT osteoblasts. (A) Real-time RT-PCR analysis of *Lcn2* mRNA levels in osteoblasts treated with siRNA specific for *Lcn2* or with control (scrambled) siRNA. (B,C) Transcriptional expression of *Alp* and *Runx2*. Data are the mean \pm SD of three independent experiments (unpaired Student's *t*-test).

4.2 ENERGY METABOLISM

Given that bone and energy metabolism are tightly linked²², we investigated whether the energy metabolism was disturbed in *Lcn2*^{-/-} mice, thus indirectly affecting the bone phenotype. We noticed that *Lcn2*^{-/-} mice were bigger in size compared to matched WT littermates. The body weight (Fig. 4A) and the weight of the gonadal fat (Fig. 4B, Supporting Fig. 4A) were significantly higher in *Lcn2*^{-/-} compared to WT mice at all ages evaluated. The *Lcn2*^{-/-} gonadal white adipose tissue showed more adipocytes (Fig. 4C), while the adipocyte area/tissue area was similar in the two genotypes (Fig. 4D). The higher body weight was likely due to a greater food intake in *Lcn2*^{-/-} compared to WT mice, measured at 3 months (Fig. 4E,F) and 12 months of age (Supporting Fig. 4B,C). To assess whether these features could be associated with an altered glucose metabolism, we measured the glycemia and observed that *ad libitum*-fed circulating glucose concentration was similar in the two genotypes, while fasted glucose was significantly lower in *Lcn2*^{-/-} mice (Fig. 5A). Consistently, dynamic measurements of glycemia by GTT confirmed lower blood glucose in the *Lcn2*^{-/-} versus the WT mice (Fig. 5B), while insulin levels measured at each time point were comparable (Supporting Fig. 5A) and ITT showed no differences in the sensitivity to insulin (Fig. 5C). To investigate the energy metabolism more deeply, and because insulin is also important for bone metabolism^{22,23}, we evaluated the insulinemia and observed that it was significantly higher in *Lcn2*^{-/-} mice compared to WT mice, under feeding conditions (Fig. 5D). In our mice, histological examination of endocrine pancreas showed a similar number of Langerhans islets in the two genotypes (Fig. 5E), although the islets were larger in 3-month-old *Lcn2*^{-/-} compared to WT mice (Fig. 5F), as confirmed also by

immunofluorescence for insulin (Fig. 5G). To better clarify this phenotype, we performed a glucose-stimulated insulin secretion (GSIS) test in ex vivo pancreatic islets freshly isolated from WT and *Lcn2*^{-/-} mice and observed a greater release of insulin from *Lcn2*^{-/-} islets after



Supporting Figure 4: Effect of *Lcn2* ablation on energy metabolism. (A) Evaluation of gonadal WAT weight normalized for the body weight. (B,C) Twelve-month-old WT *Lcn2*^{-/-} mice were housed in metabolic cages to evaluate food intake for (B) 4 or (C) 21 days (unpaired Student's *t*-test, number of mice/group=4-10)

exposure to both normal and high glucose concentrations (Fig. 5H). We next evaluated the energy metabolism phenotype in elderly mice (12 months) and observed a trend to lower fasted glucose in the *Lcn2*^{-/-} genotype (Fig. 5I). Similarly, GTT still showed lower glucose levels in *Lcn2*^{-/-} mice (Fig. 5J), while insulin sensitivity remained similar in the two genotypes (Fig. 5K). Insulinemia was significantly higher in 12-month-old *Lcn2*^{-/-} mice also (Fig. 5L), while neither number nor area of pancreatic islets were changed (Fig. 5M,N). Lower levels of fasted glucose were also observed in both adult and aged female *Lcn2*^{-/-} mice (Supporting Fig. 5B), paralleled also in this sex by a significant increase of glucose tolerance (Supporting Fig. 5C,D).

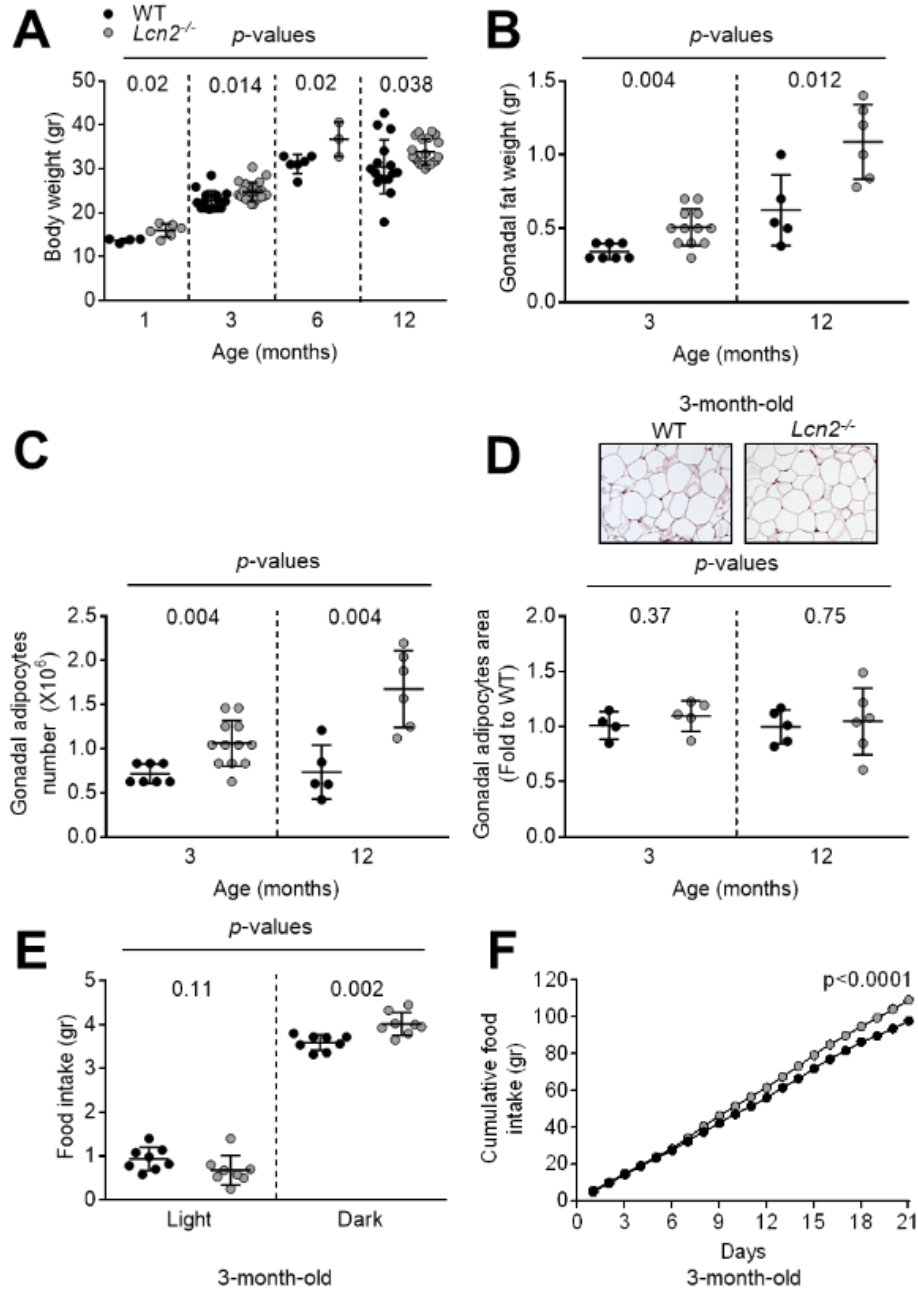


Figure 4: *Lcn2*^{-/-} knock out mice show increased body and gonadal fat weight. (A) Body weight measurements in WT and *Lcn2*^{-/-} male mice at the ages indicated in the X-axis. (B-D) Three and 12-month-old WT and *Lcn2*^{-/-} male mice were sacrificed, then gonadal fat was collected and (B) weighted. (C) Evaluation of gonadal adipocyte cell number. (D) Histological sections of gonadal fat from WT and *Lcn2*^{-/-} mice stained with hematoxylin/eosin (inset; scale bar = 50 μ m) and quantification of the adipocyte area. (E,F) Three-month-old WT and *Lcn2*^{-/-} mice were housed in metabolic cages to evaluate food intake after (E) 4 and (F) 21 days (unpaired Student's *t*-test, number of mice/group=3-10).

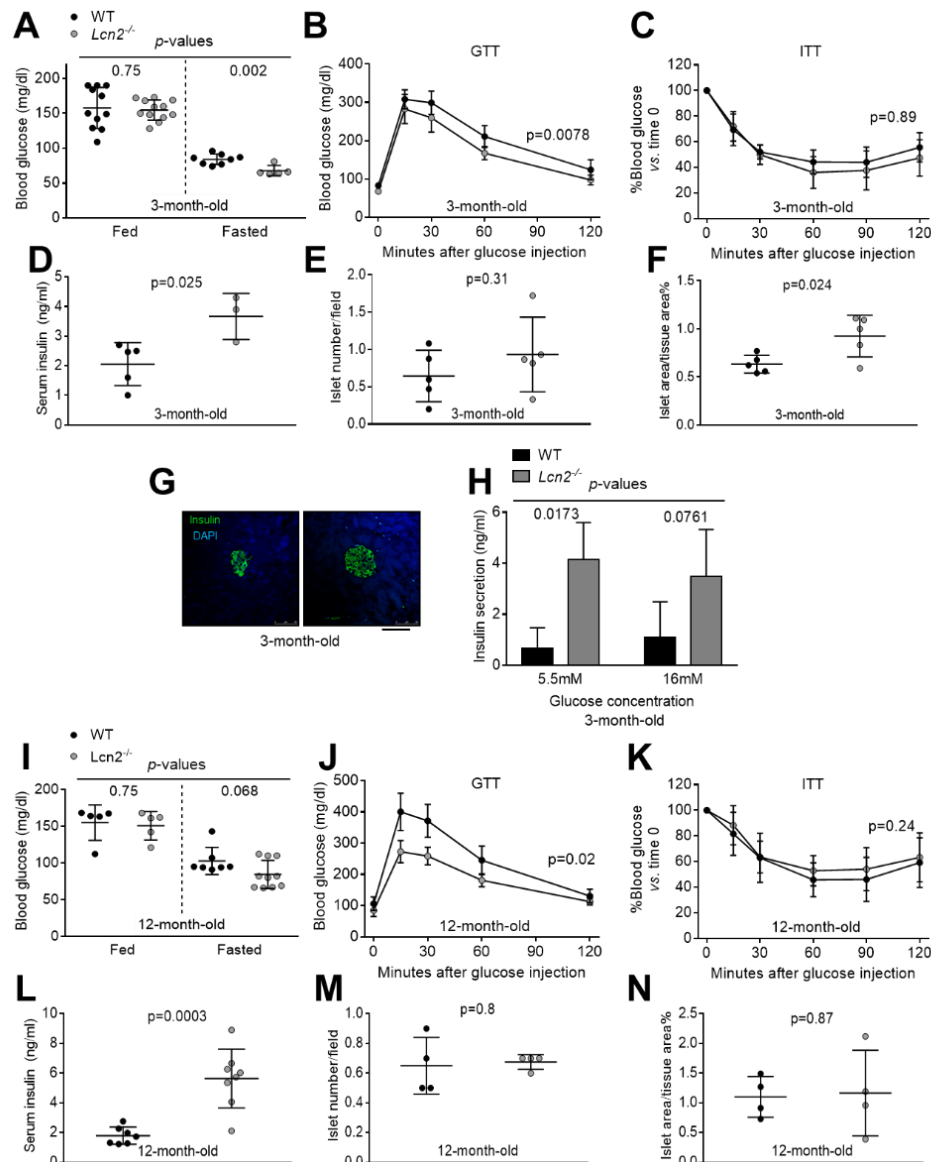
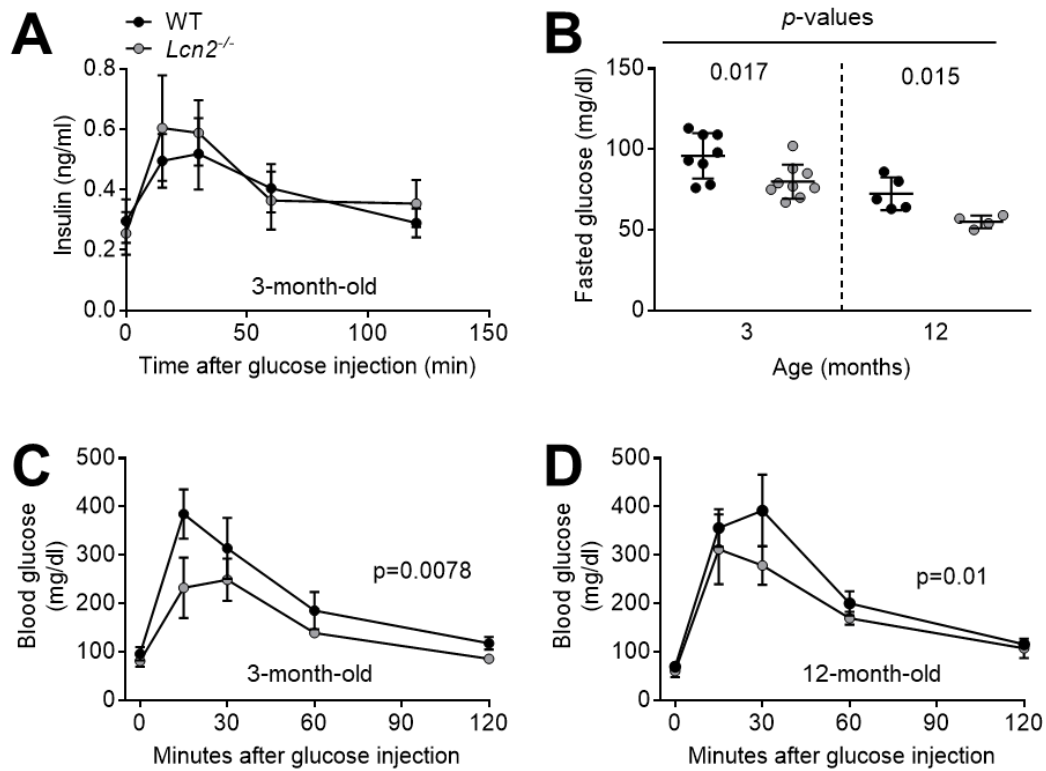


Figure 5: Effect of *Lcn2* ablation on energy metabolism. (A-H) Three-month-old WT and *Lcn2*^{-/-} male mice were evaluated (A) for their glucose levels under *ad libitum* feeding and fasting conditions. (B) WT and *Lcn2*^{-/-} mice were injected i.p. with 2 g/kg body weight of glucose and subjected to glucose tolerance test (GTT) at the times indicated in the abscissa. (C) WT and *Lcn2*^{-/-} mice were injected with 0.75UI/Kg body weight of Humulin® (rhInsulin) and subjected to insulin tolerance test (ITT) at the times indicated in the abscissa. (D) ELISA assay to assess serum levels of insulin. (E) Pancreatic islet number and (F) area over tissue area. (G) Immunofluorescence analysis of insulin in sections from pancreas of WT and *Lcn2*^{-/-} mice; scale bar = 50µm. (H) GSIS test in pancreatic islets isolated from 3-month-old WT and *Lcn2*^{-/-} male mice. (I) Twelve-month-old WT and *Lcn2*^{-/-} male mice were evaluated for their glucose levels under *ad libitum* feeding and fasting conditions. (J) Glucose and (K) insulin tolerance test. (L) Serum levels of insulin. (M) Pancreatic islet number and (N) area over tissue area (unpaired Student's *t*-test, number of mice/group=4-11).



Supporting Figure 5: Effect of *Lcn2* ablation on energy metabolism. (A) Insulin levels evaluated in the blood of 3-month-old male mice subjected to glucose tolerance test. (B) Three- and 12-month-old WT and *Lcn2*^{-/-} female mice were evaluated for their glucose levels under fasting conditions. (B) Three and (C) 12-month-old WT and *Lcn2*^{-/-} female mice were injected i.p. with 2 g/kg body weight of glucose and subjected to glucose tolerance test (GTT) at the times indicated in the abscissa (unpaired Student's *t*-test, number of mice/group=4-8).

4.3 KIDNEY ALTERATIONS

To establish whether kidney alterations could contribute to the *Lcn2*^{-/-} mouse phenotype, we measured the urine output in metabolic cage experiments. We found polyuria in *Lcn2*^{-/-} mice at both 3 and 12 months of age (Fig. 6A), while their water intake was similar to WT mice (Fig. 6B,C). Interestingly, glycosuria was also observed in *Lcn2*^{-/-} mice (Fig. 6D), likely associated with the polyuria described in Figure 6A. Moreover, *Lcn2* has been previously associated with the polyuria described in Figure 6A. Moreover, *Lcn2* has been previously associated with chronic kidney disease progression in mice and humans²⁴ and *Lcn2*^{-/-} mice showed proteinuria (Fig. 6E) and histological signs of renal cortex vacuolization (Fig. 6F,G), thus suggesting the development of kidney injury and its potential involvement in the circulating glucose depletion observed in the *Lcn2*^{-/-} mice.

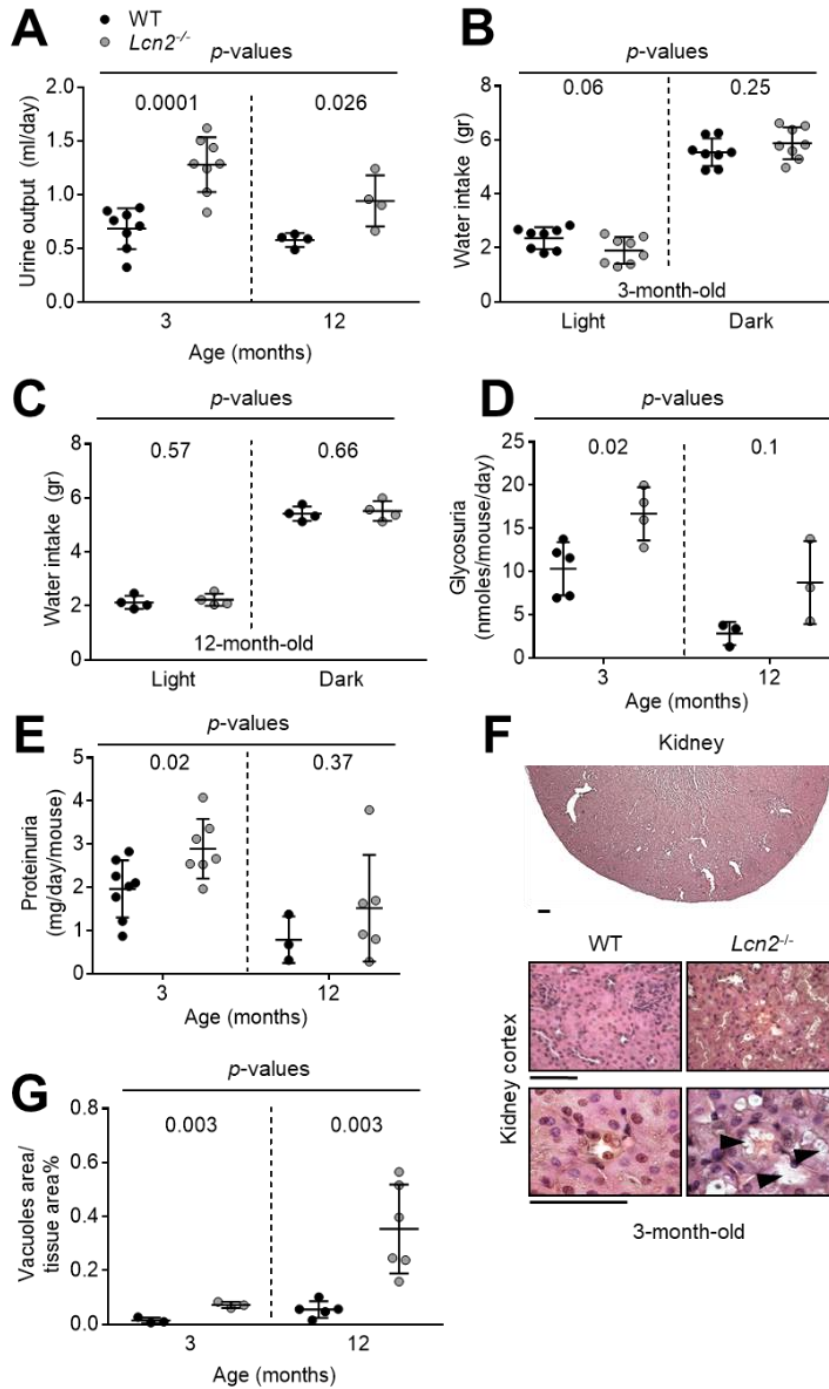
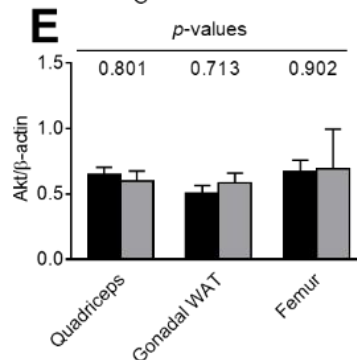
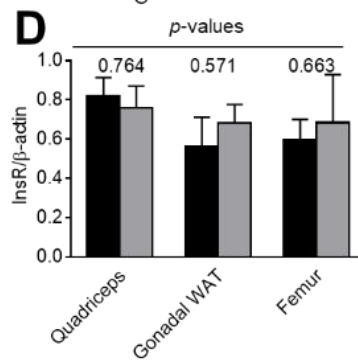
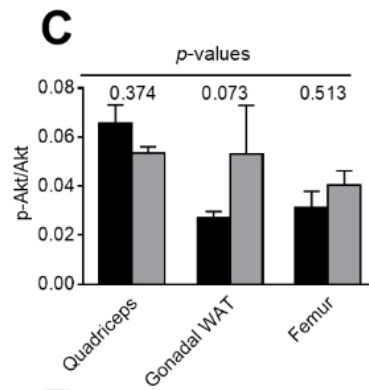
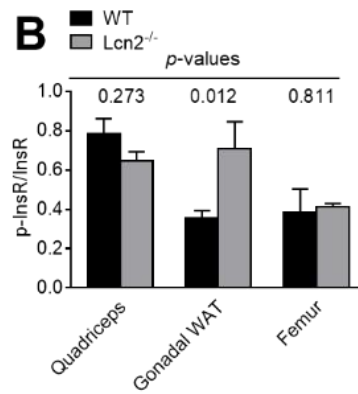
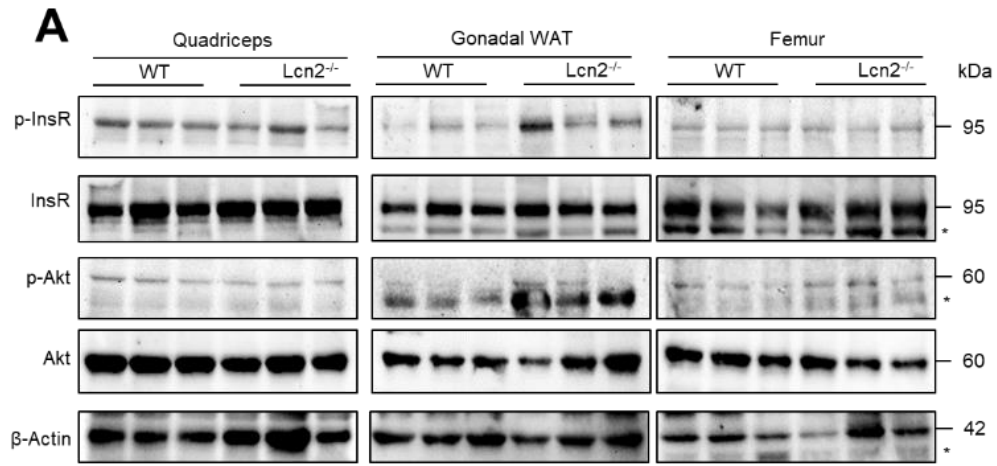


Figure 6: Effect of *Lcn2* ablation on renal functions. Three- and 12-month-old WT and *Lcn2*^{-/-} male mice were housed in metabolic cages to assess (A) urine output and (B,C) water intake. Evaluation of (D) glucose levels and (E) protein concentration in urine. (F) Histological sections of kidneys from WT and *Lcn2*^{-/-} mice stained with hematoxylin/eosin and (G) evaluation of vacuolar area in the cortical region (unpaired Student's *t*-test, number of mice/group=3-8; scale bar = 25μm).

4.4 MOLECULAR MECHANISM

To investigate the effect of *Lcn2* deletion on the overall insulin signaling, we performed Western blot analysis for the activated (ie, phosphorylated) insulin receptor (InsR) and its downstream target AKT in gonadal white adipose tissue, quadriceps, and femur protein lysates. Phosphorylation of InsR and AKT did not appear different between the two genotypes in quadriceps and femurs. In gonadal white adipose tissue, we observed a significant increase of InsR phosphorylation and a trend of increase of AKT phosphorylation (Supporting Fig. 6A–D, left panels), suggesting that the high circulating insulin in *Lcn2*^{-/-} mice targets especially the white adipose tissue. These results ruled out that the bone phenotype of *Lcn2*^{-/-} mice was associated with altered insulin signaling and led us to

hypothesize that a specific glucose-associated alteration could affect the bone. To address this hypothesis, we evaluated the expression of GLUT1, which is the transporter through which glucose enters the osteoblasts by an insulin-independent mechanism, driving osteoblast differentiation and bone deposition²⁵. Glut1 transcriptional expression was lower in bone marrow depleted femurs from *Lcn2*^{-/-} mice compared to WT, while it was higher in *Lcn2*^{-/-} liver (Fig. 7A) as expected from the insulin-induced hypoglycemic phenotype²⁶. The lower level of GLUT1 in the marrow-depleted bone was also confirmed by Western blot (Fig. 7B). Taken together, these results suggest that *Lcn2* global ablation prevents the full expression of a glucose transporter that is essential for osteogenesis²⁵, at least in part explaining the osteopenic phenotype observed in the *Lcn2*^{-/-} mice.



Supporting Figure 6: Insulin signaling in WT and Lcn2^{-/-} mice. (A) Western blot analysis of phospho insulin receptor (pINSr), INSr, phospho AKT (pAKT), AKT and β-actin in quadriceps, gonadal WAT and femurs from WT and Lcn2^{-/-} mice. Densitometry analysis of the Western blots shown in A for (B) pINSr normalized with INSr, (C) pAKT normalized with AKT, (D) INSr normalized with β-actin and (E) AKT normalized with β-actin (unpaired Student's *t*-test, number of mice/group=3). *Non-specific bands.

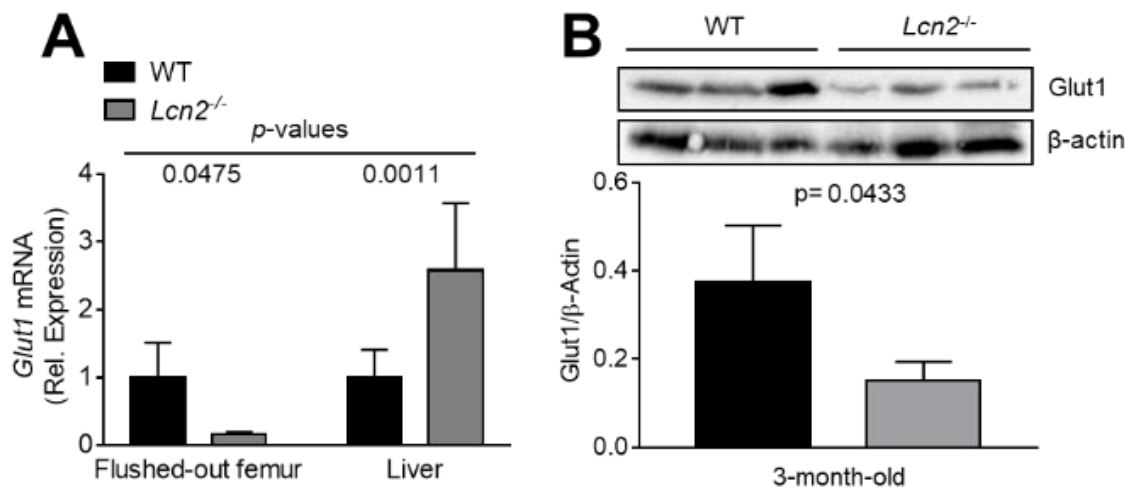


Figure 7: Glut1 expression. (A) Transcriptional expression of *Glut-1* in the indicated tissues. (B) Western blot analysis of GLUT-1 in marrow flushed-out femurs (unpaired Student's *t*-test, number of mice/group=3-5).

5. DISCUSSION

Lcn2 is a versatile protein involved in many complex and often contradictory functions. In our work, we showed that *Lcn2*^{-/-} mice had a marked osteopenic phenotype due to reduced osteoblast number and activity, with no changes in osteoclast parameters. Our data supports the concept that this phenotype was not primary, but secondary to deregulated energy metabolism and, at least in part, due to the impairment of the GLUT1 expression in the *Lcn2*^{-/-} bone. Accordingly, differentiation and *in vitro* mineralization ability of cultured calvarial osteoblasts were similar between WT and *Lcn2*^{-/-} cells, thus suggesting an *in vivo* non-cell autonomous osteoblast response to *Lcn2* ablation. *In vitro* osteoclast function and gene expression were also similar in the WT and *Lcn2*^{-/-} genotypes. This is at variance with a recent report which proposed that *Lcn2*^{-/-} mice had no bone phenotype *in vivo*, while *in vitro* osteoclasts were larger and their osteoclast precursors proliferated more due to upregulation of the M-CSF receptor, c-Fms²⁷.

This result is surprising, further strengthening the complexity of the *Lcn2* pathway in the bone. The involvement of energy metabolism reconciles this study with our previous work¹⁰, in which we showed impaired osteoblast function when *Lcn2* was overexpressed in unloading conditions. This paradox could depend on the fact that overexpression of *Lcn2*

could have a direct negative influence on osteoblasts, while in our global *Lcn2* ablated mice the negative effect on osteoblasts could be mediated by a complex alteration of energy metabolism and kidney function. Our results on the bone phenotype also diverge from those described in the elegant report by Mosialou and colleagues¹¹, who found normal bone mass in both global and osteoblast specific *Lcn2*-deleted mice, and normal circulating levels of OCN in osteoblast-specific-deleted mice, concluding that the effect of *Lcn2* deletion was not on the bone but only on appetite in the brain. These discrepancies could be explained by the fact that Mosialou and colleagues investigated the bone phenotype only in the vertebrae and only at 3 months of age. Concordantly, also the vertebral phenotype of our 3-month-old global *Lcn2*^{-/-} mice was unremarkable, while vertebral low bone mass was apparent in older mice. In contrast, we observed long-bone osteopenia at all ages, representing another piece of complexity in the *Lcn2* pathway, which seems to exhibit both time-based and site-based diversities. Another important difference between these two studies was in the osteoblast basal expression of *Lcn2*. Mosialou and colleagues showed a very high *Lcn2* level in WT osteoblasts, 10-fold more than in adipocytes. This is at variance with previous reports, which showed that *Lcn2*-producing cells are mainly adipocytes and bone marrow cells^{1-8,10,21} rather than osteoblasts^{28,29}. In Mosialou and colleagues¹¹, the bone marrow was not included in the transcriptional and protein analyses, while in our previous work, we showed that the marrow *Lcn2*-highly expressing cells did not belong to the stromal compartment, thus ruling out the osteoblast lineage^{9,10,21}. This observation was complemented in this study, in which high *Lcn2* expression was detected immunohistochemically in marrow cells and in gonadal adipocytes but not in endosteal cells, confirming previous reports^{1,2,28,29,3-8,10,21}. The role of *Lcn2* in the energy metabolism has been investigated by various groups, but again the results did not fully clarify the exact pattern, and studies diverge in their observations and conclusions. The fact that our *Lcn2*^{-/-} mice had an altered control of energy metabolism was suggested by their hyperphagia and mild obesity. The adipose tissue was clearly affected by the *Lcn2* deletion with an increase of the number of adipocytes and of the signaling response to insulin. We also showed that *Lcn2*^{-/-} mice exhibited fasted hypoglycemia and greater glucose tolerance but, at variance with Mosialou and colleagues and other reports⁶, we observed a fed hyperinsulinemia, corroborated by the detection of bigger pancreatic islets in *Lcn2*^{-/-}. Increased insulin secretion was confirmed by the GSIS test in isolated starved *Lcn2*^{-/-} islets exposed to glucose; therefore, we are confident that, in our experimental condition, hyperinsulinemia characterizes the *Lcn2*^{-/-} mouse energy phenotype. This hyperinsulinemia could be associated with the mild obesity observed in the *Lcn2*^{-/-} mice, in agreement with

reports that showed a causal association between these two conditions²⁶. In fact, it has been proposed that hyperinsulinemia can promote obesity³⁰⁻³³, whereas drugs that prevent hyperinsulinemia can lead to weight loss^{33,34}. Given that the insulin sensitivity in *Lcn2*^{-/-} mice was normal, hyperinsulinemia could indeed account for the higher glucose tolerance and fasted hypoglycemia observed in *Lcn2*^{-/-} mice. However, a previous study showed that *Lcn2* deficiency reduced glycemia and insulinemia, and enhanced insulin sensitivity in aging, dietary or genetic-induced obesity⁶, partly diverging from our observations and corroborating the observations by Mosialou and colleagues¹¹. To make the phenotype even more complex, glucose excretion and kidney function appeared altered in our *Lcn2*^{-/-} mice. *Lcn2* is very important for the iron handling and recycling in the kidney, preventing iron accumulation in tubular kidney cells³⁵. *Lcn2* has also been proposed as a biomarker of acute kidney injury³⁶ and our data showed that *Lcn2*^{-/-} kidneys presented with proteinuria and cortex vacuolization, which is morphologically consistent with iron-induced kidney injury³⁵. This could also potentially be the cause of the polyuria and glycosuria, which could contribute to the circulating glucose depletion in *Lcn2*^{-/-} mice. The mechanisms underlying the response of the bone to the *Lcn2*-induced hypoglycemia and hyperinsulinemia remain to be fully elucidated, representing a limitation of our study. The basal insulin receptor and downstream signaling pathways appeared similar in WT and *Lcn2*^{-/-} mice. However, the expression of GLUT1 in the bone was downregulated in *Lcn2*^{-/-} mice. GLUT1 transports glucose in osteoblasts, and glucose uptake stimulates osteoblast differentiation through a mechanism that stabilizes Runx2 by preventing its degradation into the proteasome²⁵. Glucose uptake by osteoblasts is independent of insulin, and in osteoblasts GLUT1 has been demonstrated to be more expressed compared to other glucose transporters²⁵. Mouse genetics showed that GLUT1 expression is enhanced by Runx2 and that Runx2 cannot induce osteoblast differentiation in the presence of low glucose. Therefore, it is conceivable, although rather speculative, that the impairment of GLUT1 expression in *Lcn2*^{-/-} bone could contribute to the low bone formation observed in these mice. In conclusion, *Lcn2* is a very peculiar protein, whose physiologic level appears to be essential for bone health, balanced energy metabolism, and normal kidney function. Together with other reports^{11,22,23}, we have highlighted that the pathways in which *Lcn2* is involved are very complex and not yet fully understood. It should be noted that *Lcn2* is also called growth factor super-inducible protein 24³⁷ because of its strong transcriptional activation in various conditions. Therefore, we cannot rule out that small experimental or environmental differences could also be responsible for the discrepancies noted in various studies. Furthermore, strategies to generate

the available Lcn2 mouse models were different, for instance deleting a 1.9-kilobase (kb) genomic fragment comprising Lcn2 exons 3 to 6 by LoxP sites within introns 2 and 6 in Mosialou and colleagues, or using a targeting vector designed to replace a 2.5-kb genomic fragment containing Lcn2 exons 1 to 5 with the PGK-neo cassette in Berger and colleagues¹², who generated the mice investigated in this study. Therefore, further research and controlled approaches will be necessary to recognize the exact multifaceted roles of Lcn2 in the organismal health, elucidate the underlying cellular and molecular mechanisms and reconcile the many divergent observations reported so far in the literature (See introduction).

6. REFERENCES

1. Lögdberg, L. & Wester, L. Immunocalins: A lipocalin subfamily that modulates immune and inflammatory responses. *Biochim. Biophys. Acta - Protein Struct. Mol. Enzymol.* **1482**, 284–297 (2000).
2. Abella, V. *et al.* The potential of lipocalin-2/NGAL as biomarker for inflammatory and metabolic diseases. *Biomarkers* **20**, 565–571 (2015).
3. Zhang, Y. *et al.* Lipocalin 2 expression and secretion is highly regulated by metabolic stress, cytokines, and nutrients in adipocytes. *PLoS One* **9**, 1–9 (2014).
4. Guo, H. *et al.* Lipocalin-2 deficiency impairs thermogenesis and potentiates diet-induced insulin resistance in mice. *Diabetes* **59**, 1376–1385 (2010).
5. Guo, H. *et al.* Lipocalin 2 deficiency alters estradiol production and estrogen receptor signaling in female mice. *Endocrinology* **153**, 1183–1193 (2012).
6. Law, I. K. M. *et al.* Lipocalin-2 deficiency attenuates insulin resistance associated with aging and obesity. *Diabetes* **59**, 872–882 (2010).
7. Jin, D. *et al.* Lipocalin 2 is a selective modulator of peroxisome proliferator-activated receptor- γ activation and function in lipid homeostasis and energy expenditure. *FASEB J.* (2011) doi:10.1096/fj.10-165175.
8. Paton, C. M. *et al.* Lipocalin-2 increases fat oxidation in vitro and is correlated with energy expenditure in normal weight but not obese women. *Obesity* (2013) doi:10.1002/oby.20507.
9. Capulli, M., Rufo, A., Teti, A. & Rucci, N. Global transcriptome analysis in mouse calvarial osteoblasts highlights sets of genes regulated by modeled microgravity and

- identifies A ‘mechanoresponsive osteoblast gene signature’. *J. Cell. Biochem.* (2009) doi:10.1002/jcb.22120.
10. Rucci, N. *et al.* Lipocalin 2: A new mechanoresponding gene regulating bone homeostasis. *J. Bone Miner. Res.* (2015) doi:10.1002/jbmr.2341.
 11. Mosialou, I. *et al.* MC4R-dependent suppression of appetite by bone-derived lipocalin 2. *Nature* (2017) doi:10.1038/nature21697.
 12. Berger, T. *et al.* Lipocalin 2-deficient mice exhibit increased sensitivity to *Escherichia coli* infection but not to ischemia-reperfusion injury. *Proc. Natl. Acad. Sci. U. S. A.* (2006) doi:10.1073/pnas.0510847103.
 13. Feldkamp, L. A., Davis, L. C. & Kress, J. W. Practical cone-beam algorithm. *J. Opt. Soc. Am. A* (1984) doi:10.1364/josaa.1.000612.
 14. Lorensen, W. E. & Cline, H. E. Marching cubes: A high resolution 3D surface construction algorithm. in *Proceedings of the 14th Annual Conference on Computer Graphics and Interactive Techniques, SIGGRAPH 1987* (1987). doi:10.1145/37401.37422.
 15. Pratt, W. K. *Processing Digital Image Processing. Image Rochester NY* (2001). doi:10.1016/S0146-664X(78)80023-9.
 16. Bouxsein, M. L. *et al.* Guidelines for assessment of bone microstructure in rodents using micro-computed tomography. *Journal of Bone and Mineral Research* (2010) doi:10.1002/jbmr.141.
 17. Rucci, N. *et al.* The glycosaminoglycan-binding domain of PRELP acts as a cell type-specific NF- κ B inhibitor that impairs osteoclastogenesis. *J. Cell Biol.* (2009) doi:10.1083/jcb.200906014.
 18. Dempster, D. W. *et al.* Standardized nomenclature, symbols, and units for bone histomorphometry: A 2012 update of the report of the ASBMR Histomorphometry Nomenclature Committee. *Journal of Bone and Mineral Research* (2013) doi:10.1002/jbmr.1805.
 19. Li, D. S., Yuan, Y. H., Tu, H. J., Liang, Q. Le & Dail, L. J. A protocol for islet isolation from mouse pancreas. *Nat. Protoc.* (2009) doi:10.1038/nprot.2009.150.
 20. Ellacott, K. L. J., Morton, G. J., Woods, S. C., Tso, P. & Schwartz, M. W.

- Assessment of feeding behavior in laboratory mice. *Cell Metabolism* (2010) doi:10.1016/j.cmet.2010.06.001.
21. Veeriah, V. *et al.* Interleukin-1 β , lipocalin 2 and nitric oxide synthase 2 are mechano-responsive mediators of mouse and human endothelial cell-osteoblast crosstalk. *Sci. Rep.* (2016) doi:10.1038/srep29880.
 22. Ferron, M. *et al.* Insulin Signaling in Osteoblasts Integrates Bone Remodeling and Energy Metabolism. *Cell* (2010) doi:10.1016/j.cell.2010.06.003.
 23. Fulzele, K. *et al.* Insulin Receptor Signaling in Osteoblasts Regulates Postnatal Bone Acquisition and Body Composition. *Cell* (2010) doi:10.1016/j.cell.2010.06.002.
 24. Viau, A. *et al.* Lipocalin 2 is essential for chronic kidney disease progression in mice and humans. *J. Clin. Invest.* (2010) doi:10.1172/JCI42004.
 25. Wei, J. *et al.* Glucose Uptake and Runx2 Synergize to Orchestrate Osteoblast Differentiation and Bone Formation. *Cell* (2015) doi:10.1016/j.cell.2015.05.029.
 26. Mastaitis, J. W., Wurmbach, E., Cheng, H., Sealfon, S. C. & Mobbs, C. V. Acute induction of gene expression in brain and liver by insulin-induced hypoglycemia. *Diabetes* (2005) doi:10.2337/diabetes.54.4.952.
 27. Kim, H.-J. *et al.* Deficiency of Lipocalin-2 Promotes Proliferation and Differentiation of Osteoclast Precursors via Regulation of c-Fms Expression and Nuclear Factor-kappa B Activation. *J. Bone Metab.* (2016) doi:10.11005/jbm.2016.23.1.8.
 28. Tsai, T. L. & Li, W. J. Identification of Bone Marrow-Derived Soluble Factors Regulating Human Mesenchymal Stem Cells for Bone Regeneration. *Stem Cell Reports* (2017) doi:10.1016/j.stemcr.2017.01.004.
 29. Wang, Y. Small lipid-binding proteins in regulating endothelial and vascular functions: Focusing on adipocyte fatty acid binding protein and lipocalin-2. *British Journal of Pharmacology* (2012) doi:10.1111/j.1476-5381.2011.01528.x.
 30. Templeman, N. M., Skovsø, S., Page, M. M., Lim, G. E. & Johnson, J. D. A causal role for hyperinsulinemia in obesity. *J. Endocrinol.* (2017) doi:10.1530/JOE-16-0449.

31. Corkey, B. E. Banting lecture 2011: Hyperinsulinemia: Cause or consequence? *Diabetes* (2012) doi:10.2337/db11-1483.
32. Odeleye, O. E., De Courten, M., Pettitt, D. J. & Ravussin, E. Fasting hyperinsulinemia is a predictor of increased body weight gain and obesity in Pima Indian children. *Diabetes* (1997) doi:10.2337/diab.46.8.1341.
33. R.H., L. *et al.* A multicenter, randomized, double-blind, placebo-controlled, dose-finding trial of a long-acting formulation of octreotide in promoting weight loss in obese adults with insulin hypersecretion. *International Journal of Obesity* (2006).
34. Alemzadeh, R., Jacobs, W. & Pitukcheewanont, P. Antiobesity effect of diazoxide in obese Zucker rats. *Metabolism*. (1996) doi:10.1016/S0026-0495(96)90287-5.
35. Schmidt-Ott, K. M. *et al.* Neutrophil gelatinase-associated lipocalin-mediated iron traffic in kidney epithelia. *Current Opinion in Nephrology and Hypertension* (2006) doi:10.1097/01.mnh.0000232886.81142.58.
36. Konno, T. *et al.* Expression and function of interleukin-1 β -induced neutrophil gelatinase-associated lipocalin in renal tubular cells. *PLoS One* (2016) doi:10.1371/journal.pone.0166707.
37. LIU Quart-Sheng, Marit Nilsen-Hamillon, X. S.-D. Synergistic regulation of the acute phase protein SIP24/24p3 by glucocorticoid and pro-inflammatory cytokines. *Acta Physiol. Sin.* **55**, 525–529 (2003).



Chapter 3

*“Lipocalin-2 in muscle in basal conditions
and after challenge”*

1. ABSTRACT

Lipocalin-2 (Lcn2) is an adipokine that carries out a variety of functions in diverse organs. Although its role in bone is being investigated and is becoming clearer and clearer, its importance in muscle and exercise biology is currently unknown. In this chapter, we observed that following acute high-intensity aerobic exercise (Gran Sasso Vertical Run), LCN2 serum levels were increased, along with muscle damage markers creatine kinase (CK) and myoglobin, while the osteoblast marker undercarboxylated osteocalcin (ucOCN) was unaffected. The Wnt pathway antagonist DKK1 was also increased after the race, positively correlating with LCN2. In mice, Western blot analyses showed that Lcn2 was indeed expressed by muscle, especially diaphragm, quadriceps and *soleus*, but not extensor digitorum longus (EDL). This prompted us to investigate the muscle phenotype of Lcn2 globally deleted mice (*Lcn2*^{-/-}) at different ages at the macroscopic, histological, functional and molecular level. *Lcn2*^{-/-} mice presented with smaller muscle fibers in the quadriceps, but no detectable fibrosis or muscle damage, at 3,6, and 12 months of age. However, this was not accompanied by a reduction of muscle performance, evaluated by grip force test, or muscle weight. Myoglobin and CK levels were also comparable to WT, while serum Interleukin 6 (IL6) was lower in *Lcn2*^{-/-} mice, consistent with the suggested role of Lcn2 as inflammatory molecule. The transcriptional profile showed a general increase of myogenic factors *MyoD*, *Myogenin* and *Pax7* at 3 months of age, which became unremarkable or was reverted at 12 months of age, in quadriceps, *soleus*, and diaphragm. *In vitro* treatment with recombinant Lcn2 caused a reduction in myogenic differentiation of C2C12 and primary mouse myoblasts, as assessed by evaluating % of myonuclei in fusion medium. Transcriptionally, Lcn2 treatment caused an increase in fatty acid-binding protein 1 (Fabp1), tumor necrosis factor-related apoptosis-inducing ligand (TRAIL), Wnt3a and other factors that are important in muscle as well as bone biology. Taken together, these results show that LCN2 is dispensable for normal muscle biology, and its absence reduces IL6. Furthermore, treating muscle cells with exogenous LCN2 reduces myogenic differentiation, suggesting that LCN2 may be a detrimental factor when upregulated in inflammatory muscle conditions.

2. INTRODUCTION

Lipocalin 2 (Lcn2), is a multifunctional protein belonging to the lipocalin superfamily¹ and involved in many pathological processes, such as inflammation², myocarditis³, acute kidney injury^{4,5} and notably, bone physiopathology⁶⁻¹¹. In particular, from our investigations, Lcn2 emerges as a complex player in bone biology, which is detrimental for bone health when upregulated in hindlimb suspension and bed rest models, which are models of mechanical unloading in mouse and humans, respectively⁶. Also, osteoblasts subjected to simulated microgravity, overexpress Lcn2⁷. However, at the same time, its absence causes osteopenia in basal conditions⁸. Although the role of Lcn2 in bone physiopathology has been studied and is still under scrutiny, its effect on muscle and exercise biology has poorly investigated so far. In fact, only 2 specific reports on skeletal muscle exist to date. One is specific to Lcn2, and demonstrated that lack of Lcn2 reduces satellite cells proliferation, impairing acute muscle damage repair¹², while another is a large-scale analysis performed on *longissimus dorsi* (LD) muscles in mice subjected to space flight, a condition of strong mechanical unloading. In this case, the investigators show a strong upregulation of Lcn2 in the space flight group in the LD¹³. Further reports claim that Lcn2 is a negative determinant of myocardial health^{3,14-16}. In this work, we aimed at characterizing LCN2 at the muscle tissue level, and to check how it responds to exercise, by means of mouse models and analysis of serum samples from healthy male human athletes.

3. MATERIAL AND METHODS

3.1 MATERIALS

Dulbecco's modified Minimum Essential Medium (DMEM), Fetal Bovine Serum (FBS), penicillin, streptomycin and trypsin were from GIBCO (Uxbridge, UK). Basic Fibroblasts growth factor was from Peprotech (Rocky hills, NJ, USA) while recombinant mouse (rm)Lcn2 was from R&D (Minneapolis, MN, USA). Vacuette serum-separator tubes were from Greiner Bio-One, Kremsmünster, Austria. Sterile plasticware and syringes were from Falcon Becton-Dickinson (Cowley, Oxford, UK) or Costar (Cambridge, MA, USA), while serum-separator tubes were from Greiner Bio-One, (Kremsmünster, Austria). TRIzol reagent, primers and reagents for RT-PCR were from Invitrogen (Carlsbad, CA, USA). The Sensimix SYBR Green QPCR master mix was from Bioline (Memphis, TN). Masson's trichrome kit was from Bio Optica (Milan, Italy). All the other reagents were of the purest grade from Sigma Aldrich Co. (St. Louis, MO, USA).

3.2 ANIMALS

Lcn2^{-/-} mice (background C57BL6/J) were generated and kindly provided by Dr. Tak Wah Mak (University Health Network, Toronto, ON, Canada)¹⁷. They are vital, with an overall normal lifespan and fertility. All procedures involving animals and their care were conducted in conformity with national and international laws and policies (European Economic Community Council Directive 86/609, OJ L 358, 1, December 12, 1987; Italian Legislative Decree 4.03.2014, n.26, *Gazzetta Ufficiale della Repubblica Italiana* no. 61, March 4, 2014) and the Animal Research: Reporting of *In Vivo* Experiments (ARRIVE) guidelines. Mice were housed in the animal facility of the University of L'Aquila, Italy, at the following conditions: temperature: 24°C; humidity: 60-65%; dark/light cycle: 12/12 hours. They had access to food and water *ad libitum* and were fed with a standard diet (Mucedola code: 4RF21) composed of 60.8% carbohydrates, 21% proteins, 3.45% fat, 6.8% fibers, 7.95% trace elements, and 12% humidity.

3.3 CELL LINES

C2C12 mouse myoblast-like cells were obtained from the European Collection of Authenticated Cell Cultures (ECACC). C2C12 cells were cultured in DMEM plus 10% FBS for maintenance, while when treating with rmLcn2 they were kept in fusion medium (DMEM plus 5% horse serum) for 4 days in total, with 2 medium changes, before fixation or RNA extraction. Cells were supplied with penicillin/streptomycin and glutamine and kept in a humidified 37°C incubator with 95% air 5% CO₂.

3.4 PRIMARY CELL CULTURES

Mouse primary myoblasts were cultured from the hindlimb muscles of 4-6 week-old CD1 mice using standard protocols^{18,19}. Cells were kept in 80% Ham's F10, 20% FBS, 25 µg/ml basic Fibroblasts Growth Factor (bFGF) before complete fibroblast depletion, and 40% DMEM, 40% Ham's F10, 20% FBS, 25 µg/ml bFGF afterwards. when treating with rmLcn2 cells were kept in fusion medium (DMEM plus 5% horse serum) for 4 days in total, with 2 medium changes, before fixation or RNA extraction. Cells were supplied with penicillin/streptomycin and glutamine and kept in a humidified 37°C incubator with 95% air 5% CO₂.

3.5 GRAN SASSO D'ITALIA VERTICAL RUN (VR)

Male runners from different European countries competed in a timed race which consisted in a 3.6 km long race with a 1.03 km vertical ascension (29.5% slope, Figure 1A), which is usually completed in 40-50 minutes (speed=75-80m/min). The run was an outdoor run, and weather was unremarkable, with no rain, very high temperature or other factors that could

significantly influence the performance of the athletes. Fifteen competitors (Table I) chose to participate in our study and were given a self-administered informed consent in English or Italian depending on their preferred language.

3.6 HUMAN SERUM SAMPLING

About 10 ml of venous blood were collected from participants 30 minutes before the race, and no more than 30 minutes after the race. Blood was collected on-site into serum-separator tubes (Greiner bio-one) by a medical doctor and brought to the laboratory in controlled-temperature boxes, before being centrifuged at 2000g for 10 minutes. Sera were then harvested in aseptic conditions and frozen at -80°C for storage. When needed for the ELISA or Reflotron tests, blood was thawed on ice and used following the manufacturer's instructions.

Table I: Features of Skyrace participants

ID	Age	Sex	Hours of training/week	Agonist (Y/N)
1	17	M	5	N
2	18	M	7	N
3	29	M	3.5	N
4	30	M	3	N
5	32	M	3.5	N
6	33	M	10	Y
7	35	M	4	Y
8	38	M	6.5	Y
9	39	M	14	Y
10	44	M	6	Y
11	45	M	3.5	Y
12	46	M	5	N
13	48	M	12	N
14	51	M	7	N
15	54	M	10	Y

3.7 MICE SERUM SAMPLING

Blood was collected by cardiac puncture from 1-, 3-, 6-, 12-months old WT C57/BL6/J (henceforth WT) or *Lcn2*^{-/-} mice after sacrifice by CO₂ inhalation, allowed to clot for 15 minutes at room temperature in 1.5ml tubes, centrifuged at 2000g for 10 minutes and stored as described for humans.

3.8 ELISA AND REFLOTRON TESTS

Sera from participants to the VR were used for detection of LCN2 (cat# DLCN20, R&D, Minneapolis, MN, USA), undercarboxylated Osteocalcin (ucOCN, cat# E-EL-H5493,

Elabscience, Houston, TX), myoglobin (cat# ab171580), DKK1 (cat# ab100501, Abcam Cambridge, UK) according to the manufacturers' instructions. Reflotron PLUS (Roche, Basel, Switzerland) reactive strips were used to evaluate creatine kinase as described in the instruction sheet.

For WT and *Lcn2*^{-/-} mice analyses, sera were used to detect Lcn2 (cat# MLCN20 R&D, Minneapolis, MN, USA), myoglobin (cat# ab210965) or IL-6 (cat# ab100712, Abcam Cambridge, UK) according to the manufacturers' instructions. Reflotron PLUS (Roche, Basel, Switzerland) reactive strips were used to evaluate creatine kinase as described in the instruction sheet.

3.9 COMPARATIVE REAL-TIME RT-PCR

Total RNA was extracted from mouse diaphragm (Diaph), quadriceps (Quad), *soleus* (SOL), *extensor digitorum longus* (EDL) muscle tissues using the TRIzol[®] method. One μ g of RNA was reverse transcribed into cDNA using Moloney Murine Leukemia Virus (M-MLV) reverse transcriptase and the equivalent of 0.1 μ g was processed using The Sensimix SYBR Green QPCR master mix for real-time PCR. Results, calculated as fold to WT average using the $\Delta\Delta$ Ct method, were normalized with the housekeeping gene beta actin.

3.10 REAL TIME RT-ARRAYS

Total RNA was extracted from mouse C2C12 cells following treatment with vehicle or rmLcn2 using the TRIzol[®] method. One 1 μ g of total RNA was reverse transcribed as described above, and the whole of the cDNA was mixed with the appropriate amount of SYBR mix and water following the manufacturer's instructions. The mix was then equally distributed among the wells of a mouse RT²-Array pathway finder (Cat# PAMM-014ZA, Qiagen, Heidelberg, Germany). A total of 3 experiments were ran and analysed using the manufacturer's online software, using an average of all available housekeeping genes as reference to calculate fold-regulations. Genes having Cts>30 in both control and treated samples were not considered for the analysis.

3.11 HISTOLOGY AND HISTOPATHOLOGY

After sacrificing mice with CO₂, hindlimbs were isolated, skin and fur removed, and limbs immersed in 10% neutral buffered formalin. After 48h of fixation, quadriceps were isolated from the limbs, and processed for paraffin embedding. Five μ m-thick cross sections were obtained within 50 μ m from the longitudinal mid-section of the muscle and stained with hematoxylin-eosin (Sigma Aldrich) or Masson's trichrome kit (Bio Optica). Finally, they were dehydrated and mounted with permanent medium (Eukitt).

For fiber size analyses, hematoxylin-eosin-stained quadriceps muscle fibers from the whole section were selected and their minimum Feret diameter was calculated using the image analysis software NIH ImageJ. This method was preferred compared to the fiber area analysis because less prone to error due to slight differences in sectioning angles²⁰. To calculate the % of intact fibers, we used well-established methods²¹. Briefly, the centrally nucleated, fibrotic, necrotic fibers were counted, and expressed as percentage of total number of fibers. To calculate % of fibrotic tissue, we used the software ImageJ to select fibrotic tissue in quadriceps muscles following Masson's trichrome staining, and calculated the %fibrotic area compared to total area²².

3.12 STATISTICS

Results were expressed as the mean±SD of at least three independent experiments or >3 mice/group. Correlation analyses were performed using Pearson's correlation test. For the Skyrace experiments, paired Student's *t*-test was used to evaluate differences between before and after the race. In every other instance, unpaired Student's *t*-test was used when comparing 2 groups. To compare curves in longitudinal studies, Graphpad Prism 7.0 was used to run curve fitting tests to evaluate whether one curve could efficiently fit the datasets compared. A *p* value <0.05 was considered statistically significant.

4. RESULTS

Fifteen male amateur of agonist runners (age 17-54 years) participated in the "Gran Sasso d'Italia vertical run" (henceforth VR). This is a race in which participants run on a 29.5% slope for 3.6 km, ascending for more than 1000 meters in altitude in 40-50 minutes (Figure 1A), which is therefore a very acutely intense physical activity. We withdrew blood right before and right after the race, to evaluate whether this exercise would influence serum levels of LCN2 and other markers. Indeed, the analyses showed that LCN2 levels were significantly increased after the race (Figure 1B). Serum levels of muscle damage markers myoglobin (Figure 1C) and creatine kinase (CK, Figure 1D) were also increased compared to before the race, reflecting the high intensity of the workout. However, when we analyzed the bone deposition marker undercarboxylated Osteocalcin (ucOCN) we found it to be unremarkable (Figure 1E). of note, the Wnt pathway inhibitor DKK1 was significantly increased after the race (Figure 1F) and correlated with serum levels of LCN2 (Figure 1G).

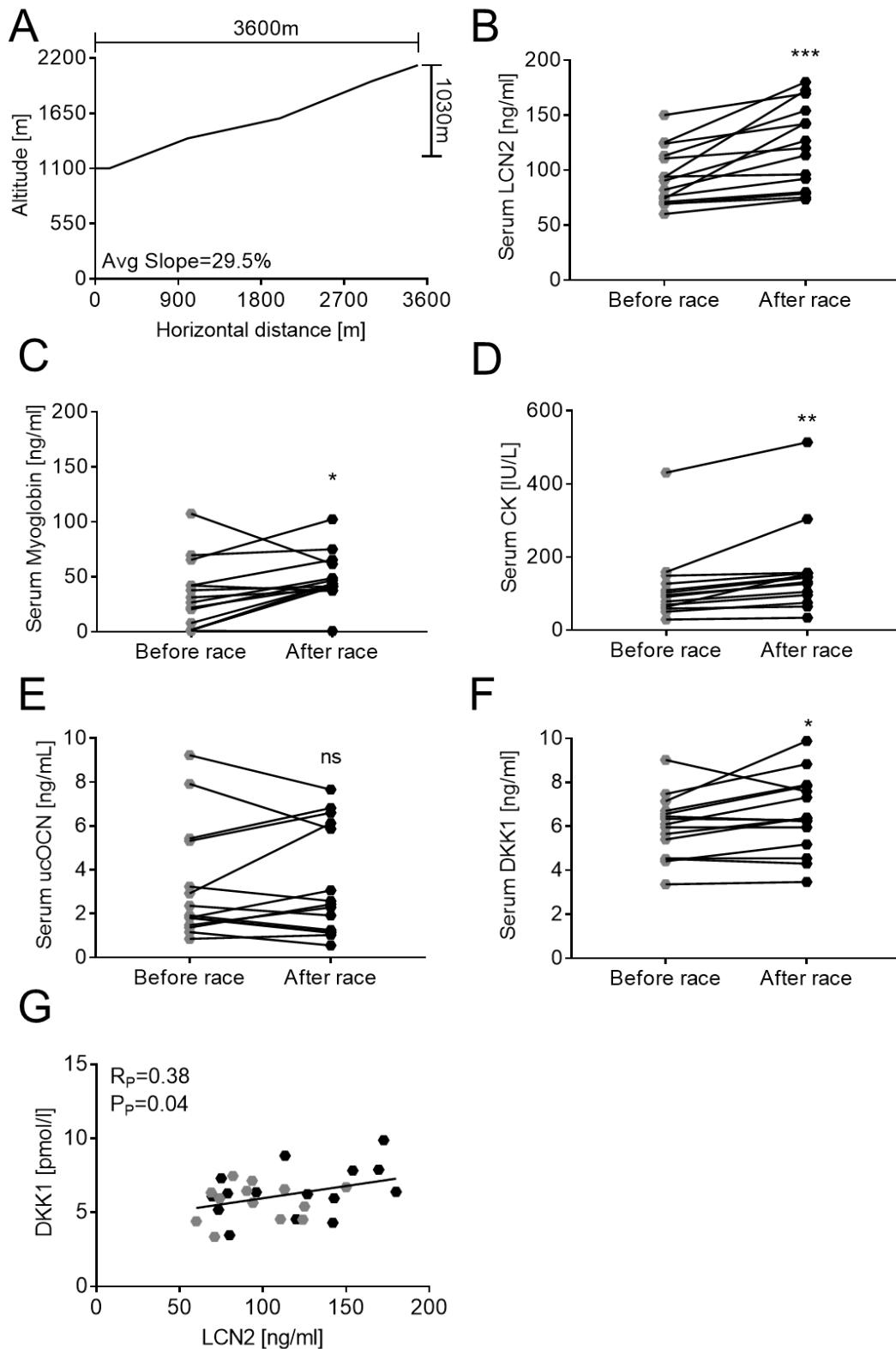


Figure 1: Gran Sasso d'Italia vertical run (VR). Fifteen male participants took part in the (A) Gran Sasso d'Italia vertical run (VR), a run where a horizontal distance of 3.6km is covered, while ascending for 1030m, averaging 29.5% slope. After informed consent administration, blood was withdrawn from participants right before, and immediately after the race. (B-G) Serum analyses showing levels of (B) Lipocalin 2 (LCN2), (C) myoglobin, (D) creatine kinase, (E) undercarboxylated osteocalcin (ucOCN), (F) DKK1. (G) Pearson's correlation analyses between DKK1 and LCN2 serum levels. R and P values are indicated in the panel. (B-F) Student's paired *t*-test and (G) Pearson's correlation. **p*<0.05; ***p*<0.01; ****p*<0.001 vs before race.

Based on these results, we next evaluated LCN2 role in muscle biology. First, we extracted RNA from diaphragm (Dia), quadriceps *femuris* (Quad), *extensor digitorum longus* (EDL) and *soleus* (SOL) from male wild type (WT) mice, and analyzed mRNA expression of *Lcn2* finding that Dia has the highest expression of *Lcn2*, compared to the muscles, with EDL showing the lowest relative expression (Figure 2A).

To better understand the role of *Lcn2* in muscle we then employed a *Lcn2* global knock out model (*Lcn2*^{-/-})¹⁷. We first confirmed, as technical control, that these mice have undetectable levels of circulating and muscle protein expression of *Lcn2* by ELISA and Western blot analysis, respectively, compared to WT littermates (Figure 2B,C). These results also showed that WT Dia, Quad and SOL expressed *Lcn2* even at the protein level, while in EDL muscle it is near-undetectable thus confirming transcriptional data.

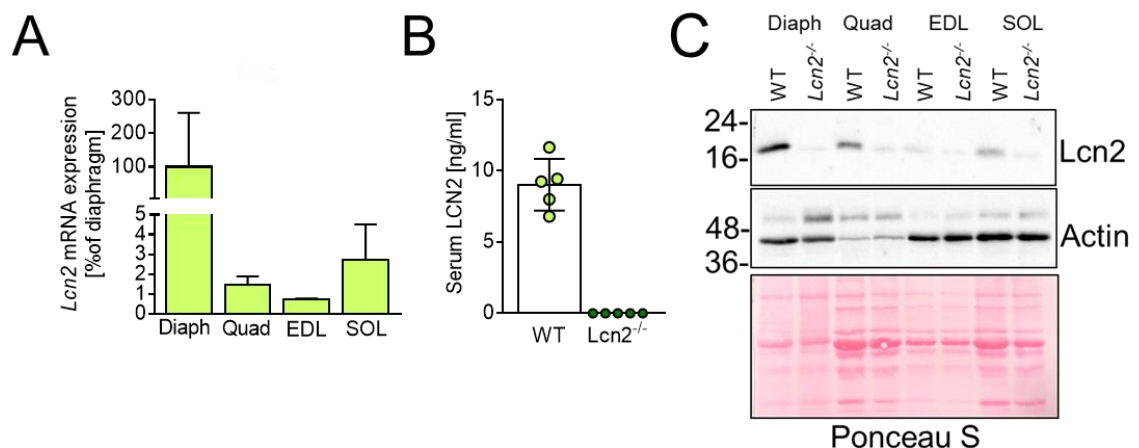


Figure 2: Lipocalin-2 expression in mouse muscle tissues. (A) Lipocalin-2 (*Lcn2*) mRNA expression was analysed in different muscle sections from WT BL6 male mice, namely diaphragm (Dia), quadriceps (Quad), *extensor digitorum longus* (EDL) and *soleus* (SOL). Results are shown as % to the average of the diaphragm Δ Cts. (B) ELISA showing circulating levels of *Lcn2* in WT and *Lcn2*^{-/-} mice. (C) Western blot representative of 3 mice per group, showing muscle expression of *Lcn2* and β -Actin as loading control. Since different levels of actin were present in Quad, ponceau S staining is included as further loading control. (A) N=5 mice per group.

To assess whether *Lcn2* could influence muscle health, we analyzed WT and *Lcn2*^{-/-} mice functionally at 3, 6 and 12 months of age, using the grip strength meter (Figure 3A). We found no difference between the genotypes, indicating normal muscle performance in *Lcn2*^{-/-} mice over the course of their lives. Quadriceps (Figure 3B), EDL (Figure 3C), SOL (Figure 3D) and *tibialis anterior* (TA, Figure 3E) weights were also unaffected during the lifespan

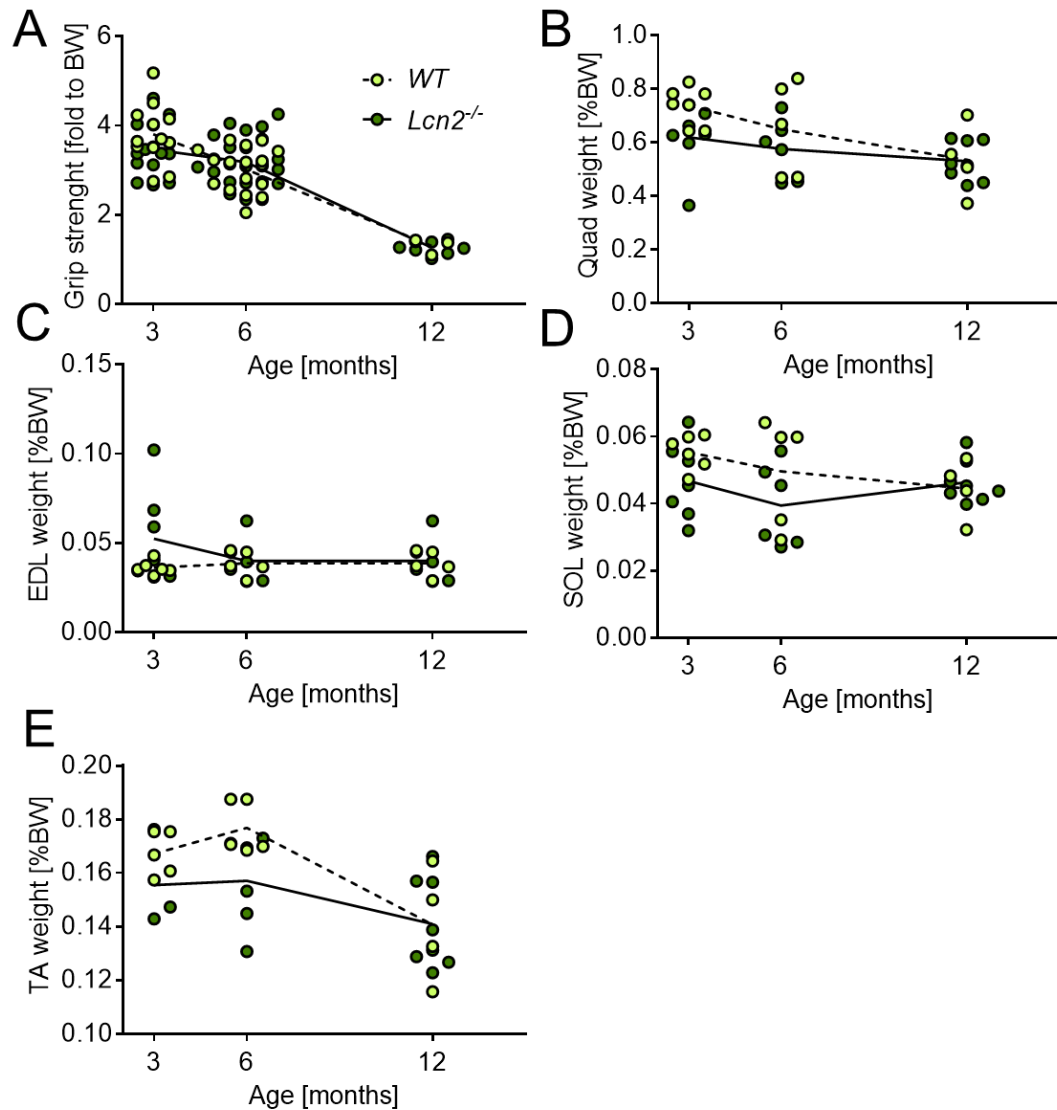


Figure 3: Functional and macroscopic analyses of *Lcn2*^{-/-} muscles. WT or *Lcn2*^{-/-} mice were subjected to (A) grip strength analysis at the ages indicated in the abscissa. Results are expressed as fold to body weight. After sacrifice, (B) quadriceps, (C) EDL, (D) SOL and (E) TA muscles from WT or *Lcn2*^{-/-} mice were weighted at the ages indicated in the abscissa and plotted as % of body weight. Curve fitting test.

of *Lcn2*^{-/-} mice. Consistently, when we analyzed sera of WT and *Lcn2*^{-/-} mice, we found no differences in muscle damage markers myoglobin (Figure 4A) and CK (Figure 4B), while IL6 ranged from 3.9 ± 6.8 pg/ml to 17.13 ± 14.93 pg/ml in WT and was consistently undetectable in *Lcn2*^{-/-} mice (Figure 4C) during their lifespan.

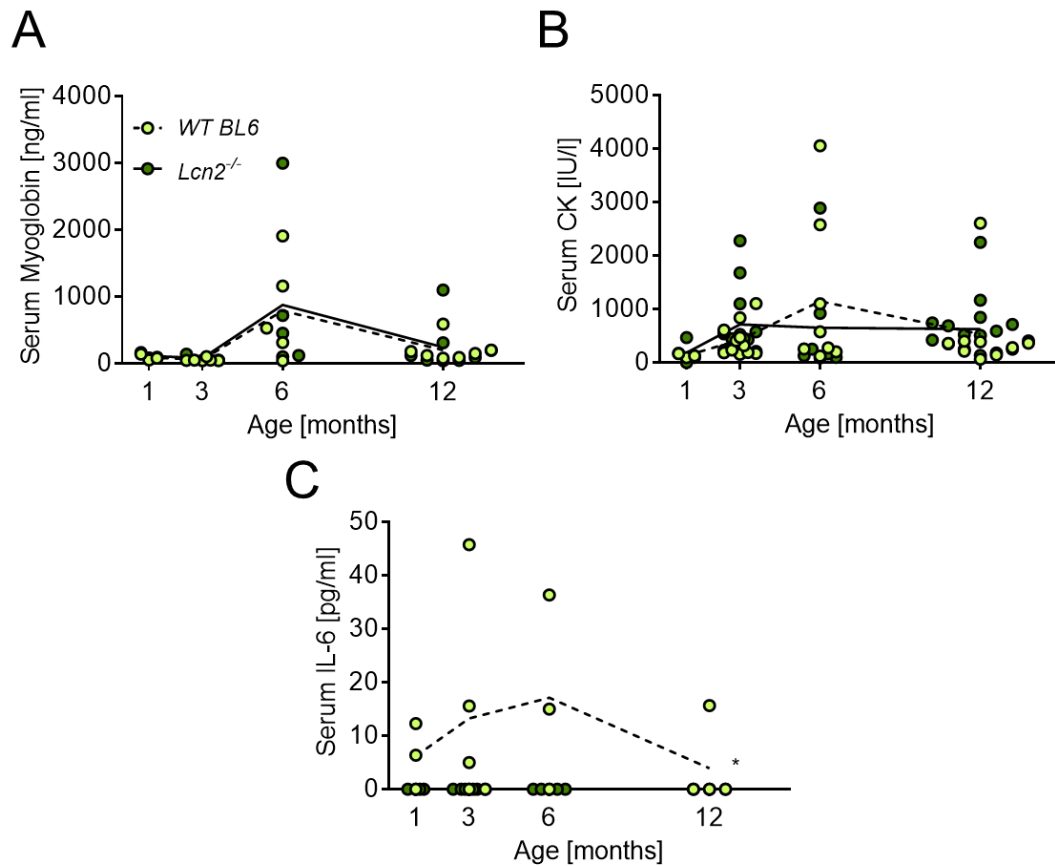


Figure 4: Serum analyses in WT and *Lcn2*^{-/-} mice. WT and *Lcn2*^{-/-} mice were sacrificed at the ages indicated in the abscissa, serum was harvested and used to analyse (A) serum myoglobin (B) CK by reflotron and (C) IL-6. **p*<0.05 vs WT. Curve fitting test.

To dig deeper into the muscle phenotyping, we paraffin-embedded, sectioned and stained quadriceps from WT and *Lcn2*^{-/-} mice of 3, 6 or 12 months of age. We found no difference in the % of intact fibers, all the ages indicated in the figures (Figure 5A-C). Muscle fibrosis was also evaluated in WT and *Lcn2*^{-/-} mice at the same ages which were fully comparable (Fig5D-F). Interestingly, when we analyzed the minimum Feret diameter of quadriceps fibers from WT and *Lcn2*^{-/-}, we found that the latter fibers were smaller (Fig. 5G-I). To further the analyses, we assessed the transcriptional profile of muscles from WT and *Lcn2*^{-/-} mice. At 3 months of age diaphragm shows upregulation of the foetal analogue of dystrophin, utrophin²³⁻²⁶ (Fig.6A). As for the quadriceps, Figure 6B shows that *Lcn2*^{-/-} mice have reduced expression of *Il1b*, increased myogenic genes myogenin (*Myog*), and *Myod1*, which

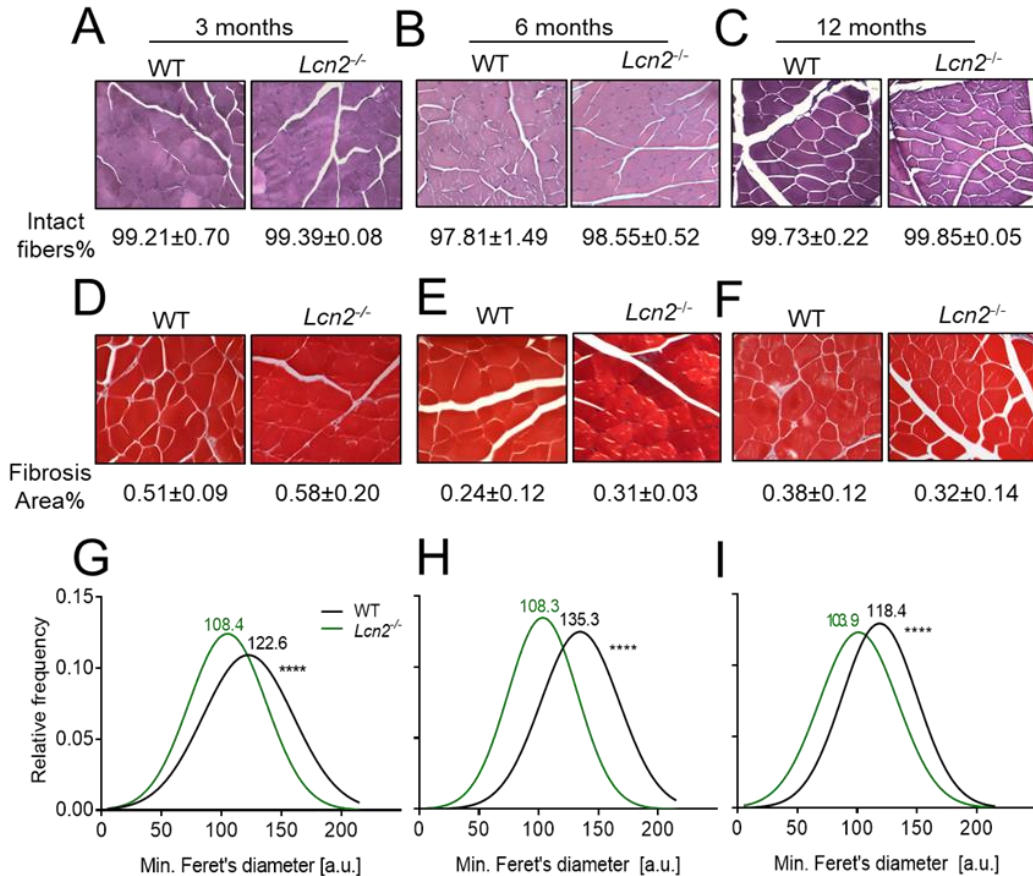


Figure 5: Histological analysis of WT and *Lcn2*^{-/-} mice quadriceps. Quadriceps muscles from WT and *Lcn2*^{-/-} mice were explanted, fixed, paraffin-embedded and sectioned at 5 μ m. (A-C) Hematoxylin-eosin staining was performed on sections from (A) 3, (B) 6, (C) 12 months old mice to analyze % of intact fibers. (D-F) Masson's trichrome staining was used to evaluate %fibrosis area at (D) 3, (E) 6, (F) 12 months. (G-I) after Hematoxylin-eosin staining, minimum Feret's diameter from quadriceps muscle fibers was assessed via software at (G) 3, (H) 6, (I) 12 months of age. Gaussian curves were interpolated to better represent the fiber size distributions. (A-F) N=3-5 mice per group; (G-I) N>1000 fibers per group, arising from N=3-5 mice per group. ****p<0.0001 vs WT. Student's *t*-test.

however only showed a trend of increase (p=0.07). Solei of 3-month old *Lcn2*^{-/-} mice also showed increased *Myog* expression, along with higher Paired box protein (*Pax*7), a marker of satellite cells (Figure 6C). However, 12-month-old mice were unremarkable for diaphragm (Figure 6D) and quadriceps (Figure 6E), while showing a trend inversion in *soleus*, where *Myog* and *Pax*7 were both significantly reduced (Figure 6F). However, tumor necrosis factor alpha (*Tnfa*) showed a trend of decrease in *Lcn2*^{-/-} mice (p=0.06).

To obtain some molecular insights about the action of *Lcn2* in muscle cells, we used *in vitro* models of myogenic progenitors culture, i.e. the widely employed C2C12 cell line²⁷, and primary

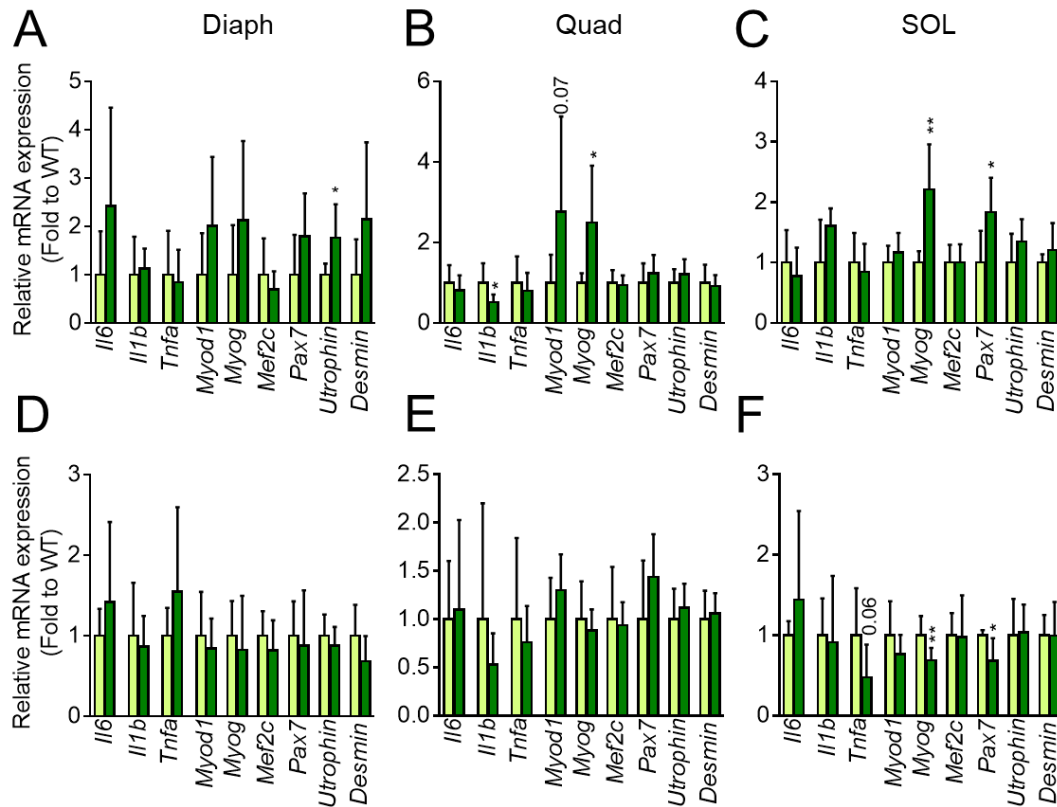


Figure 6: Transcriptional profiling of WT and *Lcn2*^{-/-} mice muscles. RNA was extracted from (A-C) 3-month-old or (D-F) 12-month-old WT or *Lcn2*^{-/-} mice muscles, and a total of 1 µg was reverse-transcribed into cDNA and used for transcriptional analyses. The genes analysed are indicated in the abscissa. The muscles assayed were (A,D) diaphragm, (B-E) quadriceps and (C-F) *soleus*. N=5-10. *p<0.05; **p<0.01 vs WT. Student's *t*-test.

mouse myoblasts. The results show that treating C2C12 myoblasts under fusion medium with recombinant mouse (rm)Lcn2, decreased their differentiation into myotubes, and hence increased the % of myoblast-like, undifferentiated cells (Figure 7A). However, the number of nuclei/myotube was not affected, indicating that the first phases of myogenesis are impaired, rather than the tube elongation after the first fusions. To confirm this finding, we used mouse primary myoblasts, finding comparable results, with increased % of myoblasts, unaffected number of nuclei/myotube, and decreased % of myonuclei (Figure 7B).

Finally, to obtain some indication on the pathway that Lcn2 could be affecting, we performed RT² pathway finder array on C2C12 cells treated with rmLcn2 in fusion medium for 4 days (Figure 7C). Intriguingly, a number of genes were upregulated, including the fat-metabolism genes fatty acid binding protein-1 (*Fabp1*) and Carnitine palmitoyltransferase II (*Cpt2*), erythropoietin (*Epo*), tumor necrosis factor superfamily, member 10 (*Tnfsf10* aka *TRAIL*), members of the Wnt family (*Wnt3a,2b,6*) bone morphogenic protein 2 (*Bmp2*) and

cellular myelocytomatosis (*Myc*). The role of most of these genes in muscle biology is unknown, and needs to be investigated further. However, when clustered using the online tool for protein-protein interaction STRING, they all seem to be linked directly or indirectly (Figure 7D), suggesting that a common pathway might be affected by LCN2 in muscle cells.

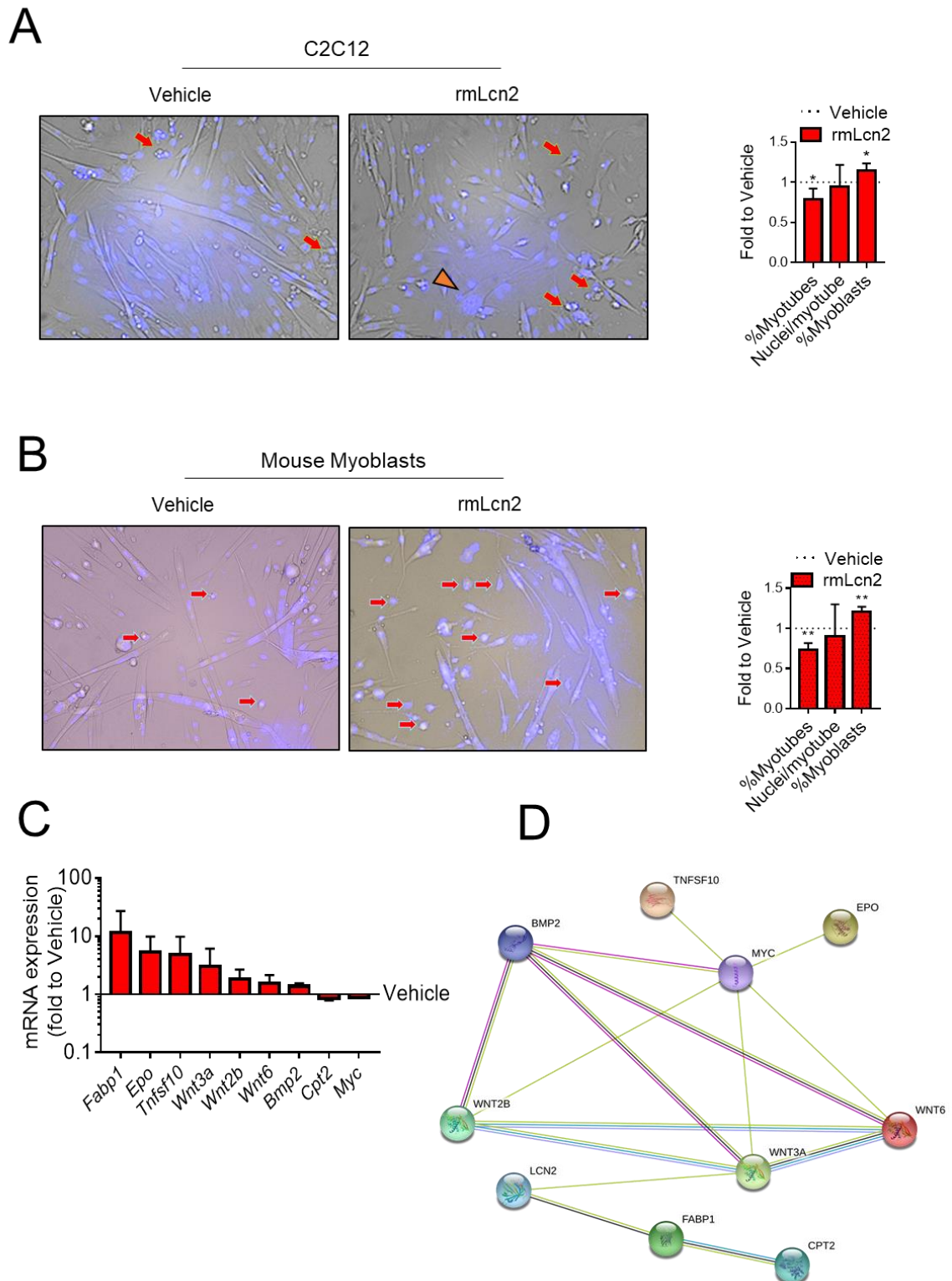


Figure 7: Effect of recombinant Lcn2 *in vitro*. (A-C) C2C12 or (B) primary mouse myoblasts were treated with recombinant mouse (rm) Lipocalin-2 (Lcn2) under myogenic differentiation (fusion) medium for 4 days. (A,B) cells were fixed, stained with DAPI to evidence nuclei, and then hybrid phase contrast-DAPI images were collected to analyse %myonuclei, %myoblasts and number of nuclei/myotube. (C) RNA was extracted from treated C2C12 cells and subjected to pathway finder RT²-array. (D) the genes that emerged from the analyses in (C) were fed to the STRING online interaction analysis software, which returned a possible interaction network. (A-C) N=3. *p<0.05; **p<0.01 vs Vehicle. Student's *t*-test.

5. DISCUSSION

Lcn2 is an interesting multifunctional protein, and new functions it exerts emerge constantly. In this work we tested its role in exercise and muscle biology, finding that it is upregulated after intense exercise, and that it correlates with the Wnt pathway inhibitor DKK1. We then found, in animal models, that *Lcn2* is expressed in some muscles, especially diaphragm, quadriceps and *soleus*. Using *Lcn2*^{-/-} mice, we found that they have normal grip force, muscle weight, muscle fibrosis and essentially all muscle fibers are intact. However, the size of the muscle fibers was consistently smaller in *Lcn2*^{-/-} mice compared to WT at all ages evaluated. This is quite an interesting observation, especially when considering that quadriceps weight was normal. This may mean that the muscle fibers are smaller, but more in number. Another intriguing observation was that the inflammatory cytokine IL6 was undetectable in the sera of *Lcn2*^{-/-} mice during their adult lives. A link between *Lcn2* and IL6 has been proposed in the past⁶, and this observation seems to play into that. The fact that *Lcn2* is also considered a flogosis-related molecule further suggests its partnership with IL-6. Furthermore, we ran transcriptional analyses on WT and *Lcn2*^{-/-} mice muscles at 3 and 12 months of age, evaluating both inflammatory molecules and muscle-related genes. The picture that emerges is that at 3 months of age, the absence of *Lcn2* increases *Utrophin* in diaphragm, *Myod1* and *Myog* in quadriceps, and *Myog* and *Pax7* in *soleus*, while reducing *I1b*, another well-described inflammatory cytokine, in quadriceps. However, this is no longer true at 12 months of age, where most genes are not significantly affected. The only significant differences are in *soleus*, where this time, *Myog* and *Pax7* are significantly reduced. *Pax7* is a satellite cells marker, and an early upregulation, which suggests a higher number of satellite cells, might lead to stem cells pool depletion later in life, leading to a downregulation in this gene. However, this speculation needs to be confirmed with more specific assays. It is however interesting to notice that this peculiar transcriptional behaviour is only observed in *soleus*, the only slow twitch fibers-enriched muscle of the lot.

Treating muscle cells with rm*Lcn2* in vitro, also led to detrimental effects, with an impairment in myogenic differentiation. Transcriptionally, rm*Lcn2* treatment led to several unexpected effects, namely the mRNA upregulation of genes coding for proteins that have never been associated to muscle biology before: *Fabp1*, *Epo*, *Tnfsf10* aka *TRAIL*, *Wnt3a,2b,6*, *Bmp2* and downregulation of *Cpt2* and *Myc*. This could open new research avenues to elucidate whether these proteins are able to influence muscle biology directly. Particular interest should be placed on *TRAIL*, which is an extrinsic apoptosis-inducing protein, that is able to bind and inactivate a very important protein in bone biology: OPG

(osteoprotegerin). Since bone is the primary partner of muscle, the Lcn2-mediated crosstalk between the two needs to be investigated. Furthermore, the fact that LCN2 is considered an adipokine, and the fact that Lcn2^{-/-} mice have increased body fat⁸, suggests that also bone marrow adipocytes (BMAs) may play a role in the phenotype of Lcn2^{-/-} mice, being usually inversely correlated to white adipose tissue. This is also consistent with the fact that Lcn2 has been suggested to influence the fate of bone marrow stromal cells²⁸. BMAs has endocrine functions²⁹, and influences both bone metabolism³⁰, which might in turn influence muscle. In conclusion, here we show that Lcn2 is dispensable for normal muscle function, while its upregulation is found in muscle damage, and reduces myogenic differentiation.

6. References

1. Lögdberg, L. & Wester, L. Immunocalins: A lipocalin subfamily that modulates immune and inflammatory responses. *Biochim. Biophys. Acta - Protein Struct. Mol. Enzymol.* **1482**, 284–297 (2000).
2. Abella, V. *et al.* The potential of lipocalin-2/NGAL as biomarker for inflammatory and metabolic diseases. *Biomarkers* **20**, 565–571 (2015).
3. Ding, L. *et al.* Lipocalin-2/neutrophil gelatinase-B associated lipocalin is strongly induced in hearts of rats with autoimmune myocarditis and in human myocarditis. *Circ. J.* (2010) doi:10.1253/circj.CJ-09-0485.
4. Mishra, J. *et al.* Kidney NGAL is a novel early marker of acute injury following transplantation. *Pediatr. Nephrol.* (2006) doi:10.1007/s00467-006-0055-0.
5. Mishra, J. *et al.* Identification of neutrophil gelatinase-associated lipocalin as a novel early urinary biomarker for ischemic renal injury. *J. Am. Soc. Nephrol.* (2003) doi:10.1097/01.ASN.0000088027.54400.C6.
6. Rucci, N. *et al.* Lipocalin 2: A new mechanoresponding gene regulating bone homeostasis. *J. Bone Miner. Res.* (2015) doi:10.1002/jbmr.2341.
7. Capulli, M., Rufo, A., Teti, A. & Rucci, N. Global transcriptome analysis in mouse calvarial osteoblasts highlights sets of genes regulated by modeled microgravity and identifies A ‘mechanoresponsive osteoblast gene signature’. *J. Cell. Biochem.* (2009) doi:10.1002/jcb.22120.
8. Capulli, M. *et al.* A Complex Role for Lipocalin 2 in Bone Metabolism: Global Ablation in Mice Induces Osteopenia Caused by an Altered Energy Metabolism. *J. Bone Miner. Res.* **33**, (2018).
9. Veeriah, V. *et al.* Interleukin-1 β , lipocalin 2 and nitric oxide synthase 2 are mechano-responsive mediators of mouse and human endothelial cell-osteoblast crosstalk. *Sci. Rep.* (2016) doi:10.1038/srep29880.
10. Mosialou, I. *et al.* MC4R-dependent suppression of appetite by bone-derived lipocalin 2. *Nature* (2017) doi:10.1038/nature21697.
11. Costa, D. *et al.* Altered bone development and turnover in transgenic mice over-expressing Lipocalin-2 in bone. *J. Cell. Physiol.* (2013) doi:10.1002/jcp.24391.
12. Rebalka, I. A. *et al.* Loss of the adipokine lipocalin-2 impairs satellite cell activation

- and skeletal muscle regeneration. *Am. J. Physiol. - Cell Physiol.* (2018) doi:10.1152/ajpcell.00195.2017.
13. Gambara, G. *et al.* Microgravity-induced transcriptome adaptation in mouse paraspinal longissimus dorsi muscle highlights insulin resistance-linked genes. *Front. Physiol.* (2017) doi:10.3389/fphys.2017.00279.
 14. Marques, F. Z. *et al.* Experimental and Human Evidence for Lipocalin-2 (Neutrophil Gelatinase-Associated Lipocalin [NGAL]) in the Development of Cardiac Hypertrophy and heart failure. *J. Am. Heart Assoc.* (2017) doi:10.1161/JAHA.117.005971.
 15. Sung, H. K. *et al.* Lipocalin-2 (NGAL) Attenuates Autophagy to Exacerbate Cardiac Apoptosis Induced by Myocardial Ischemia. *J. Cell. Physiol.* (2017) doi:10.1002/jcp.25672.
 16. Xu, G. *et al.* Lipocalin-2 induces cardiomyocyte apoptosis by increasing intracellular iron accumulation. *J. Biol. Chem.* (2012) doi:10.1074/jbc.M111.275719.
 17. Berger, T. *et al.* Lipocalin 2-deficient mice exhibit increased sensitivity to *Escherichia coli* infection but not to ischemia-reperfusion injury. *Proc. Natl. Acad. Sci. U. S. A.* (2006) doi:10.1073/pnas.0510847103.
 18. Springer, M. L., Rando, T. A. & Blau, H. M. Gene Delivery to Muscle. in *Current Protocols in Human Genetics* (2002). doi:10.1002/0471142905.hg1304s31.
 19. Keire, P., Shearer, A., Shefer, G. & Yablonka-Reuveni, Z. Isolation and culture of skeletal muscle myofibers as a means to analyze satellite cells. *Methods Mol. Biol.* (2013) doi:10.1007/978-1-62703-128-8-28.
 20. Dubach-Powell, J. Quantitative determination of muscle fiber diameter (minimal Feret's diameter) and percentage of centralized nuclei. *treat-NMD* 1–16 (2011).
 21. Grounds, M. Quantification of histopathology in Haematoxylin and Eosin stained muscle sections. *TREAT-NMD Neuromuscul. Netw.* 1–14 (2012).
 22. Gutpel, K. M., Hrinivich, W. T. & Hoffman, L. M. Skeletal muscle fibrosis in the mdx/utrn+/- mouse validates its suitability as a murine model of duchenne muscular dystrophy. *PLoS One* (2015) doi:10.1371/journal.pone.0117306.
 23. Tinsley, J. *et al.* Expression of full-length utrophin prevents muscular dystrophy in mdx mice. *Nat. Med.* (1998) doi:10.1038/4033.
 24. Tinsley, J. M. *et al.* Amelioration of the dystrophic phenotype of mdx mice using a truncated utrophin transgene. *Nature* (1996) doi:10.1038/384349a0.
 25. Song, Y. *et al.* Non-immunogenic utrophin gene therapy for the treatment of muscular dystrophy animal models. *Nature Medicine* (2019) doi:10.1038/s41591-019-0594-0.
 26. Fairclough, R. J., Wood, M. J. & Davies, K. E. Therapy for Duchenne muscular dystrophy: Renewed optimism from genetic approaches. *Nat. Rev. Genet.* (2013) doi:10.1038/nrg3460.
 27. Burattini, S. *et al.* C2C12 murine myoblasts as a model of skeletal muscle development: Morpho-functional characterization. *Eur. J. Histochem.* (2004) doi:10.4081/891.

28. Lu, M. *et al.* Lipocalin produced by myelofibrosis cells affects the fate of both hematopoietic and marrow microenvironmental cells. *Blood* (2015) doi:10.1182/blood-2014-12-618595.
29. Cawthorn, W. P. *et al.* Bone marrow adipose tissue is an endocrine organ that contributes to increased circulating adiponectin during caloric restriction. *Cell Metab.* (2014) doi:10.1016/j.cmet.2014.06.003.
30. Muruganandan, S., Govindarajan, R. & Sinal, C. J. Bone Marrow Adipose Tissue and Skeletal Health. *Current Osteoporosis Reports* (2018) doi:10.1007/s11914-018-0451-y.



Chapter 4

“Lipocalin 2 in the bone and muscle phenotype of the MDX mouse model of DMD”

1. ABSTRACT

Lipocalin 2 (Lcn2) is an adipokine linked to bone and energy metabolism. Its serum levels directly correlate to mechanical unloading and inflammation, both hallmarks of Duchenne Muscular Dystrophy (DMD). Furthermore, we found it to be upregulated after intense exercise in healthy volunteers, and to be directly correlated with a bone formation inhibitor. We therefore investigated the role of Lcn2 in muscle failure-induced bone loss in the *MDX* mouse model of DMD. We found increased Lcn2 serum levels in *MDX* mice at 1, 3, 6 and 12 months of age. Consistently, *Lcn2* mRNA was higher in *MDX* versus WT diaphragm, quadriceps, soleus and extensor digitorum longus muscles. Immunohistochemistry confirmed this and also showed that Lcn2 is mainly expressed by mononuclear cells in diaphragm and quadriceps, although positive muscle fibers were also observed. *Lcn2* also correlated with the inflammatory cytokines-coding genes *IL1B* and *TNFA*. Based on these results, we ablated *Lcn2* in *MDX* mice by crossbreeding them with *Lcn2*^{-/-} mice (*MDXxLcn2*^{-/-}, double mutant/dMUT) and analyzed their bone and muscle phenotype. MicroCT analyses showed higher trabecular Bone volume/Tissue volume (BV/TV) % and number in dMUT mice compared to *MDX*, likely due to reduced bone resorption, evaluated by serum carboxy-terminal of crosslinked collagen (CTx). Similar results were found at 6-month-old-mice, although also osteoblast number (Ob.N) was increased in dMUT, compared to *MDX*. Intriguingly, 3-month-old dMUT mice had higher muscle strength, evaluated by grip strength meter. This was consistent with the fact that dMUT had increased intact muscle fibres and strongly reduced serum creatine kinase (CK) levels, which indicates reduced muscle damage. Similar results were found in 6-month-old mice, where also quadriceps fibrosis was reduced. To strengthen these findings, we inhibited Lcn2 by treating 2-month-old *MDX* mice with a Lcn2-blocking monoclonal antibody, which increased Tb.BV/TV, and reduced osteoclast surface/bone surface compared to *MDX* mice treated with irrelevant IgG. On the muscle side, grip force was increased and diaphragm fibrosis was reduced by the Lcn2-mAb. Increased BV/TV was also observed when treating 2-week-old *MDX* to mimic a preventive treatment. These results point at Lcn2 as a possible target in DMD-induced bone and muscle wasting in the *MDX* mouse model of DMD.

2. INTRODUCTION

Lipocalin 2 (Lcn2), is a multifunctional protein that has been proposed to be important for different aspects of physiopathology. Structurally, it belongs to the lipocalin superfamily¹. Lcn2 is involved in inflammation², and many other aspects, including mechanical unloading and bone physiopathology³⁻⁸. In particular, Lcn2 emerges as a complex player in bone biology, which is detrimental for bone health when upregulated in hindlimb suspension and bed rest models³ but at the same time, its absence causes osteopenia in basal conditions⁵. These findings show that Lipocalin-2 is a complex molecule, which seems to play different roles in different contexts. Since Lcn2 is involved in both disuse and inflammation, is upregulated after muscle stress, as well as in femurs of *MDX* mice, in this chapter we aimed at characterizing LCN2 in the pathology of this mouse model of Duchenne Muscular Dystrophy (DMD), using *in vivo* mouse studies and focusing on bone and muscle biology.

3. MATERIAL AND METHODS

3.1 MATERIALS

TRIzol reagent, primers and reagents for RT-PCR were from Invitrogen (Carlsbad, CA, USA). The Sensimix SYBR Green QPCR master mix was from Bioline (Memphis, TN). Masson's trichrome kit and other histological supplies were from Bio Optica (Milan, Italy) ELISA assays: Lcn2 was from R&D, (cat# MLCN20, Minneapolis, MN, USA), Myoglobin (cat# ab210965) and interleukin (IL)-6 (cat# ab100712) were from Abcam (Cambridge, UK), IL-1 β (cat# ELM-IL1b-1) was from Raybiotech (Atlanta, GE, USA), bone alkaline phosphatase (BALP, cat# CSB-E11914m) was from Cusabio (Houston, TX, USA), carboxy terminal collagen crosslinks (CTx) EIA (Cat#AC-06F1) kit was from IDS (The Boldons, UK). Reflotron PLUS (Roche, Basel, Switzerland) reactive strips were used to evaluate creatine kinase. Reactives to analyze calcium concentration were from Randox (Crumlin, UK), while the phosphate evaluation kit (cat# ab65622) was from Abcam. All the other reagents were of the purest grade from Sigma Aldrich Co. (St. Louis, MO, USA).

3.2 ANIMALS

Lcn2^{-/-} mice (background C57BL6/J) were generated and kindly provided by Dr. Tak Wah Mak (University Health Network, Toronto, ON, Canada)⁹. *MDX* mice and C57BL10 mice were purchased from the Jackson laboratory. *MDXxLcn2*^{-/-} and C57BL6x10 mice were obtained by in-house crossbreeding. All procedures involving animals and their care were conducted in conformity with national and international laws and policies (European Economic Community Council Directive 86/609, OJ L 358, 1, December 12, 1987; Italian

Legislative Decree 4.03.2014, n.26, *Gazzetta Ufficiale della Repubblica Italiana* no. 61, March 4, 2014) and the Animal Research: Reporting of In Vivo Experiments (ARRIVE) guidelines. Mice were housed in the animal facility of the University of L'Aquila, Italy, at the following conditions: temperature: 20°C to 24°C, humidity: 60%, dark/light cycle: 12/12 hours. They had access to food and water *ad libitum* and were fed with a standard diet (Mucedola code: 4RF21) composed of 60.8% carbohydrates, 21% proteins, 3.45% fat, 6.8% fibers, 7.95% trace elements, and 12% humidity.

3.3 ANTI-LCN2 ANTIBODY TREATMENT

The antibody used to neutralize Lcn2 *in vivo* on *MDX* mice was commercially available from R&D (cat# MAB18571), and has previously been used to this end by other investigators¹⁰. According to Cheng et al.¹⁰, and Pelosi et al.¹¹, for both curative and preventive protocols we used a priming dose of 3.75 mg/kg and 3 (preventive protocol) or 6 (curative protocol) maintenance doses of 0.75 mg/kg, starting 1 week after the priming shot. The curative protocol was administered to 60-day-old mice and lasted 30 days in total (Figure 9A). The preventive protocol was administered to 15-day-old mice and lasted 15 days in total (Figure 11A). Both curative and preventive treatments were carried out in 2 *tranches* by 2 independent investigators.

3.4 COMPARATIVE REAL-TIME RT-PCR

Total RNA was extracted from mouse muscles using the TRIzol[®] method. One microgram of RNA was reverse transcribed into cDNA using Moloney Murine Leukemia Virus (M-MLV) reverse transcriptase and the equivalent of 0.1 µg was processed using The Sensimix SYBR Green QPCR master mix for real-time PCR. Results, calculated as fold to WT average using the $\Delta\Delta C_t$ method, were normalized versus the housekeeping gene glycerol-3-phosphate dehydrogenase (*GAPDH*).

3.5 HISTOLOGY AND HISTOPATHOLOGY

After sacrificing mice with CO₂, diaphragm (Diaph), *quadriceps* (Quad), *soleus* (SOL), *extensor digitorum longus* (EDL) and *tibialis anterior* (TA) muscles (depending on age and experiment) were isolated, equalized in OCT medium for 10 minutes, put into cryomolds and snap-frozen in liquid nitrogen-cooled isopentane before storage at -80°C. Seven µm sections were obtained after equalization at -25°C using a Leica CM1850 cryostat and used immediately for staining with hematoxylin-eosin or Masson's trichrome kit (Bio Optica). After staining, sections were dehydrated and mounted with permanent medium (Eukitt). To calculate the % of intact fibers, we used well-established methods¹². Briefly, the non-centrally nucleated, -fibrotic, -necrotic fibers were counted in hematoxylin-eosin stained

sections and plotted as percentage of total number of fibers. To calculate % of fibrotic tissue, we used the ImageJ software to select fibrotic tissue in muscles following Masson's trichrome staining, and calculated the % fibrotic area to total area¹³.

Immunohistochemistry for Lcn2 was performed using 5µm sections of formalin-fixed paraffin-embedded quadriceps or diaphragm. Antigen retrieval was performed using pH 6 sodium citrate, and the detection kit was from Vector Laboratories (PK-6105). The anti-Lcn2 primary antibody was from R&D (AF1857).

3.6 BONE HISTOMORPHOMETRY

Tibiae explanted from euthanized WT and *Lcn2*^{-/-} mice were fixed in 4% paraformaldehyde, dehydrated in alcohol, and processed for methyl-methacrylate embedding without decalcification. Histomorphometric measurements were carried out on 5-µm-thick sections with an interactive image analysis system (IAS 2000; Delta Sistemi, Rome, Italy)¹⁴ and with the suggested nomenclature¹⁵. Osteoclast number/bone surface (number/mm²) and osteoclast surface/bone surface (%) were evaluated after histochemically staining the sections for TRAcP activity. Osteoblast surface/bone surface (%) was evaluated in sections stained with toluidine blue.

3.7 MICRO-CT ANALYSIS

Images of tibiae previously fixed in 4% paraformaldehyde were acquired using the SkyScan 1174 (Bruker, Billerica, MA, USA) with a resolution of 6.7µm (X-ray voltage 50 kV). Image reconstruction was carried out employing a modified Feldkamp algorithm¹⁶, using the Skyscan Nrecon software. Three-dimensional (3D) and two-dimensional (2D) morphometric parameters were calculated for the trabecular bone, 100 slides (6.7µm thick) from the growth plate¹⁷. 3D parameters were based on analysis of a Marching Cubes-type model with a rendered surface¹⁸. Calculation of all 2D areas and perimeters was based on the Pratt algorithm¹⁹. Bone structural variables and nomenclature were those suggested by Bouxsein and colleagues²⁰. Cortical bone thickness was analysed 450 slides below the growth plate on 54 slides as described¹⁷.

3.8 BIODENT ® MECHANICAL TESTING

Tibiae were harvested from treated mice, cleaned free of soft tissue and stored at -80 °C. After thawing, the mechanical test was performed on the distal portion of the tibia,

immediately above the insertion of the fibula, using the Reference Point Indentation (RPI) technique by Biodent®. Bones were kept in ice-cold PBS during the test to maintain tissue hydration. All the samples were tested using 5 to 10 indentation cycles at 2 Hertz (Hz) utilizing a force of 2 or 4 Newton (N) depending on the age of the mice. Indentation distance (ID) and Total indentation distance (TID) were calculated for each test following the software's instructions.

3.9 STATISTICS

Results were expressed as the mean±SD. Correlation analyses were performed using Pearson's correlation test (R and P values are indicated in the graphs). To compare curves in longitudinal studies, Graphpad Prism 7.0 was used to run curve fitting tests to evaluate whether one curve could efficiently fit the datasets compared. In experiments with more than 2 independent experimental groups, one-way ANOVA was used to calculate significance. Unpaired Student's *t*-test was used when comparing 2 groups. A *p* value <0.05 was considered statistically significant.

4. RESULTS

To understand the role of *Lcn2* in DMD pathophysiology, we first evaluated its concentration in sera of WT BL10 and *MDX* mice, finding it was significantly higher in the latter, at 1, 3, 6 and 12 months of age (Figure 1A). We next evaluated its expression in diaphragm (Diaph), *quadriceps femoris* (Quad), soleus (SOL) and *extensor digitorum longus* (EDL), finding that it was increased in all *MDX* muscles evaluated (Figure 1B). Immunohistochemical analysis confirmed the higher amount of *Lcn2* found at the transcriptional level and showed that this protein was mainly expressed in mononuclear cells between muscle fibers, although some positivity was also found in the fibers themselves (Figure 1C). We then moved to analysing inflammation. An increase in serum *Il6* was observed at 1 and 6 months of age in *MDX* mice (Figure 2A) while circulating levels of *Il1β* were unremarkable (Figure 2B). At the transcriptional level, *Il6* was not significantly affected in diaphragm (Diaph), undetectable in SOL and EDL, while a trend of upregulation was found in *MDX* Quad, compared to WT (Figure 2C). *Il1b* was significantly upregulated in Diaph and SOL of *MDX* vs WT, and a trend of upregulation was found in Quad and EDL (Figure 2D), while *Tnfa* did not change between the two genotypes (Figure 2E). Hence, *Lcn2* was the most consistently upregulated inflammatory factor in muscle in our hands. However, we found a significant correlation between mRNA expression of *Lcn2*, *IL1B* and *TNFA* in

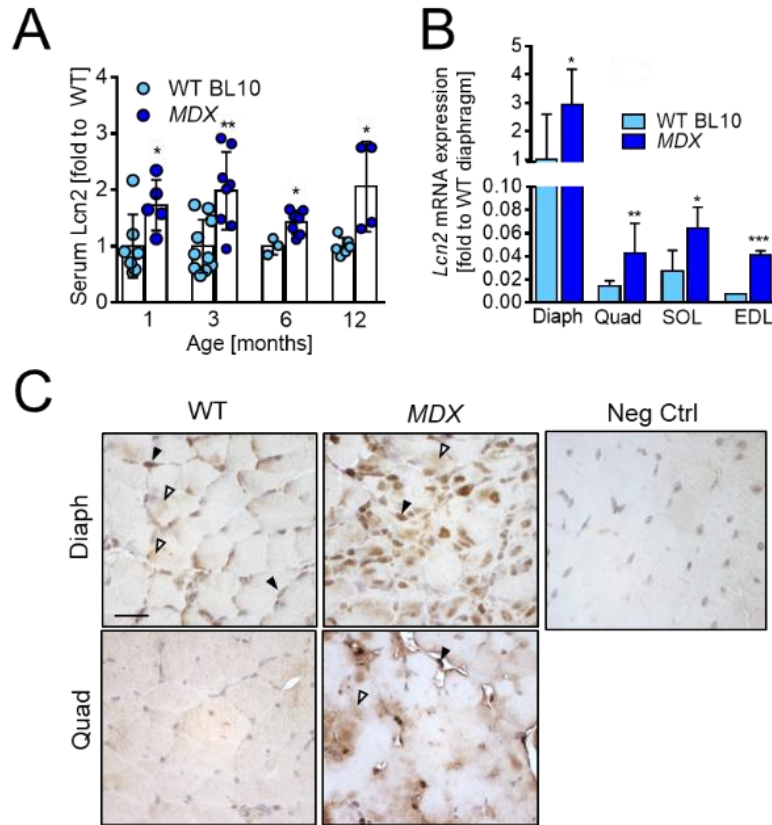


Figure 1: Lipocalin 2 expression in MDX. WT BL10 or MDX mice were sacrificed to analyse their (A) serum expression of Lcn2. Diaphragm (Diaph), quadriceps (Quad), soleus (SOL) and *extensor digitorum longus* (EDL) muscles from 1-month-old mice of the same genotypes were isolated, and RNA was extracted from them to evaluate (B) transcriptional expression of *Lcn2*. Quad and Diaph were also fixed in PFA, embedded in paraffin and sectioned. (C) shows immunohistochemical analysis for Lcn2 in said muscles. Black arrowhead: mononuclear cells positive for Lcn2; white arrowhead: positivity for Lcn2 in muscle fibers. Bar=25µm. (A,B) Student's *t*-test. **p*<0.05; ***p*<0.01; ****p*<0.001. (B) N=5

MDX (Figure 2F,G) while correlation between the former 2 was unremarkable in WT (Figure 2H). A stronger correlation was observed between *Lcn2* and *TNFA* in WT (Figure 2I) vs MDX (Figure 2G). Since we demonstrated that removing Lcn2 is not detrimental for muscle (chapter 2 of this dissertation) we crossbred *Lcn2*^{-/-} mice with MDX to obtain MDXx*Lcn2*^{-/-} mice, i.e. MDX mice genetically lacking *Lcn2*. Since the 3 mice have 3 slightly different backgrounds (C57BL6 for *Lcn2*^{-/-}, C57BL10 for MDX and C57BL6x10 for MDXx*Lcn2*^{-/-} mice) data will be presented as fold to the appropriate WT. Surprisingly, µCT analyses showed that at 3 months of age, while MDX mice have low trabecular bone volume/tissue volume (BV/TV)% vs their WT, removing Lcn2 rescues this reduction (Figure 3A), due to increased trabecular (Tb) number (N, Figure 3B) and reduced separation (Sp, Figure 3D), with no difference in thickness (Th, Figure 3C). Cortical (Ct) thickness was not affected (Figure 3F). The rescue in bone mass may be due to a reduction in osteoclast activity,

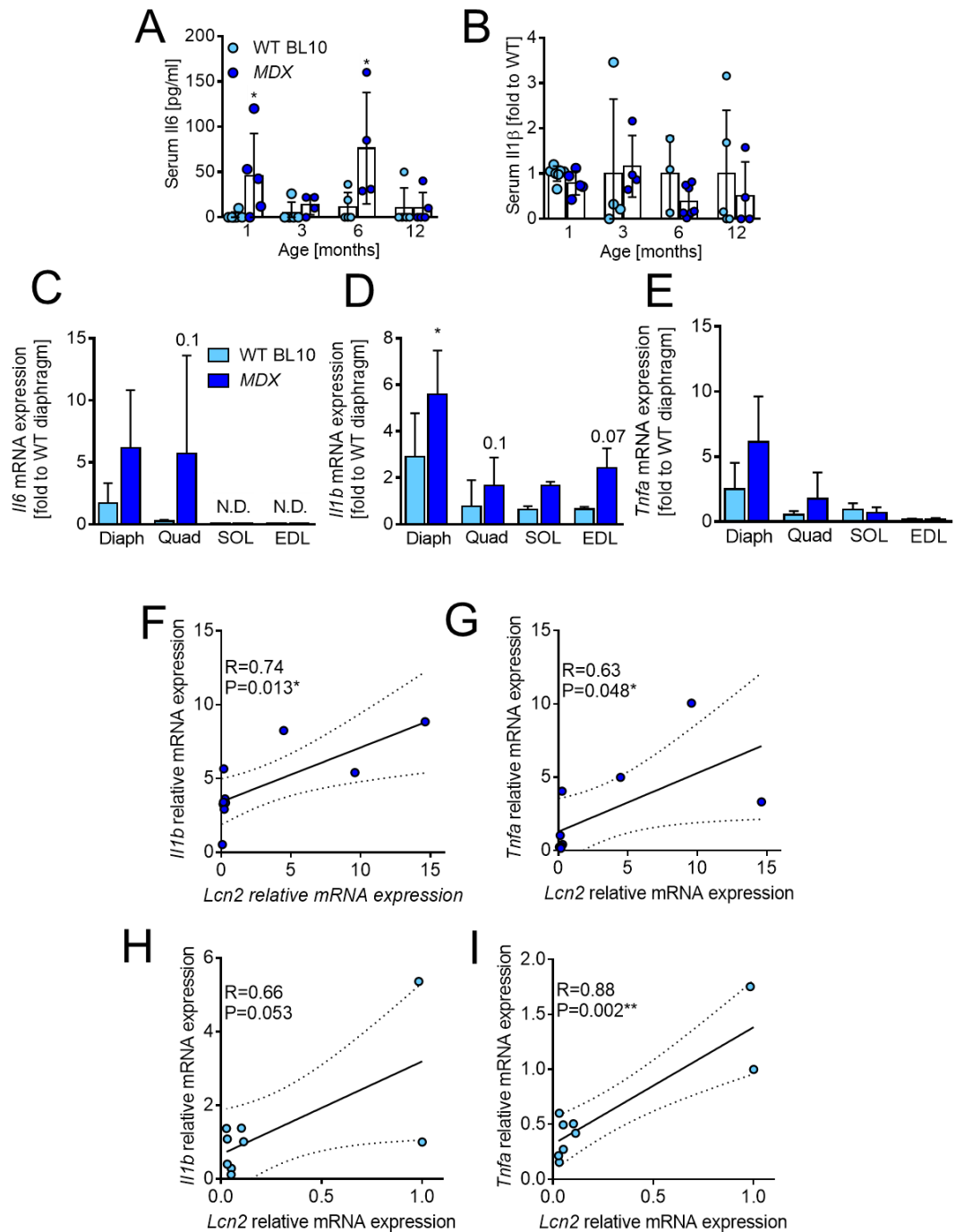


Figure 2: inflammatory cytokines and Lipocalin-2 expression in MDX mice. WT BL10 or MDX mice were sacrificed to analyse their serum expression of (A) Interleukin (IL)6 and (B) IL1 β . Diaphragm (Diaph), quadriceps (Quad), soleus (SOL) and *extensor digitorum longus* (EDL) muscles from 1-month-old mice of the same genotypes were isolated, and RNA was extracted from them to evaluate transcriptional expression of (C) *Il6*, (D) *Il1b*, (E) tumor necrosis factor (*Tnf*) α . Then, correlation studies were ran on MDX muscles between the expression of *Lcn2* and (F) *Il1b* or (G) *Tnf* α . The same was done between *Lcn2* and (H) *Il1b* or (I) *Tnf* α in WT. (C-E) N=5 mice per group. (A-E) Student's *t*-test. * $p < 0.05$; p values between 0.05 and 0.1 are explicated. (F-I) Pearson's correlation. R and P values are written in the graph.

as suggested by analysis of the bone resorption marker carboxy-terminal collagen crosslinks (CTx) in *MDXxLcn2^{-/-}* mice vs *MDX* (Figure 3F). Next, we analyzed the mechanical properties of tibiae harvested from 3-month-old mice via reference point indentation (RPI) analysis (Biodent). We assessed indentation distance (ID) and total indentation distance (TID) which are inversely correlated with mechanical proficiency of the bone. ID was not significantly affected in any of the group, although a trend of increase was found in *Lcn2^{-/-}* and *MDX* vs their WT ($p=0.056$ and $p=0.055$ respectively, Figure 3G). However, the TID was significantly reduced in *MDXxLcn2^{-/-}* mice vs *MDX*, and the latter TID was significantly higher vs WT (Figure 3H), indicating that *Lcn2* removal is able to revert the loss of bone mechanical properties observed in *MDX* mice at 3 months of age. At 6 months of age, we found a similar rescue of bone phenotype when removing *Lcn2* from *MDX* mice: BV/TV% was increased and brought back to WT levels (Figure 4A), due to increased Tb.N (Figure 4B) with no significant differences in Tb.Th (Figure 4C) and Sp (Figure 4D) in *MDXxLcn2^{-/-}* mice vs *MDX*. However, it should be noted that *MDX* mice have significantly lower Tb.Th (Figure 4C) and higher Sp (Figure 4D) compared to their WT, which is not observed in *MDXxLcn2^{-/-}* mice. Intriguingly, Ct.Th was reduced in *MDX* mice at 6 months of age as well (Figure 4E), while *MDXxLcn2^{-/-}* showed significantly higher Ct.Th compared to *MDX* alone. As for the mechanical properties of 6 months old mice, ID, which showed a trend of increase in *MDX* vs WT ($p=0.08$), was significantly reduced when removing *Lcn2* (Figure 4F), which was also true for TID (Figure 4G). Consistently with what we observed at 3 months of age, osteoclast parameters were affected: osteoclast surface/bone surface% was reduced by *Lcn2* removal in *MDX*, which had an increase in this parameter compared to WT (Figure 4H). The same was true for osteoclast number (Figure 4I). Intriguingly, also osteoblast parameters were affected, with significant increases in both osteoblast surface/bone surface (Figure 4J) and number/bone surface (Figure 4K). We then moved to analyze muscle phenotype in the same experimental groups. Investigating muscle performance at 3 months of age by grip force test showed a significant decrease in *MDX* mice vs WT, which was completely abrogated by removing *Lcn2* (Figure 5A). This was accompanied by a significant reduction of the muscle damage marker creatine kinase (CK) in *MDXxLcn2^{-/-}* mice vs *MDX*, the latter also being significantly higher than the relative WT (Figure 5B). The same trend was observed histologically, with a reduction of fibrosis evaluated by Masson's trichrome in quadriceps of *MDXxLcn2^{-/-}* mice (Figure 5C), which was however still significantly higher than the relative WT. The percentage of intact fibers was also increased in *MDXxLcn2^{-/-}* mice vs *MDX*, although still being far from WT levels (Figure 5D). Similarly, 6-month-old *MDX*

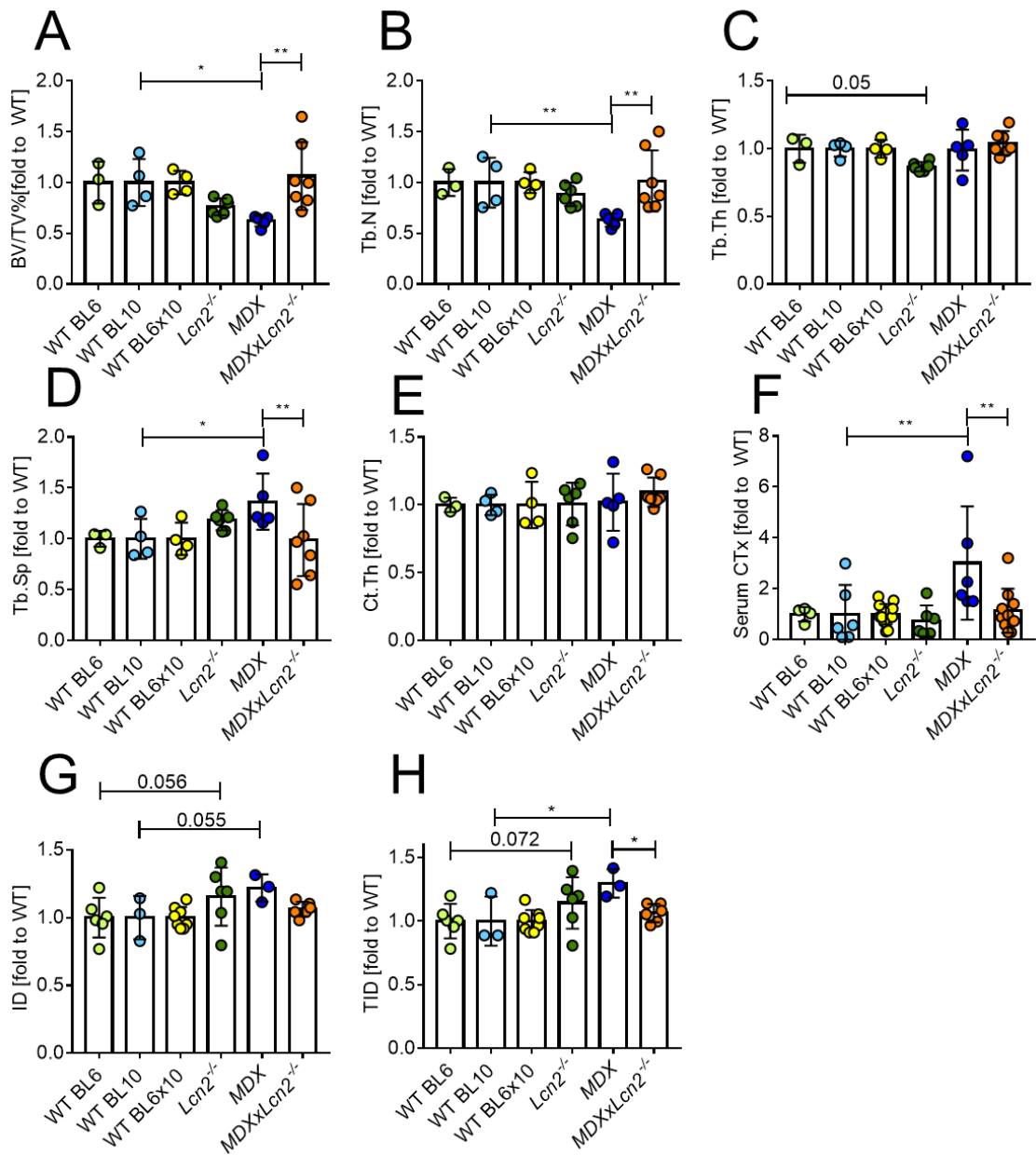


Figure 3: Bone phenotype of 3 months old mice. Tibiae were explanted from 3 months old mice and cancellous bone from proximal tibia was subjected to μ CT analysis to evaluate trabecular (A) bone volume/tissue volume%, (B) number, (C) thickness, (D) separation. Tibial cortical bone was also analysed to evaluate its (E) thickness. Serum from 3 months old mice was also harvested to evaluate (F) carboxy-terminal collagen crosslinks (CTx). Tibiae were then subjected to biomechanical testing via the Biodent reference point indentation analysis instrument, to assess (G) indentation distance and (H) total indentation distance. One-way ANOVA. * $p < 0.05$; ** $p < 0.01$; p values between 0.05 and 0.1 are explicated.

had lower grip force vs WT and MDXxLcn2^{-/-} (Figure 6A). Serum analysis showed significantly higher CK in MDX vs WT (Figure 6B), although the increase was not nearly as severe as what we observed at 3 months of age. However, similar to what we observed in younger animals, CK was significantly lower in MDXxLcn2^{-/-} vs MDX. As for the histopathological aspects, quadriceps fibrosis was higher in both MDX and MDXxLcn2^{-/-} vs

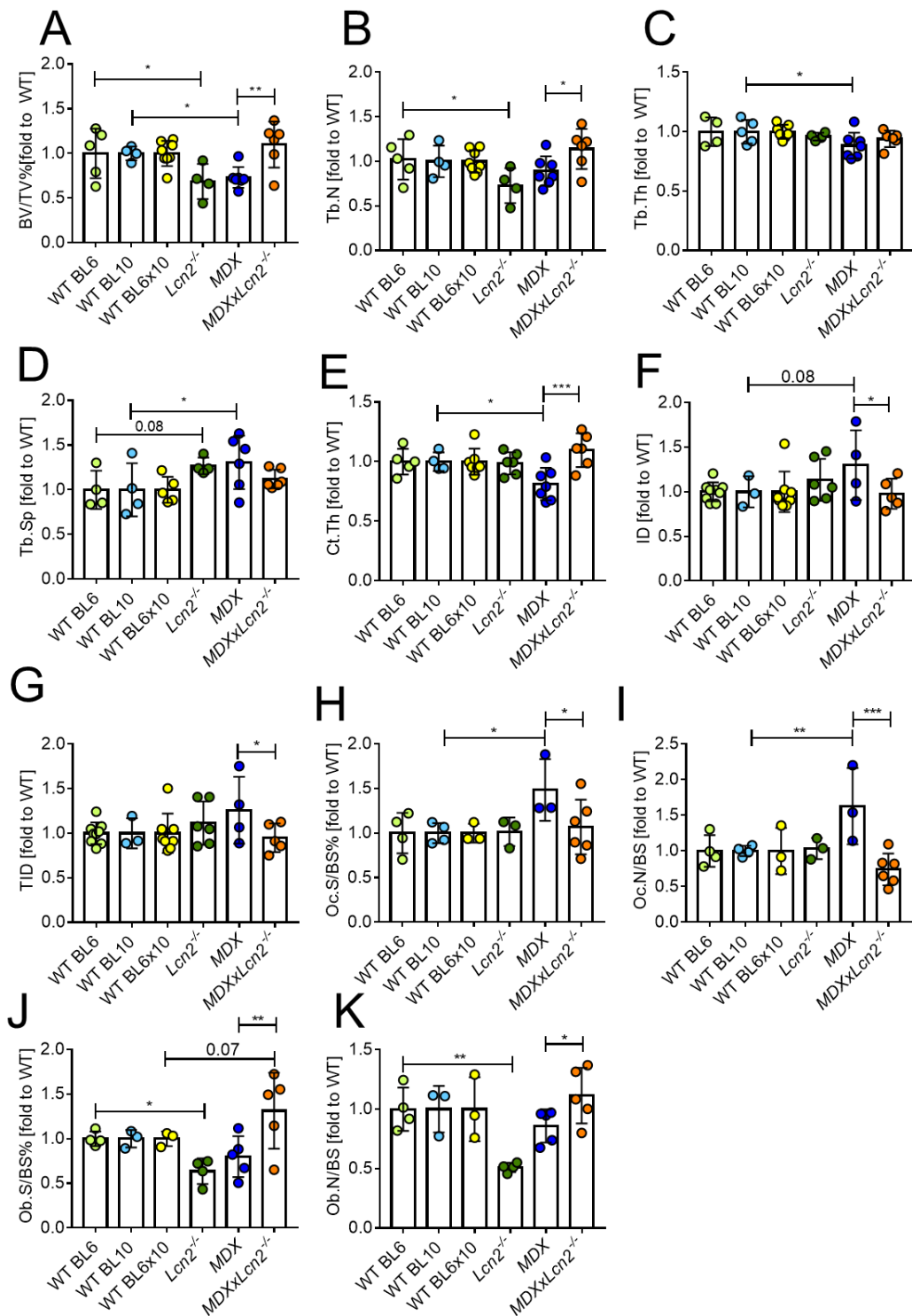


Figure 4: Bone phenotype of 6 months old mice. Tibiae were explanted from 6 months old mice and cancellous bone from proximal tibia was subjected to μ CT analysis to evaluate trabecular (A) bone volume/tissue volume%, (B) number, (C) thickness, (D) separation. Tibial cortical bone was also analysed to evaluate its (E) thickness. Tibiae were then subjected to biomechanical testing via the Biodent reference point indentation analysis instrument, to assess (F) indentation distance and (G) total indentation distance. Tibiae were embedded in plastic and sections were obtained to assess (H) Osteoclasts (Oc) surface/bone surface% (I) Oc number/bone surface by TRAcP histochemical staining, (J) Osteoblasts (Ob) surface/bone surface, (K) ob number/bone surface by toluidine blue staining. One-way ANOVA. * $p < 0.05$; ** $p < 0.01$; p values between 0.05 and 0.1 are explicated.

their respective WT (Figure 6C), while the % of intact fibers in this muscle was slightly higher in the double mutants vs *MDX* (Figure 6D). Similar regulations in bone and muscle were found when we analyzed 1-month-old mice (Supporting figure 1A-E), while most of the regulations found in younger mice seemed to fade at 12 months of age (Supporting figure 1F-J).

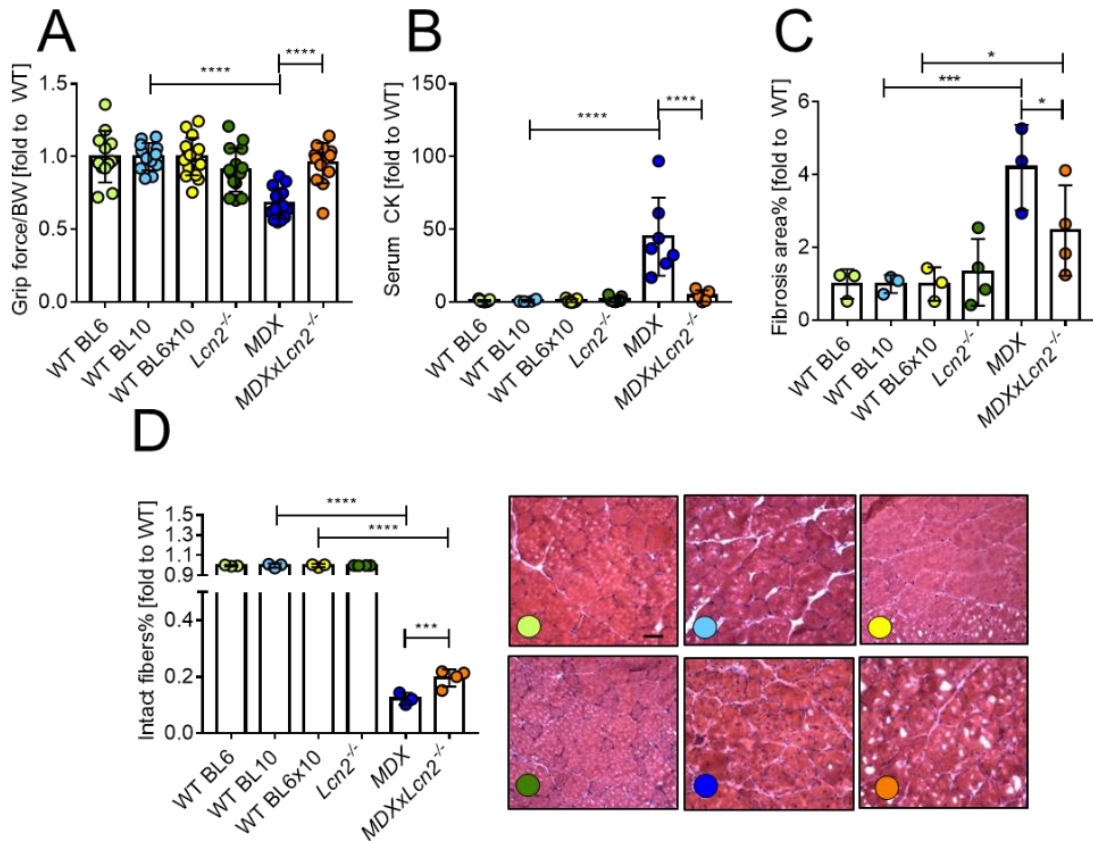


Figure 5: Muscle phenotype of 3 months old mice. 3-month-old mice were subjected to (A) grip force evaluation. (B) evaluation of serum CK. Quadriceps were snap frozen without fixation and embedded in OCT. After sectioning, quadriceps were subjected to (C) Masson’s trichrome stain to evaluate fibrosis, and (D) Hematoxylin eosin to assess % of intact fibers. Bar=30µm. One-way ANOVA. * $p < 0.05$; *** $p < 0.001$; **** $p < 0.0001$.

To reproduce the results obtained with mouse genetics, we treated *MDX* mice with a commercially available Lcn2-blocking monoclonal antibody (R&D), first using a “curative treatment” (Figure 7A). Briefly, we administered a “priming shot” of 3.75 mg/kg to 60-day-old *MDX*, which already manifested the DMD-like phenotype, and kept treating them with maintenance shots until sacrifice at 90 days of age. MicroCT results on proximal tibia trabecular bone (Figure 7B) show that the treatment with Lcn2Ab was able to significantly increase BV/TV% (Figure 7C) and Tb.N (Figure 7D), while Tb.Th (Figure 7E) was unaffected, and Tb.Sp was decreased (Figure 7F) vs irrelevant IgG. This was absolutely

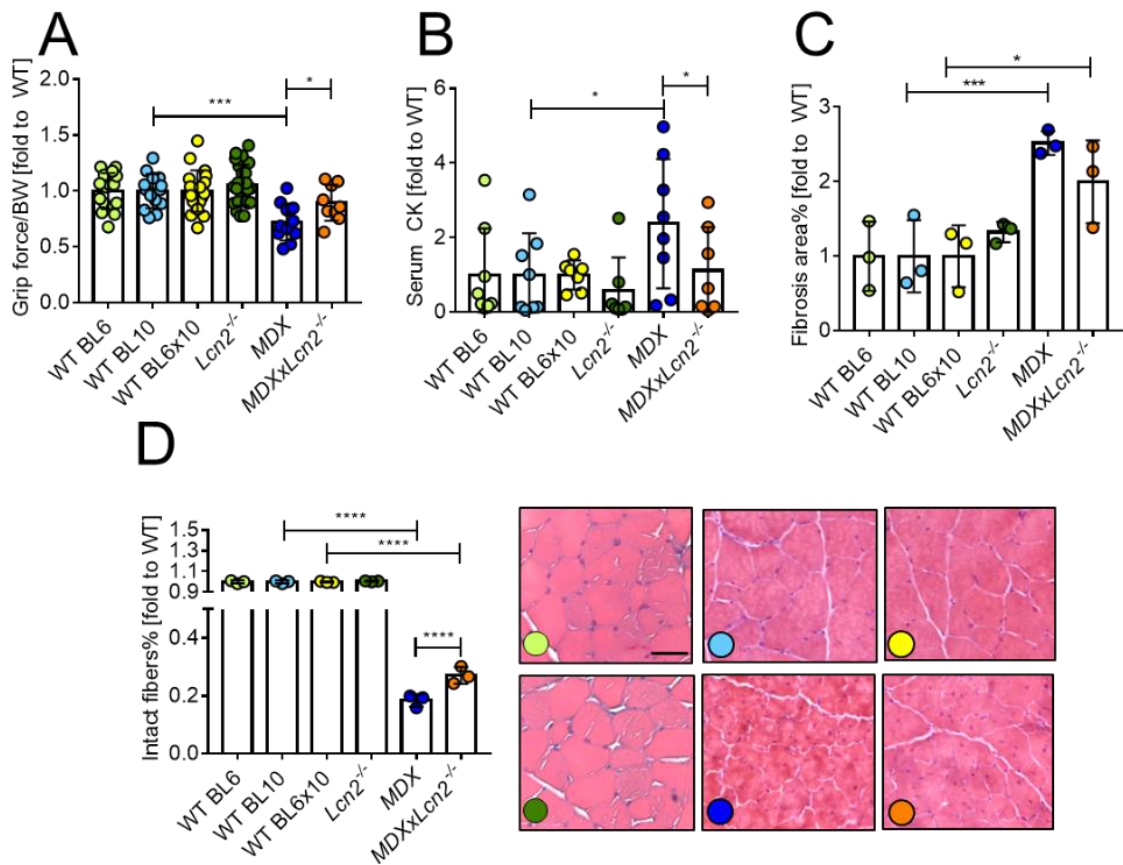
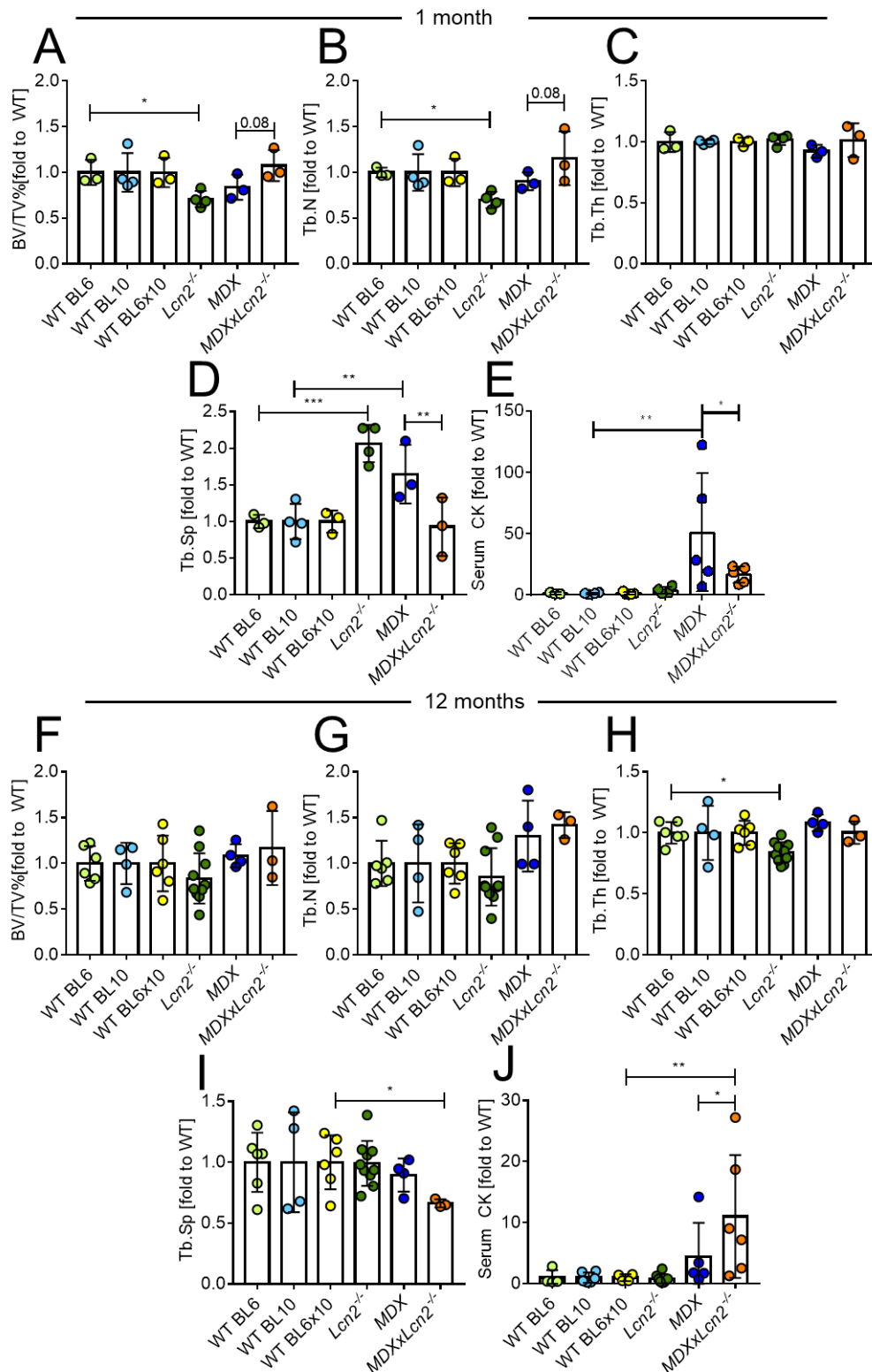


Figure 6: Muscle phenotype of 6 months old mice. 6-month-old mice were subjected to (A) grip force evaluation. (B) evaluation of serum CK. Quadriceps were snap frozen without fixation and embedded in OCT. After sectioning, quadriceps were subjected to (C) Masson's trichrome stain to evaluate fibrosis, and (D) Hematoxylin eosin to assess % of intact fibers. Bar=30µm. One-way ANOVA. *p<0.05;***p<0.001;****p<0.0001.

consistent with what was observed using mouse genetics. Ct.Th was unremarkable (Figure 7G). However, the increased bone volume was not sufficient to significantly reduce ID (Figure 7H) or TID (Figure 7I). Serum bone turnover markers CTx (Figure 7J), tartrate resistant acid phosphatase (TRAcP) 5b (Figure 7K) and free Ca²⁺ (Figure 7L) were also unremarkable.

Serum phosphate, which may be indicative of bone resorption, showed a trend of decrease following treatment with Lcn2Ab (Figure 7M), while the osteoblast marker serum bone-alkalin phosphatase (BALP), was not affected by the treatment (Figure 7N). After embedding and sectioning the tibiae, we performed histomorphometric analyses of osteoclasts and osteoblasts. TRAcP staining (Figure 7O) revealed that osteoclast surface was significantly reduced by Lcn2Ab (Figure 7P), while Oc.N showed a trend (p=0.07) of decrease (Figure 7Q). At the same time, toluidine blue (Figure 7R) showed that osteoblast surface (Figure 7S) and number (Figure 7T) were unremarkable.



Supporting Figure 1: Bone phenotype and CK levels of 1- and 12-months old mice. Tibiae were explanted from 1- or 12- months old mice and cancellous bone from proximal tibia was subjected to μ CT analysis to evaluate trabecular (A,F) bone volume/tissue volume%, (B,G) number, (C,H) thickness, (D,I) separation. Tibial cortical bone was also analysed to evaluate its (E) thickness. Serum CK was also evaluated at (E) 1- and (J) 12-months-old mice. One-way ANOVA. * $p < 0.05$; ** $p < 0.01$; *** $p < 0.001$; p values between 0.05 and 0.1 are explicited.

Hence, the increase in bone volume revealed by μ CT is probably due to a reduction in osteoclasts. We also ran longitudinal studies of weight, which was unremarkable between the two treatments and grip force, which showed a significant increase in Lcn2Ab treated mice (Figure 8A and B respectively), consistent with what we found in the double mutant studies. We then ran histological studies on diaphragm, quadriceps and *soleus*. Hematoxylin-eosin staining showed that diaphragm had a trend of increase in intact fibers, while the other muscles were unaffected (Figure 8C). Fibrosis, evaluated by Masson's trichrome was significantly lower in diaphragm (Figure 8D), while no differences were found in quadriceps (Figure 8E), and *soleus* (Figure 8F). No differences were observed in CK (Figure 8G) and myoblobin (Figure 8H). When we ran transcriptional analyses in diaphragm and quadriceps of Lcn2Ab-treated mice, we found no differences in diaphragm expression of the myogenic factors myogenic differentiation 1 (*Myod1*, Figure 9A) and Myogenin (*Myog*, Figure 9B), the satellite cells marker paired box protein 7 (*Pax7*, Figure 9C) and *Il6* (Figure 9D). However, while *Colla1* showed no difference between IgG and Lcn2Ab treatments (Figure 9E), *Col3a1*, the main fibrillar collagen in muscle, showed a trend of decrease following Lcn2Ab treatment (Figure 9F), consistently with the histological data. Quadriceps analyses revealed no difference in *Myod1* (Figure 9G), *Myog* (Figure 9H), *Pax7* (Figure 9I), but a significant reduction of *Il6* (Figure 9J), *Colla1* (Figure 9J) and *Col3a1* (Figure 9L). We next performed a similar treatment with anti-Lcn2 Ab, but following a preventive protocol (Figure 10A). Briefly, 15-day-old mice were given a priming shot and 3 maintenance shots for a total of 15 days of treatment and were then sacrificed. Tibial trabecular bone, analyzed by μ CT (Figure 10B), revealed an increase in BV/TV% (Figure 10C) following Lcn2Ab treatment vs IgG, again due to increased Tb.N (Figure 10D) with no differences in Th (Figure 10E), Sp (Figure 10F) or Cortical thickness (Figure 10G). Consistent with the lack of differences in cortical thickness, biomechanical testing revealed no difference in ID (Figure 10H) or TID (Figure 10I). The serum marker CTx showed no statistically significant difference, although the distribution would suggest that the analysis is underpowered (Figure 10J) due to high variability. Intriguingly, body weight was significantly lower in Lcn2Ab treated mice (Figure 10K), although % quadriceps (Figure 10L) and %TA (Figure 10M) weight were unaffected.

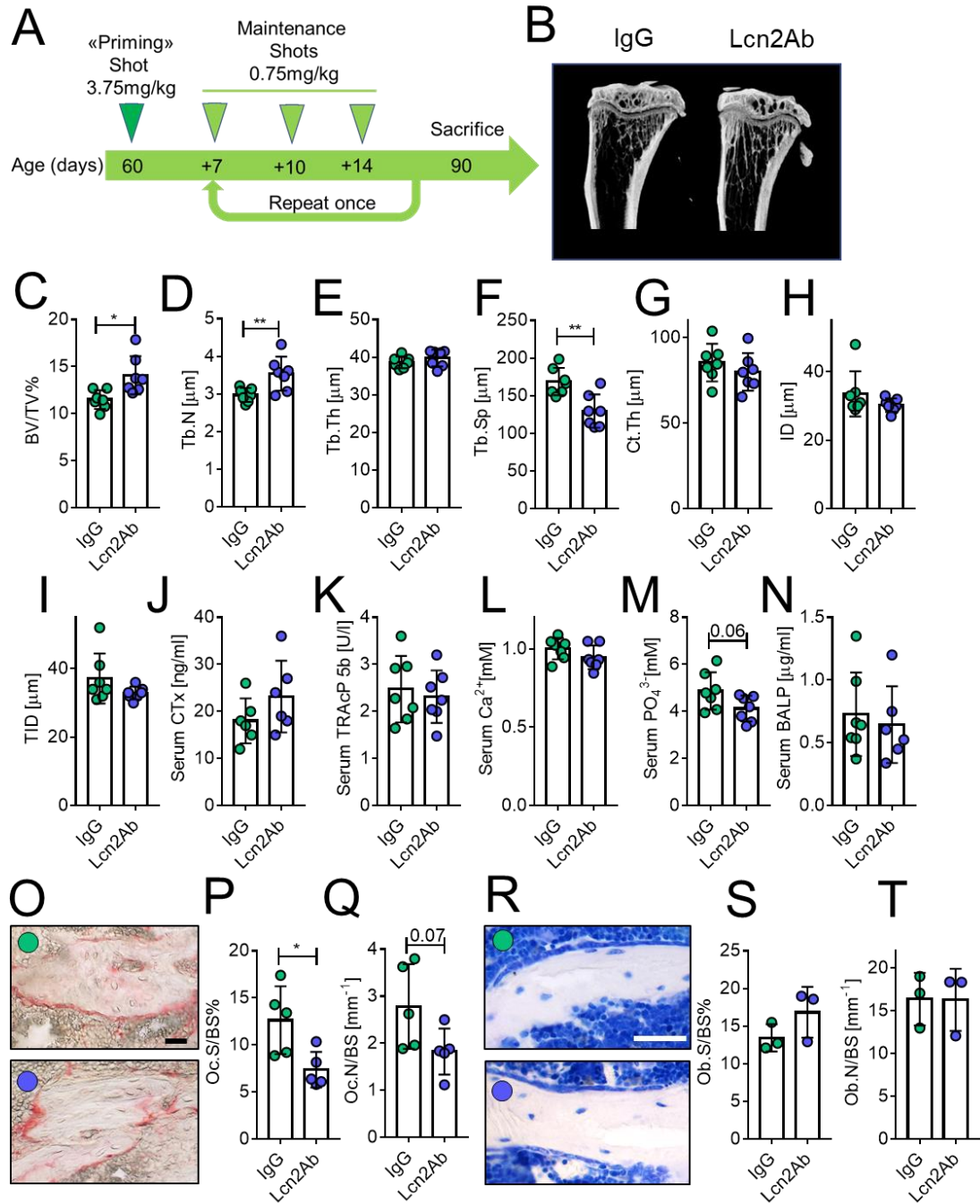


Figure 7: Treatment of MDX with anti-Lcn2 antibody, curative protocol: bone phenotype. Following treatment of MDX mice with a monoclonal antibody against Lcn2 (curative protocol, schematized in **A**), tibiae were explanted and cancellous bone from the proximal epiphysis was subjected to (**B**) μ CT analysis to evaluate trabecular (**C**) bone volume/tissue volume%, (**D**) number, (**E**) thickness, (**F**) separation. Tibial cortical bone was also analysed to evaluate its (**G**) thickness. Tibiae were then subjected to biomechanical testing via the Biodent reference point indentation analysis instrument, to assess (**H**) indentation distance and (**I**) total indentation distance. Serum from treated mice were also harvested to evaluate (**J**) carboxy-terminal collagen crosslinks (CTx), (**K**) tartrate resistant acid phosphatase 5b, (**L**) calcium and (**M**) phosphate ions, and (**N**) bone-specific alkaline phosphatase. Tibiae were then embedded in plastic and sections were obtained to perform (**O**) TRAcP histochemical staining in order to evaluate (**P**) osteoclasts (Oc) surface/bone surface% (**Q**) Oc number/bone surface. (**R**) Toluidine blue staining was also performed to assess (**S**) Osteoblasts (Ob) surface/bone surface, (**T**) ob number/bone surface by toluidine blue staining. Bar=30 μ m. Student's *t*-test. * $p < 0.05$; ** $p < 0.01$; p values between 0.05 and 0.1 are explicated.

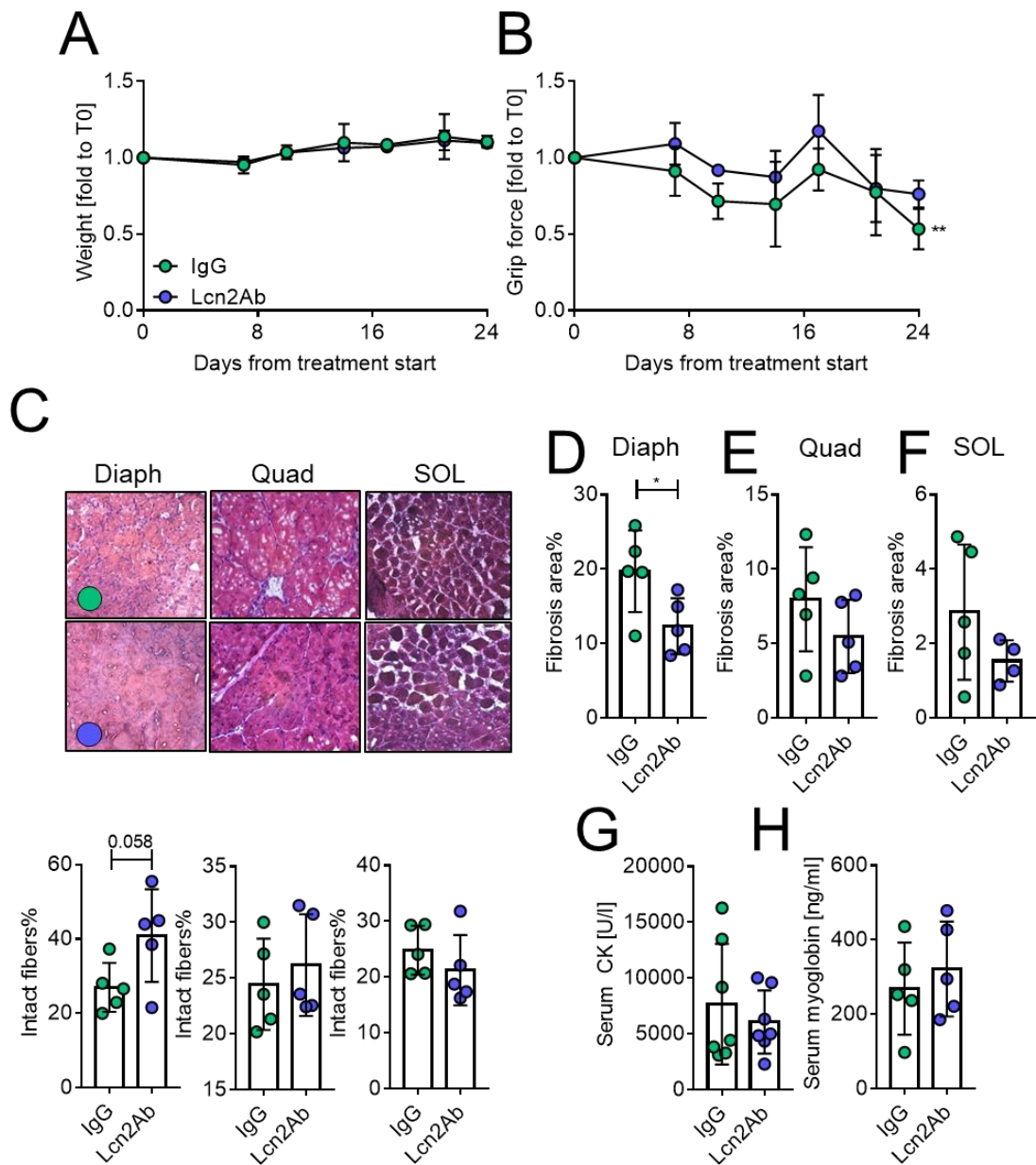


Figure 8: Treatment of MDX with anti-Lcn2 antibody, curative protocol: muscle phenotype. During treatment of MDX mice with a monoclonal antibody against Lcn2 (curative protocol, schematized in figure 7), mice were (A) weighed, after being subjected to (B) grip force test. After sacrifice, (C) diaphragm (diaph), quadriceps (Quad) and soleus (SOL) were snap frozen without fixation and embedded in OCT. After sectioning, muscles were subjected to (C) Hematoxylin eosin staining to assess % of intact fibers and (D-F) Masson's trichrome stain to evaluate fibrosis. Serum from treated mice were also harvested to evaluate (G) serum CK and (H) myoglobin. (A,B) curve fitting test, (C-H) Student's *t*-test. * $p < 0.05$; ** $p < 0.01$; p values between 0.05 and 0.1 are explicated.

Taken together, the results demonstrate that removing Lcn2 from MDX mice improves their bone health and has beneficial effects on muscle performance and damage. The fact that elder mice showed little or no differences suggests that the treatment is not curative, but probably keeps the damage at bay and slows the onset of muscle and bone disruption down.

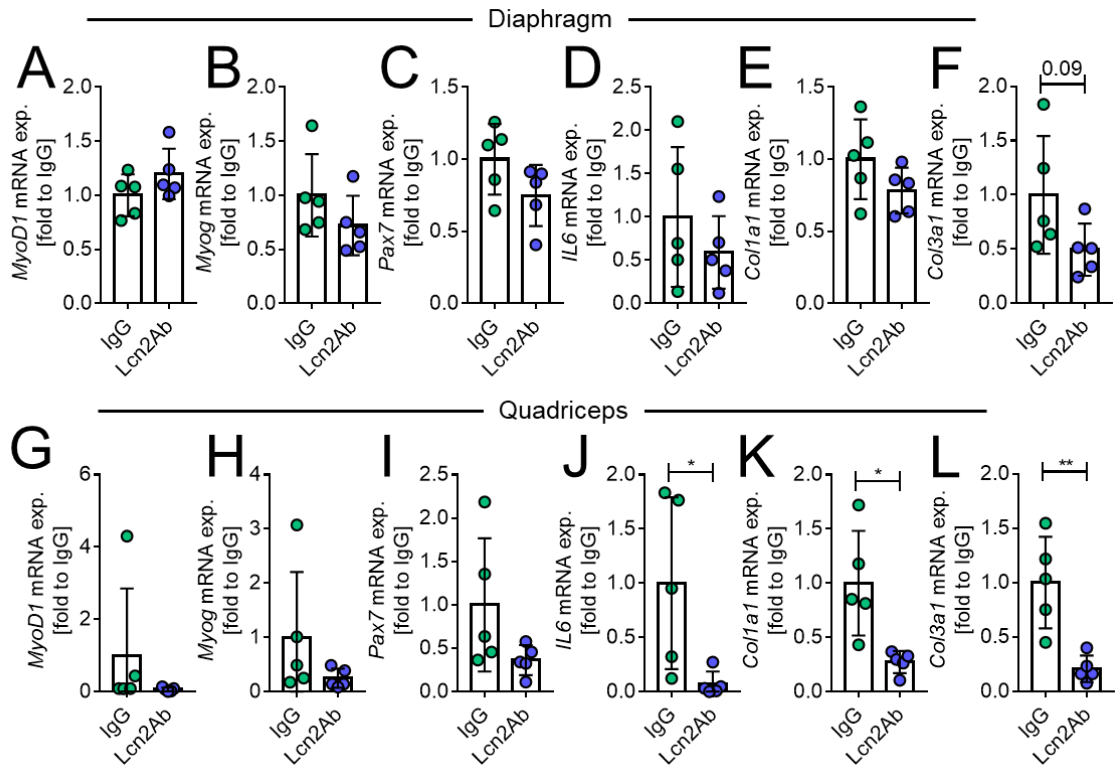


Figure 9: Treatment of MDX with anti-Lcn2 antibody, curative protocol: transcriptional analyses. Following treatment of MDX mice with a monoclonal antibody against Lcn2 (curative protocol, schematized in figure 7), (A-F) diaphragm and (G-L) quadriceps were explanted and subjected to RNA extraction, cDNA synthesis and transcriptional analysis via real time PCR. The genes analysed were (A,G) myogenic differentiation d1 (*MyoD1*), (B,H) myogenin (*Myog*), (C,I) paired box protein 7 (*Pax7*), (D,J) interleukin (*IL6*), (E,K) collagen (*Col1a1*) and (F,L) *Col3a1*. Student's *t*-test. * $p < 0.05$; ** $p < 0.01$; p values between 0.05 and 0.1 are explicitated.

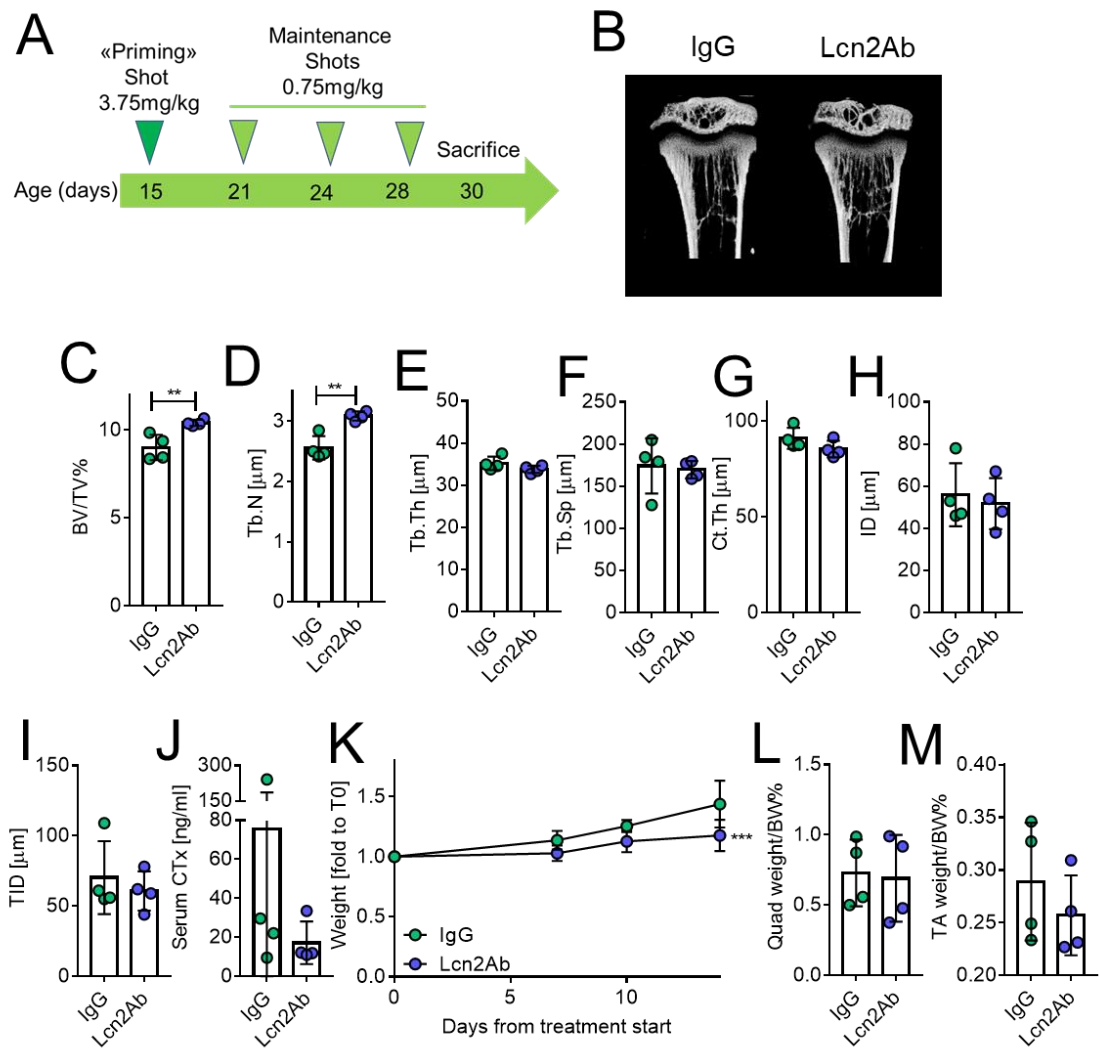


Figure 10: Treatment of MDX mice with anti-Lcn2 antibody, preventive protocol. Following treatment of MDX mice with a monoclonal antibody against Lcn2 (preventive protocol, schematized in A), tibiae were explanted and cancellous bone from the proximal epiphysis was subjected to (B) μ CT analysis to evaluate trabecular (C) bone volume/tissue volume%, (D) number, (E) thickness, (F) separation. Tibial cortical bone was also analysed to evaluate its (G) thickness. Tibiae were then subjected to biomechanical testing via the Biodent reference point indentation analysis instrument, to assess (H) indentation distance and (I) total indentation distance. Serum from treated mice were also harvested to evaluate (J) carboxy-terminal collagen crosslinks (CTx). (K) body weight was also evaluated during the timeframe of the experiment, while (L) quadriceps and (M) tibialis anterior (TA) weight was assessed at sacrifice. (A-J,L,M) Student's *t*-test. (K) curve fitting test. * $p < 0.05$; ** $p < 0.01$; p values between 0.05 and 0.1 are explicated.

5. DISCUSSION

In this chapter, we show that removing *Lcn2* genetically or by means of a blocking antibody from the *MDX* mouse model of DMD, is able to prevent the bone loss that is observed in the *MDX* mouse. However, as we stated in chapter 2, *Lcn2*^{-/-} mice are osteopenic as well. Although this might seem like a contradiction, in the previous chapter we discussed the possibility of divergent roles of this protein in physiological conditions, and in inflammatory conditions. In the *MDX*, characterized by muscle damage and flogosis, the “inflammatory” *Lcn2* might be more important, and the osteopenia-inducing effect of the lack of *Lcn2* (see Chapter 2), is lower than the damage it causes when it is present in the *MDX* mouse. The net result is that removing *Lcn2* in *MDX* mice, is beneficial for bone mass. As for muscle, while surprising, the general improvement of muscle condition when *Lcn2* is removed is not completely unexpected: in fact, in chapter 2 we showed that removing *Lcn2* is able to induce, at least in younger mice, the expression of myogenic factors. Furthermore, treating myoblasts with *Lcn2* reduces their myogenic differentiation.

The fact that after 6 months of age, the phenotypical improvements conferred by *Lcn2* removal fade, or are even reverted in the case of CK, is consistent with the fact that the damage is not prevented, but only delayed. This, along with the positive correlation we and others found between inflammation and *Lcn2*, suggests that *Lcn2* is a driving component in the chronic flogistic damage and bone loss, and removing it only provides a temporary benefit.

Although Removing *Lcn2* is not curative in DMD, this is an attractive therapeutic target to reduce bone loss, since it does not present all the known drawbacks of using bisphosphonates or PTH-mimics in pediatric patients, with the added bonus of positive effects on muscle.

Another possible advantage of using anti-*Lcn2* in DMD is that recent reports^{21,22} suggest a link between glucocorticoids and *Lcn2*. In particular, Conde et al.²¹ suggest that glucocorticoids (GCs) are able to induce *Lcn2* expression through IL1. This would be consistent with our data showing that *Ili1b* correlates with *Lcn2*, and if confirmed in DMD, would strengthen the rationale behind anti-*Lcn2* treatment, since it might be able to limit the side effects of GCs treatment on bone.

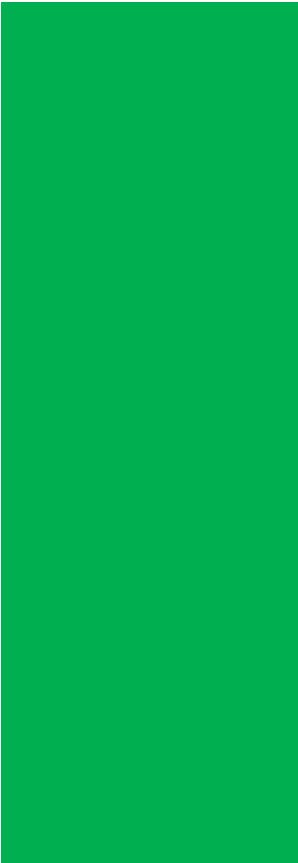
In conclusion, we showed that *Lcn2* is a detrimental factor for bone and muscle health in the *MDX* mouse model of DMD, and removing it genetically is able to revert the bone loss induced by this disease. Using a blocking antibody against *Lcn2* yields similar results,

significantly increasing bone mass, while improving muscle health. More studies will confirm whether this molecule is also important in human DMD, and whether glucocorticoid-induced osteoporosis may be prevented by targeting this molecule.

6. REFERENCES

1. Lögdberg, L. & Wester, L. Immunocalins: A lipocalin subfamily that modulates immune and inflammatory responses. *Biochim. Biophys. Acta - Protein Struct. Mol. Enzymol.* **1482**, 284–297 (2000).
2. Abella, V. *et al.* The potential of lipocalin-2/NGAL as biomarker for inflammatory and metabolic diseases. *Biomarkers* **20**, 565–571 (2015).
3. Rucci, N. *et al.* Lipocalin 2: A new mechanoresponding gene regulating bone homeostasis. *J. Bone Miner. Res.* (2015) doi:10.1002/jbmr.2341.
4. Capulli, M., Rufo, A., Teti, A. & Rucci, N. Global transcriptome analysis in mouse calvarial osteoblasts highlights sets of genes regulated by modeled microgravity and identifies A ‘mechanoresponsive osteoblast gene signature’. *J. Cell. Biochem.* (2009) doi:10.1002/jcb.22120.
5. Capulli, M. *et al.* A Complex Role for Lipocalin 2 in Bone Metabolism: Global Ablation in Mice Induces Osteopenia Caused by an Altered Energy Metabolism. *J. Bone Miner. Res.* **33**, (2018).
6. Veeriah, V. *et al.* Interleukin-1 β , lipocalin 2 and nitric oxide synthase 2 are mechano-responsive mediators of mouse and human endothelial cell-osteoblast crosstalk. *Sci. Rep.* (2016) doi:10.1038/srep29880.
7. Mosialou, I. *et al.* MC4R-dependent suppression of appetite by bone-derived lipocalin 2. *Nature* (2017) doi:10.1038/nature21697.
8. Costa, D. *et al.* Altered bone development and turnover in transgenic mice over-expressing Lipocalin-2 in bone. *J. Cell. Physiol.* (2013) doi:10.1002/jcp.24391.
9. Berger, T. *et al.* Lipocalin 2-deficient mice exhibit increased sensitivity to *Escherichia coli* infection but not to ischemia-reperfusion injury. *Proc. Natl. Acad. Sci. U. S. A.* (2006) doi:10.1073/pnas.0510847103.
10. Cheng, L. *et al.* Lipocalin-2 promotes M1 macrophages polarization in a mouse cardiac ischaemia-reperfusion injury model. *Scand. J. Immunol.* (2015) doi:10.1111/sji.12245.
11. Pelosi, L. *et al.* Functional and Morphological Improvement of Dystrophic Muscle by Interleukin 6 Receptor Blockade. *EBioMedicine* (2015) doi:10.1016/j.ebiom.2015.02.014.
12. Grounds, M. Quantification of histopathology in Haematoxylin and Eosin stained muscle sections. *TREAT-NMD Neuromuscul. Netw.* 1–14 (2012).
13. Gutpel, K. M., Hrinivich, W. T. & Hoffman, L. M. Skeletal muscle fibrosis in the mdx/utrn+/-mouse validates its suitability as a murine model of duchenne muscular dystrophy. *PLoS One* (2015) doi:10.1371/journal.pone.0117306.
14. Rucci, N. *et al.* The glycosaminoglycan-binding domain of PRELP acts as a cell

- type-specific NF- κ B inhibitor that impairs osteoclastogenesis. *J. Cell Biol.* (2009) doi:10.1083/jcb.200906014.
15. Dempster, D. W. *et al.* Standardized nomenclature, symbols, and units for bone histomorphometry: A 2012 update of the report of the ASBMR Histomorphometry Nomenclature Committee. *Journal of Bone and Mineral Research* (2013) doi:10.1002/jbmr.1805.
 16. Feldkamp, L. A., Davis, L. C. & Kress, J. W. Practical cone-beam algorithm. *J. Opt. Soc. Am. A* (1984) doi:10.1364/josaa.1.000612.
 17. Rufo, A. *et al.* Mechanisms inducing low bone density in duchenne muscular dystrophy in mice and humans. *J. Bone Miner. Res.* (2011) doi:10.1002/jbmr.410.
 18. Lorensen, W. E. & Cline, H. E. Marching cubes: A high resolution 3D surface construction algorithm. in *Proceedings of the 14th Annual Conference on Computer Graphics and Interactive Techniques, SIGGRAPH 1987* (1987). doi:10.1145/37401.37422.
 19. Pratt, W. K. *Processing Digital Image Processing. Image Rochester NY* (2001). doi:10.1016/S0146-664X(78)80023-9.
 20. Bouxsein, M. L. *et al.* Guidelines for assessment of bone microstructure in rodents using micro-computed tomography. *Journal of Bone and Mineral Research* (2010) doi:10.1002/jbmr.141.
 21. Conde, J. *et al.* Corticoids synergize with IL-1 in the induction of LCN2. *Osteoarthr. Cartil.* (2017) doi:10.1016/j.joca.2017.01.017.
 22. Kamble, P. G., Pereira, M. J., Almy, K. & Eriksson, J. W. Estrogen interacts with glucocorticoids in the regulation of lipocalin 2 expression in human adipose tissue. Reciprocal roles of estrogen receptor α and β in insulin resistance? *Mol. Cell. Endocrinol.* (2019) doi:10.1016/j.mce.2019.04.002.



Chapter 5

Conclusions

CONCLUSIONS

In this dissertation we described the role of LCN2 in bone and muscle physiopathology.

The data present in literature on this topic, as well as other physiological aspects related to LCN2 is not always consistent (See **Chapter 1**). This should not come as a surprise, since LCN2 expression appears to be regulated by several different mechanisms, and its expression is very responsive to different stimuli. In these conditions, confounding factors that are beyond the investigator's control may be present, and lead to controversial or discordant results. Having said that, a consensus is (for the most part) present on certain aspects related to LCN2, including its increase in obesity, and the fact that its lack increases food intake¹⁻⁶. The same can be said with even more certainty about its increase in acute kidney injury (AKI), where the small size of this protein, along with the strong increase in its expression in AKI kidneys concur to making it an ideal biomarker for this condition, that can be easily pass through the Bowman capsule and be detected in urines by ELISA or similar assays⁷.

The role of LCN2 in bone physiopathology, on the other hand, is quite complex and has not been completely understood to date. As shown in **Chapter 2** of this dissertation, lack of *Lcn2* causes osteopenia, whereas overexpression of this cytokine increases osteoblast production of IL6 and RANKL, leading to reduced osteoblast differentiation and increased osteoclast activity, thus leading to osteopenia⁸. This is consistent with the fact that in our hands, osteoblasts express very little *Lcn2*, and its sudden increase may signal through inflammation pathways, being recognized by the osteoblast as a noxious "unexpected" stimulus, as is often the case for inflammatory molecules such as interleukins, ATP, High Mobility Group Box 1, autologous DNA and other molecules⁹. However, a recent report by Mosialou et al.⁶ stated that in their hands *Lcn2* is highly enriched in bone, particularly in osteoblasts. We currently have no perfect answer to this divergence of results (also see **Chapter 2** discussion), but it should be noted that our mouse models are different, since they mainly employ osteoblast-specific *Lcn2*-KO mice, while our model is one of global deletion.

It is interesting to note that LCN2 also has a role to play in muscle. In **Chapter 3** we noticed that following acute high intensity exercise, LCN2 was increased in healthy athletes, and correlated with the Wnt pathway inhibitor DKK1, which reduces bone formation. This led us to think that maybe LCN2 could be a linker between muscle and bone. Upon further investigation, using mouse models, we found that removing *Lcn2* does not have any major issue in muscle, and causes only mild changes in phenotype, such as a small reduction of

fiber size in quadriceps, and few changes in gene expression, pointing at increased myogenic differentiation in young animals, which is then reverted in older animals. When we treated muscle cells with Lcn2 in vitro, this reduced their differentiation ability. That, along with the fact that Lcn2 is increased in inflammatory conditions¹⁰⁻¹², and mechanical unloading^{8,13,14}, led us to think that Lcn2 might be involved in a disease characterized by all these factors: Duchenne Muscular Dystrophy (DMD). Another indication came from our previous report, showing Lcn2 expression is increased in femurs from *MDX* mice, a model for DMD⁸.

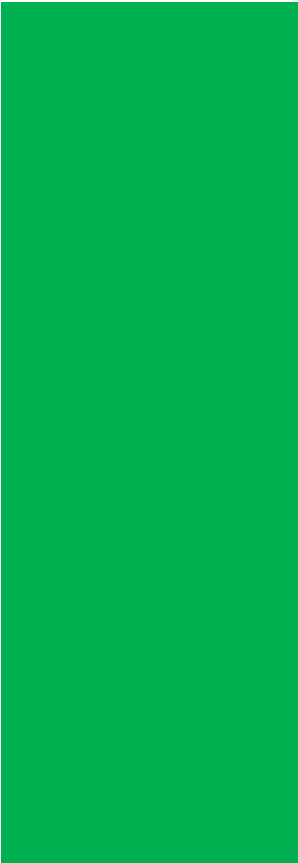
In **Chapter 4** we pursue this idea, and we reason that since *MDX* mice have low bone mass due to osteoclast activity exacerbation¹⁵, contrasting the increase in Lcn2 could potentially prevent bone loss associated with this disease, without causing any more trouble to muscle, or even helping it. This was indeed the case: removing Lcn2 genetically (via crossbreedings) or functionally (with a blocking antibody) is able to increase bone mass and improve muscle phenotype of the *MDX* mouse model of DMD. This could be potentially important for preserving bone health in DMD, since current standard of care includes bisphosphonates, which are known to “freeze” the bone, preventing bone modelling and remodeling. In young boys this can lead to failure to grow, delay in teeth eruption and atypical fractures. The alternative would be anabolic drugs, which are either dangerous or not tested in pediatric patients (See **Chapter 1**). Anti-Lcn2 agents would potentially enable us to maintain bone health, without adding any foreseeable side effects, with the bonus of improved of muscle performance. Of course, the interaction of Lcn2 with glucocorticoids such as Deflazacort or Prednisolone must be investigated before taking this route. However, there is some encouraging (albeit scarce) evidence showing that Lcn2 is increased by glucocorticoids¹⁶⁻¹⁸, which would further exacerbate bone loss, and give more rationale to Lcn2 blocking strategies. Expectedly, there is some degree of complexity in how Lcn2 acts on muscle. In fact, one recent literature report on the matter states that Lcn2 is necessary for acute skeletal muscle damage healing¹⁹, while other reports state that another similar muscle, hearth, benefits from the lack of Lcn2²⁰⁻²⁴.

In conclusion, this dissertation provides a comprehensive overview over the role of Lipocalin-2 in bone and muscle biology and provides evidence that blocking Lcn2 in the *MDX* mouse model of DMD could be a viable therapeutic option for bone loss in this disease.

REFERENCES

1. Wang, Y. *et al.* Lipocalin-2 is an inflammatory marker closely associated with obesity, insulin resistance, and hyperglycemia in humans. *Clin. Chem.* (2007) doi:10.1373/clinchem.2006.075614.
2. De La Chesnaye, E. *et al.* Lipocalin-2 plasmatic levels are reduced in patients with long-term type 2 diabetes mellitus. *Int. J. Clin. Exp. Med.* (2015).
3. Yan, Q. W. *et al.* The adipokine lipocalin 2 is regulated by obesity and promotes insulin resistance. *Diabetes* (2007) doi:10.2337/db07-0007.
4. Jun, L. S., Parker Siddall, C. & Rosen, E. D. A minor role for lipocalin 2 in high-fat diet-induced glucose intolerance. *Am. J. Physiol. - Endocrinol. Metab.* (2011) doi:10.1152/ajpendo.00147.2011.
5. Capulli, M. *et al.* A Complex Role for Lipocalin 2 in Bone Metabolism: Global Ablation in Mice Induces Osteopenia Caused by an Altered Energy Metabolism. *J. Bone Miner. Res.* **33**, (2018).
6. Mosialou, I. *et al.* MC4R-dependent suppression of appetite by bone-derived lipocalin 2. *Nature* (2017) doi:10.1038/nature21697.
7. Bolignano, D. *et al.* Neutrophil Gelatinase-Associated Lipocalin (NGAL) as a Marker of Kidney Damage. *Am. J. Kidney Dis.* (2008) doi:10.1053/j.ajkd.2008.01.020.
8. Rucci, N. *et al.* Lipocalin 2: A new mechanoresponding gene regulating bone homeostasis. *J. Bone Miner. Res.* (2015) doi:10.1002/jbmr.2341.
9. Roh, J. S. & Sohn, D. H. Damage-associated molecular patterns in inflammatory diseases. *Immune Network* (2018) doi:10.4110/in.2018.18.e27.
10. Xiao, X., Yeoh, B. S. & Vijay-Kumar, M. Lipocalin 2: An Emerging Player in Iron Homeostasis and Inflammation. *Annu. Rev. Nutr.* (2017) doi:10.1146/annurev-nutr-071816-064559.
11. Moschen, A. R., Adolph, T. E., Gerner, R. R., Wieser, V. & Tilg, H. Lipocalin-2: A Master Mediator of Intestinal and Metabolic Inflammation. *Trends in Endocrinology and Metabolism* (2017) doi:10.1016/j.tem.2017.01.003.
12. Abella, V. *et al.* The potential of lipocalin-2/NGAL as biomarker for inflammatory and metabolic diseases. *Biomarkers* **20**, 565–571 (2015).
13. Capulli, M., Rufo, A., Teti, A. & Rucci, N. Global transcriptome analysis in mouse calvarial osteoblasts highlights sets of genes regulated by modeled microgravity and identifies A ‘mechanoresponsive osteoblast gene signature’. *J. Cell. Biochem.* (2009) doi:10.1002/jcb.22120.
14. Veeriah, V. *et al.* Interleukin-1 β , lipocalin 2 and nitric oxide synthase 2 are mechano-responsive mediators of mouse and human endothelial cell-osteoblast crosstalk. *Sci. Rep.* (2016) doi:10.1038/srep29880.
15. Rufo, A. *et al.* Mechanisms inducing low bone density in duchenne muscular dystrophy in mice and humans. *J. Bone Miner. Res.* (2011) doi:10.1002/jbmr.410.
16. Kamble, P. G., Pereira, M. J., Almby, K. & Eriksson, J. W. Estrogen interacts with glucocorticoids in the regulation of lipocalin 2 expression in human adipose tissue.

- Reciprocal roles of estrogen receptor α and β in insulin resistance? *Mol. Cell. Endocrinol.* (2019) doi:10.1016/j.mce.2019.04.002.
17. Liu, Q. S., Nilsen-Hamilton, M. & Xiong, S. D. Synergistic regulation of the acute phase protein SIP24/24p3 by glucocorticoid and pro-inflammatory cytokines. *Acta Physiol. Sin.* (2003).
 18. Conde, J. *et al.* Corticoids synergize with IL-1 in the induction of LCN2. *Osteoarthr. Cartil.* (2017) doi:10.1016/j.joca.2017.01.017.
 19. Rebalka, I. A. *et al.* Loss of the adipokine lipocalin-2 impairs satellite cell activation and skeletal muscle regeneration. *Am. J. Physiol. - Cell Physiol.* (2018) doi:10.1152/ajpcell.00195.2017.
 20. Marques, F. Z. *et al.* Experimental and Human Evidence for Lipocalin-2 (Neutrophil Gelatinase-Associated Lipocalin [NGAL]) in the Development of Cardiac Hypertrophy and heart failure. *J. Am. Heart Assoc.* (2017) doi:10.1161/JAHA.117.005971.
 21. Sung, H. K. *et al.* Lipocalin-2 (NGAL) Attenuates Autophagy to Exacerbate Cardiac Apoptosis Induced by Myocardial Ischemia. *J. Cell. Physiol.* (2017) doi:10.1002/jcp.25672.
 22. Xu, G. *et al.* Lipocalin-2 induces cardiomyocyte apoptosis by increasing intracellular iron accumulation. *J. Biol. Chem.* (2012) doi:10.1074/jbc.M111.275719.
 23. Ding, L. *et al.* Lipocalin-2/neutrophil gelatinase-B associated lipocalin is strongly induced in hearts of rats with autoimmune myocarditis and in human myocarditis. *Circ. J.* (2010) doi:10.1253/circj.CJ-09-0485.
 24. Cheng, L. *et al.* Lipocalin-2 promotes M1 macrophages polarization in a mouse cardiac ischaemia-reperfusion injury model. *Scand. J. Immunol.* (2015) doi:10.1111/sji.12245.



Chapter 6

Achievements

CURRICULUM VITAE ET STUDIORUM

Marco Ponzetti



Born in Teramo (Italy), 24th December 1991,
Italian Citizenship



OrcidID QR code

ADDRESS

Frazione Colliberti, 295,
Isola del Gran Sasso d'Italia
64045, Teramo (TE)
Italy

PHONE AND EMAIL

Home +39 0861868856
Mobile +39 3290332245
Fax +39 0862433523
mp.univaq@gmail.com
marcoPON@univaq.it

ACADEMIC DEGREES

- 07/2016 Master's Degree in Medical Biotechnologies *cum laude*. University of L'Aquila, Italy.
- 07/2014 Bachelor's degree in Biotechnologies *cum laude*. University of L'Aquila, Italy.
- 2007 B1-level english certificate for foreigners (Preliminary English Test) Cambridge University, vote: "Pass with merit".

PROFESSIONAL EXPERIENCES

- 01-07/2018 Marie Curie fellowship in the RUBICON project in Prof. Malcolm Collins' lab. Department of Human Biology & Sport Science institute of South Africa, University of Cape Town, South Africa
- 11/2016-pres PhD candidate in Experimental Medicine (with scholarship, XXXII cycle) in the University of L'Aquila, Italy, in the "Skeletal Diseases Lab" (Prof. Nadia Rucci)
- 03-11/2016 Research fellow in the "Skeletal Diseases Lab" (Prof. Nadia Rucci)
- 11/2015- 03/2016 Research fellow in the "Bone Biopathology Lab" funded by AIRC, supervised by Prof. Anna Teti (Project: AIRC investigator grant IG12713)
- 01-06/2015 Marie Curie fellowship in the INTERBONE project, in Prof. Stavroula Kousteni's Lab, Department of Physiology and Cellular Biophysics, Columbia University Medical Center, New York, NY.
- 10/2014-10/2015 Research fellow in the "Bone Biopathology Lab" funded by AIRC, supervised by Prof. Nadia Rucci (Project: AIRC investigator grant IG11950)
- 2012-2015 Trainee in the "Bone Biopathology Lab" (Prof. Anna Teti) supervised by Prof. Nadia Rucci

NATIONAL AND INTERNATIONAL MEETINGS:

- 14-17/05/2016 European calcified tissue society (ECTS) annual congress, Roma, Italy
- 23-25/11/2016 Associazione italiana colture cellulari (AICC) meeting, L'Aquila, Italy
- 13-16/05/2017 ECTS annual congress, Salzburg, Austria
- 20-21/07/2018 RUBICON meeting, Manchester, UK
- 10-14/05/2019 ECTS Annual congress and pre-congress, Budapest, Hungary
- 21/06/2019 Symposium on Muscle-Bone Interaction in Duchenne Muscular Dystrophy. Salzburg, Austria
- 18-19/09/2019 Endocrine Fellow Foundation (EFF) forum on metabolic bone diseases, Orlando, FL, USA.
- 19-23/09/2019 American Society for Bone and Mineral Research (ASBMR) annual congress and pre-congress, Orlando, FL, USA.

CONFERENCE PRESENTATIONS, GRANTS AND AWARDS:

Associazione italiana per la ricerca sul cancro (AIRC)

- 2019 research “fellowship for Italy” awardee. Project title: “Role of extracellular vesicle-shuttled miRNAs in the reprogramming of the breast cancer bone metastatic microenvironment” (project code 24019) **€25000**

ASBMR congress, Orlando, FL, USA. 20-23 September 2019

- Plenary oral presentation
- Felix Bronner young investigator award **\$1000**

ASBMR pre-congress, Orlando, FL, USA. 19 September 2019

- Poster presentation

EFF (Endocrine Fellow Foundation) forum on metabolic bone diseases, Orlando, FL, USA. 18-19 September 2019

- Poster presentation
- Grant to attend the forum and the ASBMR **\$1370**

ECTS (European calcified tissue society) annual congress PhD Training course (7-10 September 2019, Bologna, Italy)

- Oral presentation

ECTS annual congress, Budapest, 10-14 May 2019

- Plenary oral presentation
- New investigator award **€750**

OTHER INITIATIVES:

- AIRC nelle scuole, Ancona 2017, Teramo 2018 (Italy)
- Telethon fundraiser, L'Aquila (2012-2018)

PUBLICATIONS:

- Loftus A, Cappariello A, George C, Ucci A, Shefferd K, Green A, Paone R, **Ponzetti M**, Delle Monache S, Muraca M, Teti A, Rucci N. “Extracellular Vesicles from Osteotropic Breast Cancer Cells Affect Bone Resident Cells.” JBMR 2019 Oct;14. doi: 10.1002/jbmr.3891. [Epub ahead of print]
- Suijkerbuijk MAM*, **Ponzetti M***, Rahim M, Posthumus M, Häger CK, Stattin E, Nilsson KG, Teti A, Meuffels DE, van der Eerden BJC, Collins M, September AV. “Functional polymorphisms within the inflammatory pathway regulate expression of extracellular matrix components in a genetic risk dependent model for anterior cruciate ligament injuries.” J Sci Med Sport. 2019 Nov;22:1219-1225
**Authors contributed equally to the work*

- Marino S, de Ridder D, Bishop RT, Renema N, **Ponzetti M**, Sophocleous A, Capulli M, Aljeffery A, Carrasco G, Gens M D, Khogeer A, Ralston SH, Gertsch J, Lamoureux F, Heymann D, Rucci N, Idris AI. “Paradoxical effects of JZL184, an inhibitor of monoacylglycerol lipase, on bone remodelling in healthy and cancer-bearing mice.” *EBioMedicine*. 2019 Jun;44:452-466.
- **Ponzetti M**, Rucci N. “Updates on Osteoimmunology: What's New on the Cross-Talk Between Bone and Immune System.” *Front Endocrinol (Lausanne)*. 2019 Apr 18;10:236.
- Aielli F, **Ponzetti M**, Rucci N. “Bone Metastasis Pain, from the Bench to the Bedside.” *Int J Mol Sci*. 2019 Jan 11;20(2).
- Capulli M, **Ponzetti M**, Maurizi A, Gemini-Piperni S, Berger T, Mak TW, Teti A, Rucci N.” A Complex Role for Lipocalin 2 in Bone Metabolism: Global Ablation in Mice Induces Osteopenia Caused by an Altered Energy Metabolism.” *JBMR* 2018 Jun;33(6):1141-1153
- **Ponzetti M**, Capulli M, Angelucci A, Ventura L, Monache SD, Mercurio C, Calgani A, Sanità P, Teti A, Rucci N. “Non-conventional role of haemoglobin beta in breast malignancy.” *Br J Ca* 2017 Sep 26;117(7):994-1006.
- Di Pompo G, Lemma S, Canti L, Rucci N, **Ponzetti M**, Errani C, Donati DM, Russell S, Gillies R, Chano T, Baldini N, Avnet S. “Intratumoral acidosis fosters cancer-induced bone pain through the activation of the mesenchymal tumor-associated stroma in bone metastasis from breast carcinoma.” *Oncotarget* 2017 Apr 13;8(33):54478-54496.
- Cappariello A, **Ponzetti M**, Rucci N. “The "soft" side of the bone: unveiling its endocrine functions.” *Horm Mol Biol Clin Investig*. 2016 Oct 1;28(1):5-20.
- Galán-Díez M, Isa A, **Ponzetti M**, Nielsen MF, Kassem M, Kousteni S. “Normal hematopoiesis and lack of β -catenin activation in osteoblasts of patients and mice harboring Lrp5 gain-of-function mutations.” *Biochim Biophys Acta*. 2016 Mar;1863(3):490-8

Marco Ponzetti

Date of preparation: January 2020

